

# CANADIAN THESES ON MICROFICHE

## THÈSES CANADIENNES SUR MICROFICHE



National Library of Canada  
Collections Development Branch

Canadian Theses on  
Microfiche Service

Ottawa, Canada  
K1A 0N4

Bibliothèque nationale du Canada  
Direction du développement des collections

Service des thèses canadiennes  
sur microfiche

### NOTICE

The quality of this microfiche is heavily dependent upon the quality of the original thesis submitted for microfilming. Every effort has been made to ensure the highest quality of reproduction possible.

If pages are missing, contact the university which granted the degree.

Some pages may have indistinct print especially if the original pages were typed with a poor typewriter ribbon or if the university sent us an inferior photocopy.

Previously copyrighted materials (journal articles, published tests, etc.) are not filmed.

Reproduction in full or in part of this film is governed by the Canadian Copyright Act, R.S.C. 1970, c. C-30. Please read the authorization forms which accompany this thesis.

**THIS DISSERTATION  
HAS BEEN MICROFILMED  
EXACTLY AS RECEIVED**

### AVIS

La qualité de cette microfiche dépend grandement de la qualité de la thèse soumise au microfilmage. Nous avons tout fait pour assurer une qualité supérieure de reproduction.

S'il manque des pages, veuillez communiquer avec l'université qui a conféré le grade.

La qualité d'impression de certaines pages peut laisser à désirer, surtout si les pages originales ont été dactylographiées à l'aide d'un ruban usé ou si l'université nous a fait parvenir une photocopie de qualité inférieure.

Les documents qui font déjà l'objet d'un droit d'auteur (articles de revue, examens publiés, etc.) ne sont pas microfilmés.

La reproduction, même partielle, de ce microfilm est soumise à la Loi canadienne sur le droit d'auteur, SRC 1970, c. C-30. Veuillez prendre connaissance des formules d'autorisation qui accompagnent cette thèse.

**LA THÈSE A ÉTÉ  
MICROFILMÉE TELLE QUE  
NOUS L'AVONS REÇUE**

**Canada**



National Library of Canada

Bibliothèque nationale du Canada

Canadian Theses Division

Division des thèses canadiennes

Ottawa, Canada  
K1A 0N4

67358

102

**PERMISSION TO MICROFILM — AUTORISATION DE MICROFILMER**

• Please print or type — Écrire en lettres moulées ou dactylographier

Full Name of Author — Nom complet de l'auteur

*Edmund Sumbar*

Date of Birth — Date de naissance <i>November 17, 1954</i>	Country of Birth — Lieu de naissance <i>Canada</i>
---	---

Permanent Address — Résidence fixe  
*11320 - 102 ST.  
Edmonton, Alta.  
T5G 2E4*

Title of Thesis — Titre de la thèse  
*Design and Performance of a 280 kV Ion Accelerator*

University — Université  
*University of Alberta*

Degree for which thesis was presented — Grade pour lequel cette thèse fut présentée  
*Doctor of Philosophy*

Year this degree conferred — Année d'obtention de ce grade <i>1984</i>	Name of Supervisor — Nom du directeur de thèse <i>R.P.W. Lawson / F.E. Vermeulen</i>
---	---

Permission is hereby granted to the NATIONAL LIBRARY OF CANADA to microfilm this thesis and to lend or sell copies of the film.

L'autorisation est, par la présente, accordée à la BIBLIOTHÈQUE NATIONALE DU CANADA de microfilmer cette thèse et de prêter ou de vendre des exemplaires du film.

The author reserves other publication rights, and neither the thesis nor extensive extracts from it may be printed or otherwise reproduced without the author's written permission.

L'auteur se réserve les autres droits de publication; ni la thèse ni de longs extraits de celle-ci ne doivent être imprimés ou autrement reproduits sans l'autorisation écrite de l'auteur.

Date <i>July 12, 1984</i>	Signature <i>Edmund Sumbar</i>
------------------------------	-----------------------------------

THE UNIVERSITY OF ALBERTA

Design and Performance of a 280 kV Ion Accelerator

by

Edmund Sumbar



A THESIS

SUBMITTED TO THE FACULTY OF GRADUATE STUDIES AND RESEARCH  
IN PARTIAL FULFILMENT OF THE REQUIREMENTS FOR THE DEGREE  
OF Doctor of Philosophy

Department of Electrical Engineering

EDMONTON, ALBERTA

Fall, 1984

THE UNIVERSITY OF ALBERTA

RELEASE FORM

NAME OF AUTHOR Edmund Sumbar

TITLE OF THESIS Design and Performance of a 280 kV Ion Accelerator

DEGREE FOR WHICH THESIS WAS PRESENTED Doctor of Philosophy

YEAR THIS DEGREE GRANTED\* Fall, 1984

Permission is hereby granted to THE UNIVERSITY OF ALBERTA LIBRARY to reproduce single copies of this thesis and to lend or sell such copies for private, scholarly or scientific research purposes only.

The author reserves other publication rights, and neither the thesis nor extensive extracts from it may be printed or otherwise reproduced without the author's written permission.

(SIGNED)

*Edmund Sumbar*

PERMANENT ADDRESS:

*11320-102 Street*

*Edmonton, Alberta*

*T5G 2E4*

DATED

*July 12, 1984*

THE UNIVERSITY OF ALBERTA  
FACULTY OF GRADUATE STUDIES AND RESEARCH

The undersigned certify that they have read, and recommend to the Faculty of Graduate Studies and Research, for acceptance, a thesis entitled Design and Performance of a 280 kV Ion Accelerator submitted by Edmund Sumbar in partial fulfilment of the requirements for the degree of Doctor of Philosophy.

*Ronald P.W. Law*

Supervisor

*F.R. Vermaseren*

Supervisor

*James McMullin*  
*G. Roy*

*J.D. Stephens*

External Examiner

Date *June 25 1984*

### **Dedication**

The work of this thesis project was done in a spirit intended to honor my father, Stefan Sumbar, who died January 17, 1972. If there is any good in this thesis or in the accelerator that has been built, let it be a tribute to the lives of my father and mother.

### Abstract

An oil insulated 60 Hz half-wave voltage doubler circuit, whose output is continuously variable to a maximum of 280 kV at 5.5 mA, supplies the high potential for an open air ion accelerator. A novel constant gradient acceleration tube design was adopted to simplify construction and minimize cost of materials. The 1000 mm tube is built with the electrodes and interelectrode voltage grading resistors inside a one piece 7-in. o.d. glass pipe. Small plastic cylinders that are coated with resistance paint separate 46 intermediate tube electrodes and at the same time make up the voltage divider chain. The potential gradient along the tube, that was established by this technique, deviated less than 6% from a constant value at 50 kV, decreasing with applied voltage to less than 2% at 280 kV. An ion source, electrostatic three-cylinder lens, vertical deflection plates, and Wein-type mass filter are located inside the positive high voltage terminal. This ion gun injects a 4 kV mass filtered beam into the acceleration tube. Power to run the terminal mounted electronic equipment comes from an ac generator. An electric motor located at ground potential drives a hydraulic pump which transfers power via an insulating fluid-circuit to a hydraulic motor in the high voltage terminal. The hydraulic motor, in turn, drives the generator. The efficiency of this system, from electric motor shaft to generator load, is about 13%. Sufficient power was generated to operate the ion gun. The accelerator generated ion beams of  $N_2^+$  at potentials from 50 to 280 kV. Beam currents ranging from 0.6 to 1.5  $\mu A$  were collected 460 mm from the acceleration tube exit in a Faraday cup. As well, the beam cross section was viewed on a roughened quartz window. The intensity of the scintillations observed on the window was concentrated in a roughly circular area, 2 to 3 mm in diameter. Moreover, the images were stationary, indicating the acceleration tube was adequately designed to shield the beam from asymmetric charges on the tube walls and, conversely, to shield the tube walls from the beam.

## Preface

Much of the design work for this project was done using the English system of units. This includes units for length, pressure and stress, volume flow rate, and so on. Modern scientific writing, however, requires the use of metric—preferably SI—units. Inasmuch as there is still a transition going on in engineering practice, all quantities in this thesis will be expressed in both SI and nonstandard units, with the unconventional measure enclosed in brackets. An exception to this is where standard engineering units are appropriate, as in, for example, 3/8-in. diameter rod material and 1/4-in. drill. In addition, manufacturer's equipment specifications are given without conversion. The unit pounds-force (as in pounds-force per square inch) is indicated by the symbol lbf.



### Acknowledgments

My deepest appreciation goes to Ron Lawson and Fred Vermeulen who supervised me in this project. I owe them thanks for the opportunity to choose the particular work that I did, thereby allowing me to fulfill a boyhood dream. They provided an environment that stimulated creative thought and study. As such, graduate work has been an invaluable education.

My tenure as a graduate student was financially supported at various times by the National Research Council of Canada, the Natural Sciences and Engineering Research Council of Canada, and by the University of Alberta. To these bodies, I express my gratitude.

Perhaps my most enjoyable experiences were had cooperating with the staff of the electrical engineering machine shop. Their assistance aided the design process and contributed greatly to the success of the final product. Over 100 jobs were submitted in the course of the project, and from the simplest turning to the most complex assemblies, I could count on excellent craftsmanship. Therefore, I wish to thank Barry Arnold, Herbert Dexel, Konrad Doerrbecker, George Fij, Herb Gans, Henry Loeder, Bernie Munawich, Gerry Soligo, and the late Steve Gomez.

On the same note, I am especially indebted to Roy Schmaus who single-handedly designed and built all of the original electronic apparatus. Without his contribution, the project would surely never have been completed.

In a project such as this in which the range of design topics is broad, consultation with informed individuals was essential. Among those who contributed their opinions and advice are Jaeshin Ahn, Jim Fearn, Bob King, and Bob McCroary. In addition, I should like to thank Steve Tam who initiated computer modelling of the mass filter. And in a supporting role, I mention Allan Hiebert, Alan Mitchell, and Dennis Simeoni. Finally, I would not have had this experience if it had not been for the advice and encouragement of Ben Korbutiak.

## Table of Contents

Chapter	Page
1. General Introduction .....	1
2. Engineering of the Accelerator .....	3
2.1 Overview .....	3
2.2 Component Description .....	4
2.2.1 Beam Line .....	4
2.2.1.1 Introduction .....	4
2.2.1.2 Acceleration Tube .....	6
2.2.1.3 Ion Gun .....	16
Introduction .....	16
Ion Source .....	16
Lens .....	22
Mass Filter .....	26
2.2.1.4 Target Chamber .....	29
2.2.2 High Voltage Apparatus .....	29
2.2.2.1 Introduction .....	29
2.2.2.2 High Voltage Power Supply .....	32
2.2.2.3 Structures .....	35
2.2.3 Beam Line Support Systems .....	35
2.2.3.1 Introduction .....	35
2.2.3.2 Vacuum Equipment .....	35
2.2.3.3 Electrical Systems .....	<del>37</del>
Electronic Power Supply and Control Scheme .....	37
Power Source Inside the Terminal .....	42
2.2.3.4 Coolant Flow System .....	47
2.2.4 Radiation Shielding .....	47

2.3	Component Testing and Evaluation .....	51
2.3.1	Introduction .....	51
2.3.2	Acceleration Tube .....	54
2.3.3	Ion Gun .....	58
2.3.3.1	Ion Source .....	58
2.3.3.2	Ion Source with Lens .....	60
2.3.3.3	Ion Source with Lens and Filter .....	65
2.3.4	Terminal Mounted Power Supply .....	71
3.	Accelerator Performance and Analysis .....	75
3.1	Introduction .....	75
3.2	Performance Data .....	75
3.3	Analysis of Performance Data .....	80
3.4	Radiation Pattern .....	84
3.5	Recommendations .....	86
4.	Conclusions .....	89
	References Cited .....	91
	Appendix: Operating Instructions .....	94
	Vita .....	101

## List of Figures

Figure	Page
2.1 Block Diagram I .....	5
2.2 Acceleration Tube Design Schematic .....	9
2.3 Acceleration Tube Assembly Detail .....	10
2.4 Spacer-Resistor Construction Detail .....	11
2.5 Cardinal Points of the Tube .....	17
2.6 Block Diagram II .....	18
2.7 Ion Source Detail .....	20
2.8 Ion Source Schematic .....	21
2.9 Lens Detail .....	23
2.10 Lens Potential Contours .....	24
2.11 Lens Focal Properties .....	25
2.12 Mass Filter Detail .....	27
2.13 Mass Filter Schematic .....	28
2.14 Mass Selection Aperture .....	30
2.15 Target Detail .....	31
2.16 Block Diagram III .....	33
2.17 High Voltage Generator .....	34
2.18 Terminal Supports .....	36
2.19 Block Diagram IV .....	38
2.20 Vacuum System Schematic (AVS 7.1-1966) .....	39
2.21 Block Diagram V .....	40
2.22 Control System .....	41
2.23 Block Diagram VI .....	44
2.24 Hydraulic System Schematic (ANSI Y32.10-1967) .....	45
2.25 Generator Unit .....	46

Figure	Page
2.26 Hose Layout in the Lab .....	48
2.27 Block Diagram VII .....	49
2.28 Coolant System Schematic (ANSI Y32.10-1967) .....	50
2.29 Block Diagram VIII .....	52
2.30 Accelerator Room Plan View .....	53
2.31 Spacer-Resistor Performance Data .....	55
2.32 Acceleration Tube Column Current .....	57
<hr/>	
2.33 Ion Source Performance .....	59
2.34 Collector Geometry .....	61
2.35 Lens Imaging Characteristics .....	63
2.36 Magnet Characteristics .....	66
2.37 Ion Beam Envelope .....	70
2.38 Hydraulic System Load-Test Data .....	72
2.39 Hydraulic Hose Insulation-Test Results .....	74
3.1 Plan View of the Accelerator Beam Line .....	76
3.2 Control Panels Inside the High Voltage Terminal .....	77
3.3 Legend for Fig. 3.2 .....	78
3.4 Remote Control Unit .....	79
3.5 Accelerator Beam Current .....	81
3.6 Beam Spots .....	82
3.7 Radiation Intensity Pattern .....	85

## 1. General Introduction

A need was perceived in the Department of Electrical Engineering at the University of Alberta for an ion accelerator that could be used for the Rutherford backscattering (RBS) analysis of thin films (Chu, Mayer, and Nicolet 1978) and the ion implantation of semiconductors (Wilson and Brewer 1973, Chap. 4; Carter and Grant 1976). In response, I undertook the design of an accelerator system that could partially satisfy this need; specifically, a 280 kV open air Cockcroft-Walton-type positive-ion accelerator has been constructed that generates a mass filtered beam which is collected at a simple target. A description of the design, construction, and testing of this accelerator is the subject of my thesis.

Planning for the accelerator started with preliminary design studies. The first proposal was to modify an existing 280 kV Cockcroft-Walton machine that had been used for colloidal beam experiments (Hepburn 1973). The conversion would have required installing an ion source and mass filter and enlarging the high voltage terminal. But this was not done. Because of poor high voltage insulation, that accelerator could not operate above 90 kV, which was only one third the maximum output of the high voltage generator. Consequently, a decision was made to dismantle that system and to use some of its components—the high voltage terminal, terminal support structure, radiation shielding, and the Cockcroft-Walton voltage generator—in a new accelerator system which is the subject of this discourse. Of course, this new structure must, in some way, be unique. To appreciate how this Cockcroft-Walton machine may differ from all of the others, consider the following historical sketch of particle accelerator development.

Particle accelerator development was initiated in the late 1920s, motivated by the needs of nuclear physicists. In fact, accelerator history is generally acknowledged to have begun in 1932 with the first successful device to artificially induce a nuclear transmutation—the 700 kV accelerator of Cockcroft and Walton (1932a, 1932b). As such, progress in the early years of accelerator development was characterized by the attainment of higher particle energies. Several accelerator types were introduced in that period (Livingston and Blewett 1962): besides the

Cockcroft-Walton machine, there was the electrostatic generator, the cyclotron, the linear accelerator, and the betatron. Later, after World War II, the accelerator—in the form of the synchrotron (Livingston and Blewett 1962)—became a tool of the elementary particle physicist, who demanded still higher energies and who continues to do so in the present.

Meanwhile, the basic air insulated Cockcroft-Walton machine had reached a practical limit of 2 MV for acceleration voltage in the 1960s (Bromely 1974). But this does not mean that the development of such machines has been abandoned. Accelerators have been used in a wide range of research and practical applications, especially since the 1960s (see for example, Jiggins and Demetsopoulos 1970; Ziegler 1975). Most of these applications do not require extreme particle energies—like RBS and ion implantation. Therefore, advancements in accelerator technology have been characterized by innovations in design.

In this dissertation, I will introduce two such innovations that have been implemented in the present Cockcroft-Walton accelerator. Those innovations are (1) an alternative acceleration tube construction and (2) a new system for the generation of electrical power inside the high voltage terminal. That these are unique and—more important—that a working ion accelerator system has been produced are the theses of this work.

And so, in Chap. 2 of the following discourse, the design of each accelerator system component is presented. The order of presentation reflects the logic of system development adopted for the present accelerator. The design innovations are introduced at appropriate stages in the presentation, and they are given emphasis through an extended treatment in which I will show, by a comparison with established practices, that they have indeed contributed to low energy accelerator technology. The results of accelerator component tests are also given. Then, in Chap. 3, I will show that a working accelerator system has been produced by recapitulating the results of beam trials. These trials consisted of observing the current and cross section of a beam of  $N_2^+$  ions at a fixed target position for a range of acceleration voltages. I will conclude, with Chap. 4, by summarizing the significance of the present work.

## 2. Engineering of the Accelerator

### 2.1 Overview

The aim in this chapter is to recall the engineering processes that guided the construction of each accelerator system component. Design work began with the following objective: to produce a 280 kV Cockcroft-Walton-type accelerator that could generate a mass filtered positive-ion beam which would be subsequently collected at a fixed target position. The first step was to recognize what system components were required in such an apparatus.

There had to be an evacuated pathway for the ion beam, that is, a beam line, from the ion source, where the ions are generated, to the target, where they are collected. Between source and target, the beam would have to be filtered, accelerated, and otherwise manipulated, which meant that a decision had to be made regarding the composition and configuration of the beam line. Furthermore, the beam line required ancillary equipment: vacuum, electrical, and ion source cooling systems. Another aspect of accelerator design was the high voltage apparatus, including the voltage generator and the high voltage terminal. And finally, as in all accelerators, there was the question of radiation shielding.

Once having identified the major areas of accelerator design—beam line, beam line support equipment, high voltage, and radiation shielding—each area could be considered in detail. Accordingly, in Sec. 2.2, design topics are addressed in decreasing order of importance, which is not the order in which construction proceeded. The numerous design studies that were carried out yielded the two innovations that are the focus of this thesis. There is one innovation in the beam line and one in the beam line support equipment. The framework of the accelerator design is illustrated in a sequence of eight block diagrams. In Sec. 2.3, test results are presented showing how each component behaved. This test data, along with the theory given in parts of Sec. 2.2, will be an aid in the analysis of accelerator system performance which is the subject of Chap. 3.



## 2.2 Component Description

### 2.2.1 Beam Line

#### 2.2.1.1 Introduction

Essentially, the beam line of any high voltage accelerator, including this Cockcroft-Walton machine, comprises an acceleration tube with an ion source at one end and a target apparatus at the other. In the proposed system, mass filtering was a further basic requirement. Normally, this would have raised a question regarding the location of the mass filter (Wilson and Brewer 1973, pp. 400-402). It could be located at the ion source end or the target end of the tube. In other words, either a beam of low or high energy ions could be filtered. This issue, however, was not specifically addressed because it was decided that a commercially available ion gun which includes a mass separator should be used in the beam line. In particular, the Colutron ion gun was chosen because its operating characteristics had already become familiar, through its application in other research, to workers in the University of Alberta's Department of Electrical Engineering—individuals who would likely be using the accelerator in the future. On this basis, it was an advantage to design the beam line with this piece of equipment. The consequences of this beam line configuration are outlined in Sec. 2.2.2.1, which is an introduction to the high voltage apparatus. To summarize, a block diagram of the resultant beam line is given in Fig. 2.1.

The following sections describe the design and construction of individual beam line elements, beginning with the acceleration tube. This is a pivotal structure, dictating the requirements of the beam line components that precede it and follow it, and for this reason, it is dealt with first. The innovation in the beam line, that was referred to in the Overview, concerns acceleration tube design. The ion gun is considered next, although it is equally as important as the acceleration tube. Discussion of the beam line is closed with a look at the target arrangement.



Figure 2.1 Block Diagram I

### 2.2.1.2 Acceleration Tube

**Background.** During the evolution of acceleration tubes, two major influences on voltage holding capacity were recognized. It was learned that higher voltages could be held by evenly distributing the acceleration voltage along the tube and by preventing the accumulation of charge on the tube insulators.

The acceleration tube in Cockcroft and Walton's 1930 accelerator was a long glass pipe with tubular metal electrodes at either end (Cockcroft and Walton 1930). That is, the acceleration voltage was applied across a single electrode gap, and the positive ions travelled down the bore. This structure operated at about 300 kV. In 1932, Cockcroft and Walton constructed their 700 kV voltage multiplier machine in which the acceleration tube, or discharge tube as they referred to it, was composed of three tubular electrodes (Cockcroft and Walton 1932a). The center electrode was connected to a point on the rectifier tower giving it a potential half that of the acceleration voltage. Hence, ions were accelerated across two gaps. Before this, Tuve, Breit, and Hafstad (1930) developed an acceleration tube which was an adaptation of the principle proposed by Coolidge (1926) for a cascade-type x-ray tube. Accordingly, the acceleration voltage was divided among several long cylindrical electrodes that were mounted in line and with a regular spacing down the entire length of a glass pipe. Particles were therefore accelerated in steps between several electrode gaps. This type of tube was subsequently used in the first practical electrostatic accelerators, built by Tuve, Hafstad, and Dahl (1935). The voltage on each electrode was established by electric induction. The result was a nearly constant potential distribution which eliminated the concentration of high local electric fields. This, together with the fact that the cylindrical electrodes shielded the glass pipe from any stray ion flux, allowed high voltages to be held. Tuve, Hafstad, and Dahl had no difficulty at 1.2 MV, and they suggested that their tube could operate at higher potentials. To accommodate still higher voltages, however, the concept of a multiple electrode tube was refined by increasing the number of electrode gaps. By the late 1930s, the acceleration tube assumed

its present form—the constant gradient tube (Van de Graaff, Trump, and Beuchner 1946; Livingston and Blewett 1962, p. 56; Galejs and Rose 1967, p. 297). This type of tube is suited to applications where the acceleration voltage exceeds 100 kV (Wilson and Brewer 1973, p. 402 and p. 420).

In its basic form, a modern constant gradient acceleration tube is a vacuum-tight assembly of many thin flat-disc or reentrant style electrodes made of mild steel, stainless steel, aluminum, or titanium that are bonded to short glass or ceramic ring-shaped spacers. The induction method of establishing electrode voltage has been replaced by the voltage divider which is made up of a bank of resistors or point-to-plane corona discharge gaps that are connected to the electrodes from outside the vacuum of the tube (Beuchner et al. 1947; Herb 1959, pp. 73-74; Michael et al. 1959). In the case of Cockcroft-Walton machines, voltage grading of the tube is often achieved by linking points of intermediate potential in the voltage multiplier stack through very high resistance to appropriate tube electrodes (Arnold 1950; Reinhold, Minkner, and Adler 1965). An independent potential divider chain can also perform the task (Kovarik, Lankshear, and Sluyters 1971).

**Present design.** The acceleration voltage for this machine is generated by an oil insulated voltage doubler circuit (see Sec. 2.2.2.2). The one intermediate voltage in the circuit is inaccessible, and as a consequence, the present constant gradient acceleration tube was designed with an independent voltage grading device, in particular, a chain of resistors. Unlike the conventional practice, however, the plan was to install the resistors inside the vacuum of the tube.

This innovation led to a simplification of tube construction. Since no external connections to the tube electrodes were required for voltage grading, a single piece of insulating pipe was used as the vacuum envelope, thereby avoiding the usual layered style of tube construction. Further simplification was realized by making the intermediate tube electrodes in the shape of thin flat discs. This had the added advantage of maximizing space between adjacent electrodes, which is important since the resistors are mounted

inside the tube. Even so, there was insufficient space to install conventional metal oxide or composition resistors. The problem was overcome, however, by painting resistor elements on to the insulators that separate adjacent electrodes.

The present tube design simplified fabrication and reduced cost of materials. The basic features of the tube design are summarized in a simplified schematic diagram that appears in Fig. 2.2.

**Details of tube construction.** The acceleration tube comprises two units: the vacuum envelope and the electrode structure. Figure 2.3 shows the details. The vacuum envelope was made of a 7-in. o.d. pyrex glass tube that was cemented to aluminum end flanges with continuous beads of Araldite epoxy (composition unknown), forming a vacuum-tight unit. The electrode structure is a stack of aluminum discs. There are two end electrodes and 46 intermediate electrodes. Each electrode is 165.0 mm (6.50 in.) in diameter and has a 38.1 mm (1.50 in.) diameter beam aperture in its center. The intermediate electrodes, as shown in Fig. 2.3, were made from 1/8-in. thick sheet stock. Four Dupont Delrin (acetal plastic) cylinders separate each group of two adjacent electrodes in the stack. With a coating of resistance paint, the electrode spacers became resistor elements in the voltage divider chain. A total of 188 spacer-resistors were required: four in each of 47 intermediate sections. The following paragraphs outline how these spacer-resistors were made.

Figure 2.4 shows a typical spacer-resistor as it is assembled into the tube. The Delrin cylinders were cut to a length of 16.76 mm (0.661 in.) from 3/8-in. diameter rod material. Semicircular grooves of 0.64 mm (0.025 in.) radius were then machined 0.64 mm (0.025 in.) deep into the ends, as shown in Fig. 2.4. These grooves provide a grip for the epoxy since it does not adhere to the acetal plastic. Next, 376 washers, 7/32-in. i.d. and 9/16-in. o.d., were stamped out of 22-gauge (0.0253 in. thick) aluminum sheet. All the Delrin cylinders and aluminum washers were cleaned in acetone prior to being cemented with Araldite epoxy (composition unknown). Burrs on the edges of the washers that were

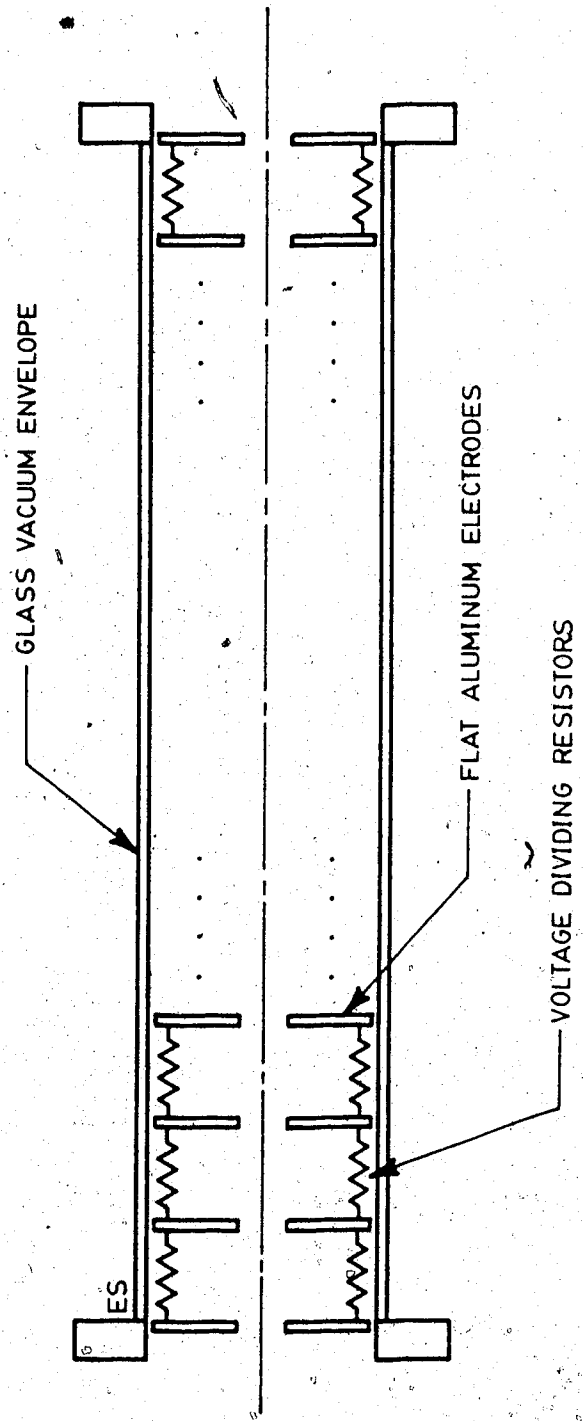


Figure 2:2 Acceleration Tube Design Schematic

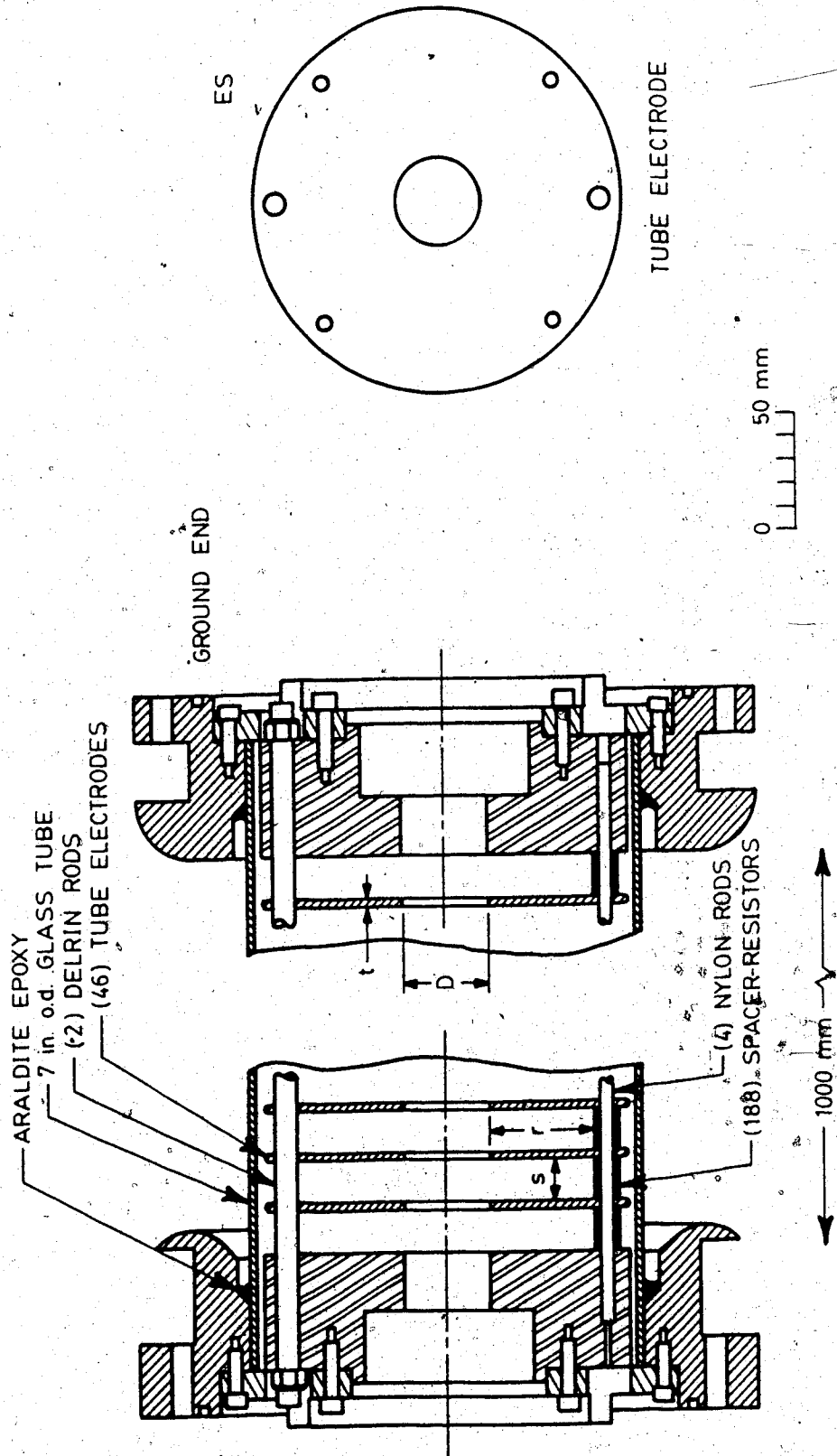


Figure 2.3 Acceleration Tube Assembly Detail

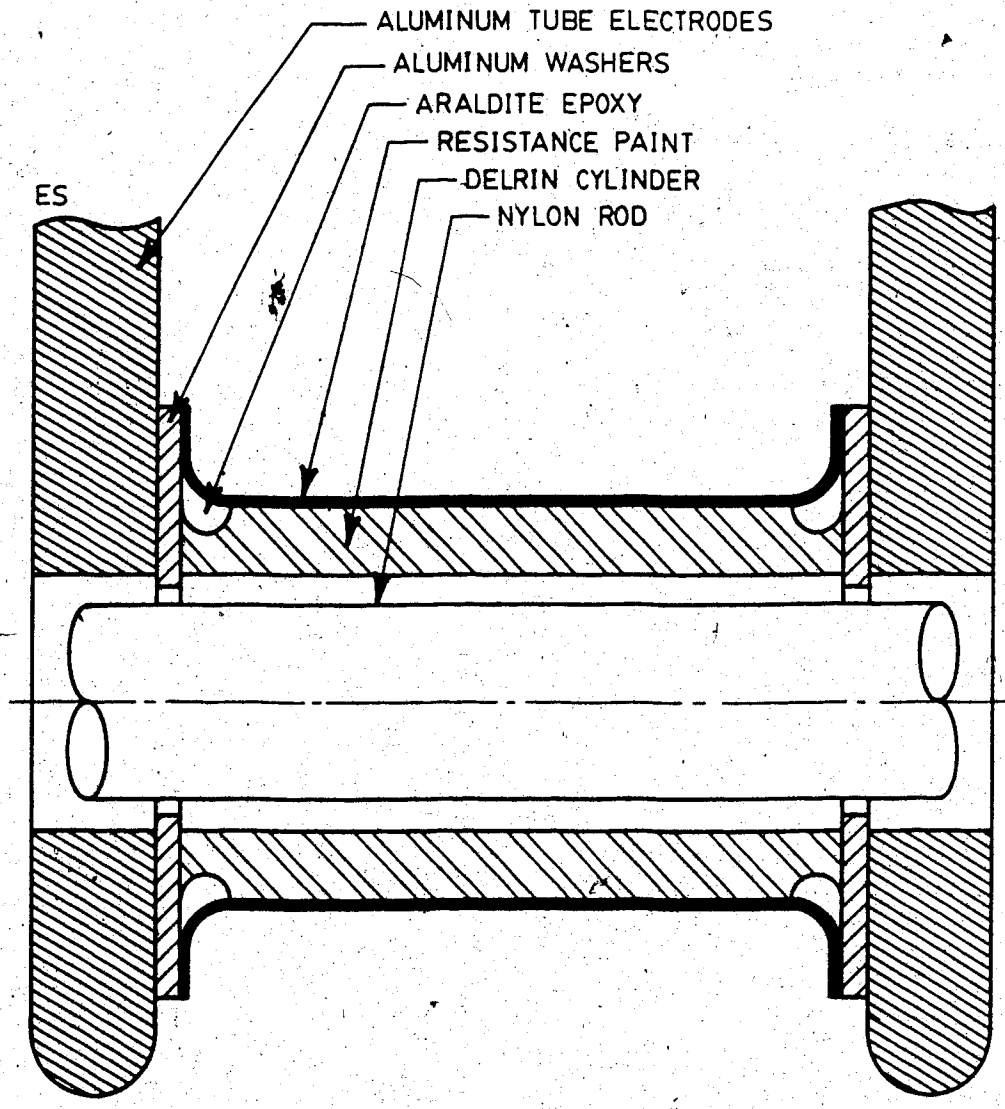


Figure 2.4 Spacer-Resistor Construction Detail



produced during the stamping process were oriented away from the Delrin cylinders so that they face the tube electrodes upon assembly into the electrode structure. In this way, they help to make contact with tube electrodes if a cylinder is, by chance, too short.

The epoxy was allowed to cure for one day at room temperature, about 23°C (73°F), after which two coats of resistance paint† were applied. Two coats were applied to more effectively cover irregularities and scratches that are present in the rod stock from which the plastic cylinders were cut and also to try to achieve uniformity in paint thickness among all the spacers. Two hours of drying time were allowed between coats. The painting was done with a No. 6 (medium size) artist's brush while the spacers, mounted one at a time on a mandrel, rotated at 85 rev/min in a lathe. The outer surface of each plastic cylinder was covered as well as that part of the aluminum washer that is not held against a tube electrode.

As a last step and following the paint manufacturer's recommendations, the painted spacers were baked, in a conventional oven, to stabilize their resistance. An oven temperature of 80°C (176°F) was maintained for approximately two hours on each of two consecutive days.

To assemble the tube, the electrodes and spacer-resistors were slid on to four 3/16-in. diameter nylon rods and two 3/8-in. diameter Delrin rods as shown in Fig. 2.3. The glass tube, plastic rods, and aluminum electrodes were washed with soap and water prior to assembly. All six rods extended the length of the electrode structure. The nylon rods fix the spacer-resistors in an equal spacing around the edge of each electrode. The Delrin rods are threaded at the ends and are fitted with steel nuts to compress the stacked assembly and hold it together. This unit was then lowered into the glass envelope and bolted to the two end flanges to form the acceleration tube.

---

†Ultra-high resistance paint, #R10KM5, available from Micro-circuits Company of New Buffalo, Michigan 49117, U.S.A. The paint provides  $10^4$  M $\Omega$  per unit area of coverage.

**Design considerations.** The mechanical layout of the tube that has just been described was influenced by several design considerations. These will now be reviewed.

**Electrode thickness.** In an ideal constant gradient acceleration tube, tube voltage varies linearly with distance along the axis of the tube. In a practical tube, however, the nonzero thickness of the tube electrodes in relation to the beam aperture causes a modulation of this pattern. Referring to Fig. 2.3, the maximum voltage deviation can be made small, less than 1%, by ensuring that  $D/t > 8$  (Galejs and Rose 1967, p. 303, Fig. 3). In the present design  $D/t = 12$ , and the deviation is predicted to be about 0.5%.

**Shielding.** The presence of stray charge on the interelectrode insulators is a limiting factor in the voltage holding capacity of any acceleration tube. There are several sources of stray charge in an acceleration tube: (1) leakage current along the insulator surfaces; (2) secondary electrons that are liberated by stray ions and electrons as they strike tube electrodes; and (3) electrons generated on the insulators by the photoelectric effect as x rays are produced when backstreaming electrons impact on tube electrodes (bremsstrahlung) and, with high beam currents, as ultraviolet radiation is emitted by the beam plasma (Hepburn, Shubaly, and Ungrin 1980). These mechanisms are a function of increasing beam current.

In the present design, where there is no direct voltage grading of the glass vacuum envelope, any stray charge that is generated is likely to accumulate on the glass and eventually precipitate electrical breakdown. Hence, the tube design that is described here is suitable for use with low beam currents (much less than 1 mA), where the production of stray charge by the aforementioned mechanisms is low. As it is, proper electrode dimensions and interelectrode spacing can be selected in an attempt to shield the insulating surfaces in the tube from the beam, and conversely, to shield the beam from any asymmetric electric charge accumulation that may be present on the interior surfaces of the tube (Herb 1959, pp. 84-85). Herb has determined that an  $r/s$  value (refer to Fig. 2.3) of 2.5 to 3.0 should provide adequate shielding. In the present tube,  $r/s = 2.58$ .

*High voltage design.* The possible electric breakdown of the evacuated tube must be considered. Herb (1959, p. 85 and p. 87) indicates that an interelectrode spacing of 13 to 25 mm (0.5 to 1.0 in.) is optimum in acceleration tube design. For the present design, the electrodes are 18.06 mm apart, and if a uniform potential distribution is assumed, the maximum interelectrode voltage will be 5.96 kV for an applied acceleration potential of 280 kV. The maximum field strength is therefore 3.3 kV/cm. Van de Graaff et al. (1946) suggest that only for tube gradients greater than 13.1 kV/cm (400 kV/ft) is the breakdown in vacuum a limiting factor in the voltage holding limit of an acceleration tube. Now, Hawley (1968, p. 89) gives the breakdown voltage gradient between two flat aluminum electrodes separated 22 mm by a pyrex insulator under vacuum conditions as 17.7 kV/cm. This indicates a safety factor of five or more for the present acceleration tube. The breakdown gradient of a long tube composed of several electrode sections, however, is much lower than the breakdown gradient for one section—the long tube effect (Herb 1959, p. 87; Van de Graaff, Rose, and Wittkower 1962). The Kilpatrick breakdown criterion (Hawley 1968, p. 87) which is an empirical guideline for the minimum sparking voltage in a vacuum indicates the present acceleration tube design is in the no-breakdown operating region.

*Spacer-resistor installation.* The resistance paint on each spacer-resistor must make electrical contact with adjacent tube electrodes. The aluminum washers that are used in the construction of each spacer-resistor provide this while eliminating direct contact between a painted surface and a tube electrode. Direct contact would otherwise cause cracking of the paint layer that would result from mechanical stresses exerted on each spacer-resistor upon assembly into the tube.

When tested under high voltage conditions (Sec. 2.3.2), the spacer-resistors displayed a lower value of resistance than was expected on the basis of resistance paint manufacturer's specifications. In fact, because of nonuniformity in paint thickness among resistors, it is different from one resistor to the next. Furthermore, the resistance is a

function of applied voltage. Consequently, before they were installed into the acceleration tube, individual spacer-resistors were matched to one another so that each parallel group of four displayed approximately the same voltage-versus-current characteristic.

The resistance paint manufacturer supplied a caution that the heat dissipated by the resistor surface should not exceed  $0.16 \text{ W/cm}^2$  ( $1 \text{ W/in}^2$ ). There was no difficulty satisfying this criterion as will be shown in Sec. 2.3.2.

*Mechanical strength of the tube.* The acceleration tube is mounted horizontally (see Sec. 2.2.3) and fixed at both ends. Hence, the mechanical strength of the tube had to be evaluated. For this purpose, a uniform load is assumed, consisting of a  $146 \text{ N/m}$  ( $12 \text{ lbf/ft}$ ) contribution due to the glass tube and  $292 \text{ N/m}$  ( $20 \text{ lbf/ft}$ ) due to the aluminum electrodes. Using the nominal tube dimensions  $178 \text{ mm o.d.}$ ,  $170 \text{ mm i.d.}$ , by  $1000 \text{ mm}$  long ( $7.0 \text{ in. o.d.}$ ,  $6.7 \text{ in. i.d.}$ , by  $39.4 \text{ in.}$  long), the maximum normal stress, which occurs at the ends of the tube where the glass is anchored to the flanges, is calculated to be  $369 \text{ kPa}$  ( $53.6 \text{ lbf/in}^2$ ) (Mott 1978, Chap. 9). For glass, the design stress, which includes a safety factor of 10, is  $4.48 \text{ MPa}$  ( $650 \text{ lbf/in}^2$ ) (Miner and Seastone 1955, p. 4-152). Consequently, the glass is strong enough to withstand the mechanical load.

*Vacuum conductance.* This is important because with a plasma type ion source, such as the one being used here (Sec. 2.2.1.3 Ion Source), there is a high gas load that must be effectively pumped; otherwise, the pressure in the beam line would be high. In this design, the pumping on the ion source is done solely from the target end of the tube (see Sec. 2.2.3.2), and the only gas flow path is through the acceleration tube. With respect to its pumping conductance, the acceleration tube is a series of 47 identical short tubes interspersed with 46 identical apertures. Applying standard formulae to evaluate the conductance (Lewin 1965, pp. 12-16), the following result is obtained for nitrogen (mass 28) at room temperature,  $20^\circ\text{C}$  ( $68^\circ\text{F}$ ):  $10.1 \text{ m}^3/\text{h}$  ( $2.8 \text{ liter/s}$ ). This is a low value, but acceptably low gas pressures were obtained (see Sec. 2.3.2 and the Appendix).

*Ion optics.* The quantities of interest are the Gaussian, or first order, principal plane locations and the focal lengths (Galejs and Rose 1967, p. 312). These were theoretically evaluated using Timm's method (Galejs and Rose 1967, p. 317) with an assumed axial potential distribution given by Wilson and Brewer (1973, p. 230). Figure 2.5 charts the result for a range of acceleration potentials, assuming a 4 kV injected beam of singly charged ions.

### 2.2.1.3 Ion Gun

#### Introduction

This device was designed after the Colutron Corporation ion gun model G-1. The model G-1 is an integrated group of four beam line elements: an ion source at the head, followed by an electrostatic three cylinder lens, a set of vertical deflection plates, with a Wein-type mass filter at the tail. A drift tube and beam defining aperture are installed downstream of the mass filter and are considered part of the ion gun for this accelerator. The block diagram for this system is given in Fig. 2.6 (compare Fig. 2.1).

Ions are extracted from the plasma that is in the discharge region with a negatively biased electrode. The energetic ions are then collected by the lens to form a beam which is directed through the mass filter. The Wein-type filter allows those ions of a particular mass-to-charge ratio to pass through undeflected, dispersing all others. The desired ion species is finally transmitted through the mass selection aperture and into the acceleration tube.

#### Ion Source

The ion source used in this ion gun is a modified version of the Colutron Corporation model 100-0 ion source and model 103-B heat sink. A prototype for the Colutron device is described by Menzinger and Wählin (1969). Design changes to the boron nitride ion source body were made by Jun Amano in the Department of Electrical Engineering at the University of Alberta in 1976. A detailed diagram of the

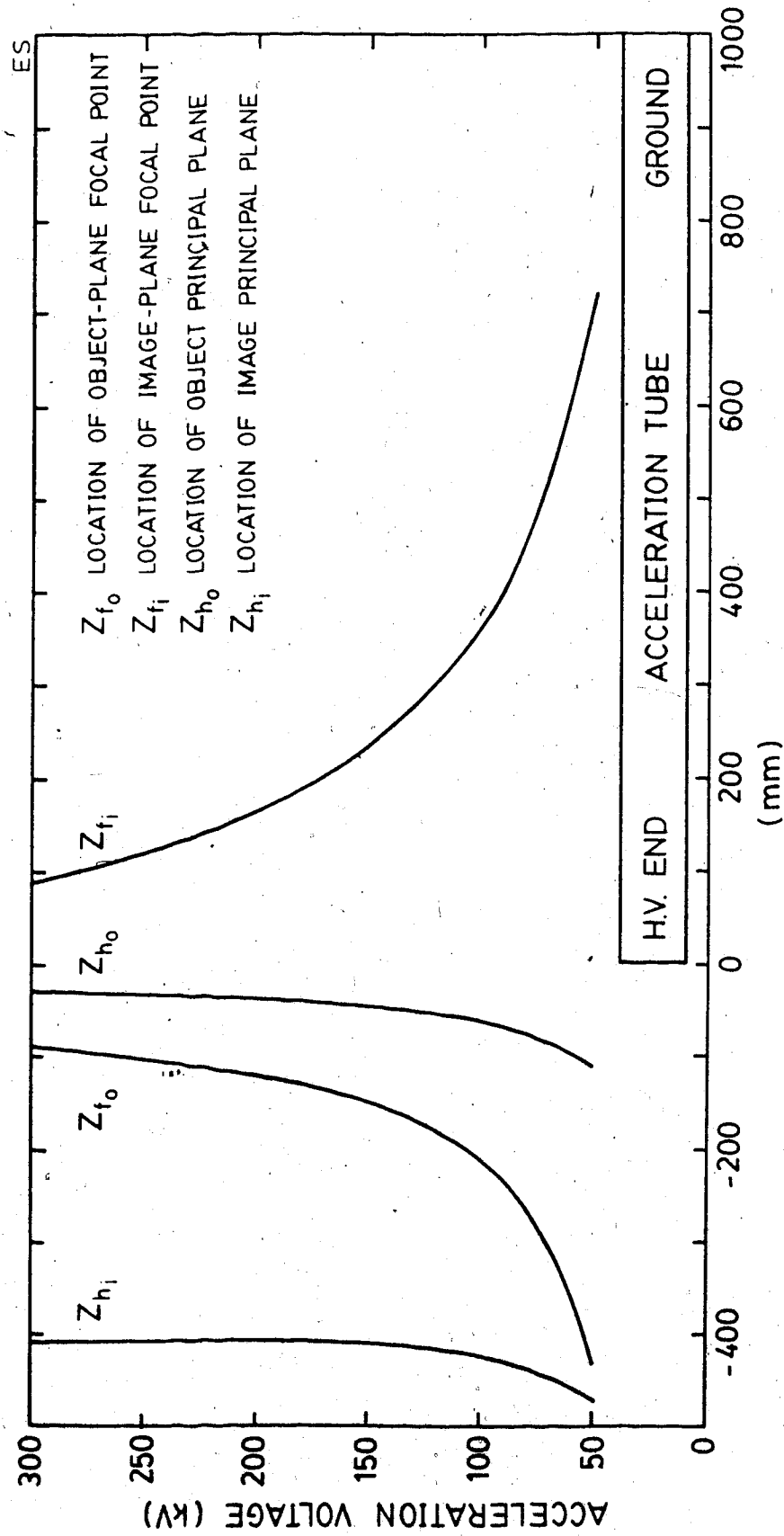


Figure 2.5 Cardinal Points of the Tube

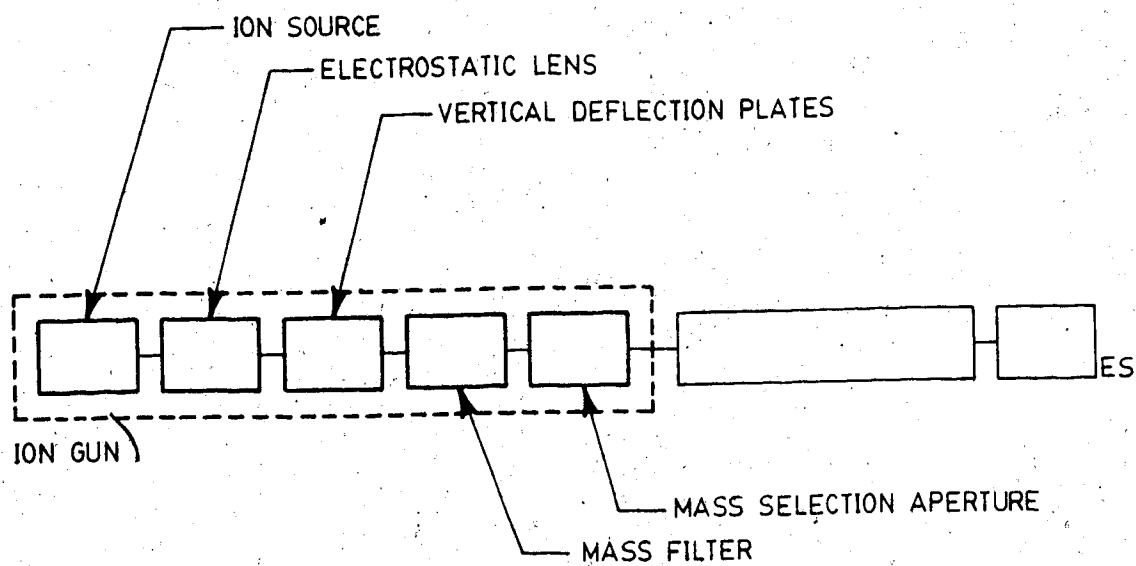


Figure 2.6 Block Diagram II

present ion source and heat sink is given in Fig. 2.7. A simplified schematic diagram of the ion source and its recommended power supply connections is given in Fig 2.8. The extraction electrode is at chassis ground, and the ion source along with the heat sink are maintained at positive extraction potential.

This is a hot cathode arc discharge ion source that uses no magnetic field (Sidenius 1977). It generates a plasma with a gas pressure on the order of 7 Pa (0.05 Torr). The gas is supplied directly from a reservoir or from the adjoining furnace in which solid materials can be vapourized. The principle of operation of such an ion source is outlined by Reich (1944, Chap. 11), von Engel (1965, pp. 282-286), and Wilson and Brewer (1973, pp. 19-21, pp. 48-53, pp. 84-89).

Colutron Corporation specifies that a filament current of 17.5 A and an anode-to-cathode voltage of 100 V are required to initiate an arc discharge. The quoted procedure is then to slowly increase gas pressure from a background level of about 0.7 Pa (0.005 Torr) to between 3 and 10 Pa (0.025 and 0.1 Torr) until an anode-to-cathode current of 0.5 A is established. (The apparatus for admitting gas into the ion source is described in Sec. 2.2.3.2). The anode-to-cathode voltage is then lowered until a maximum ion current is extracted from the source. To simplify accelerator operation, however, filament current and gas pressure are established before switching the anode supply on (see the Appendix). Furthermore, the present system employs a current regulated anode-to-cathode power supply which adjusts its voltage to maintain a preset discharge current. (In the remainder of this thesis, it will be referred to as the anode power supply.) An extraction field strength in the range 1 to 5 kV/cm is recommended. The emittance characteristics of the source are not given by Colutron Corporation. In the present system, the anode-to-extraction electrode distance is approximately 20 mm, and an extraction voltage of 4 kV is used. The coolant flow system is described in Sec. 2.2.3.4.



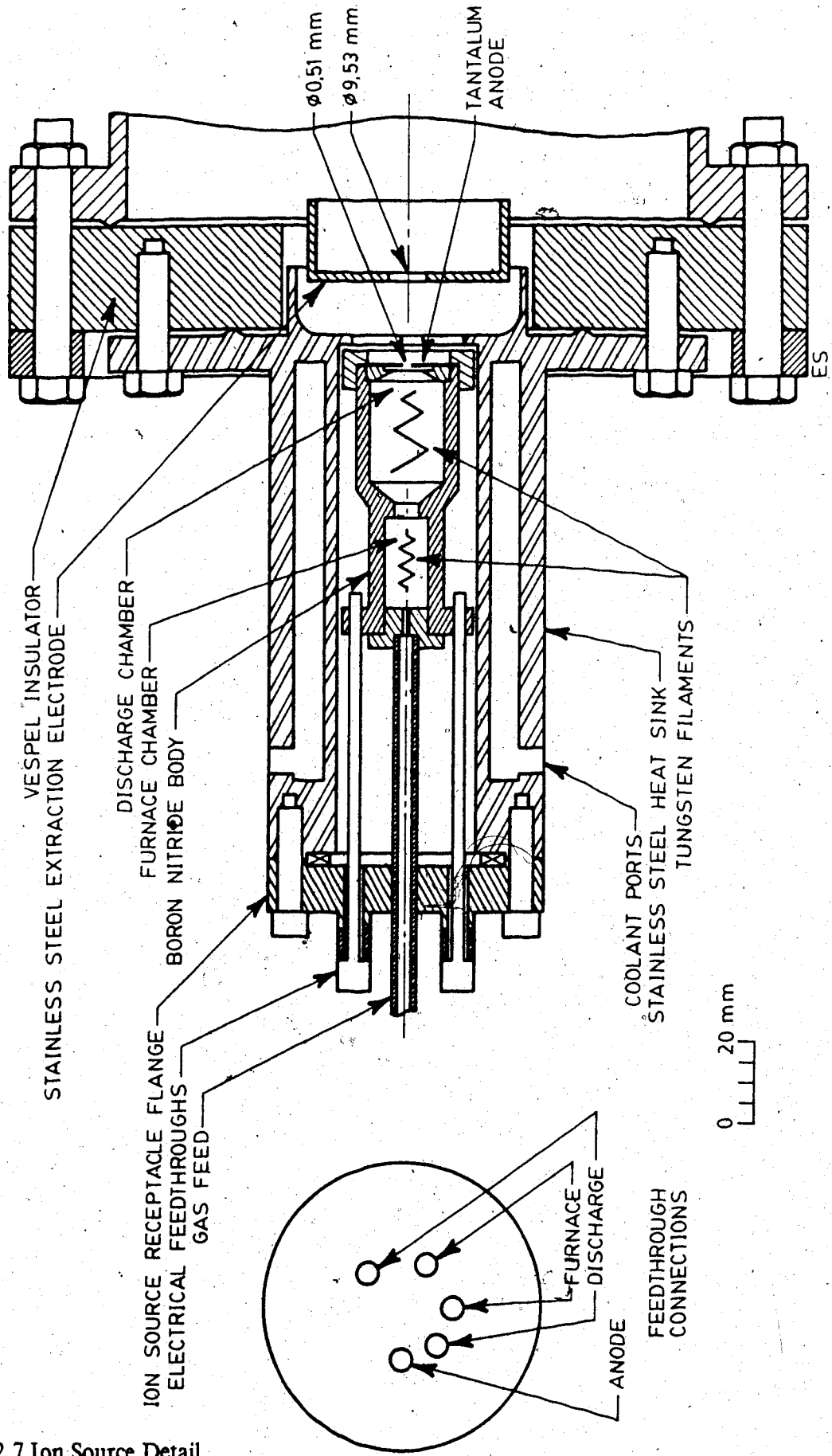


Figure 2.7 Ion Source Detail

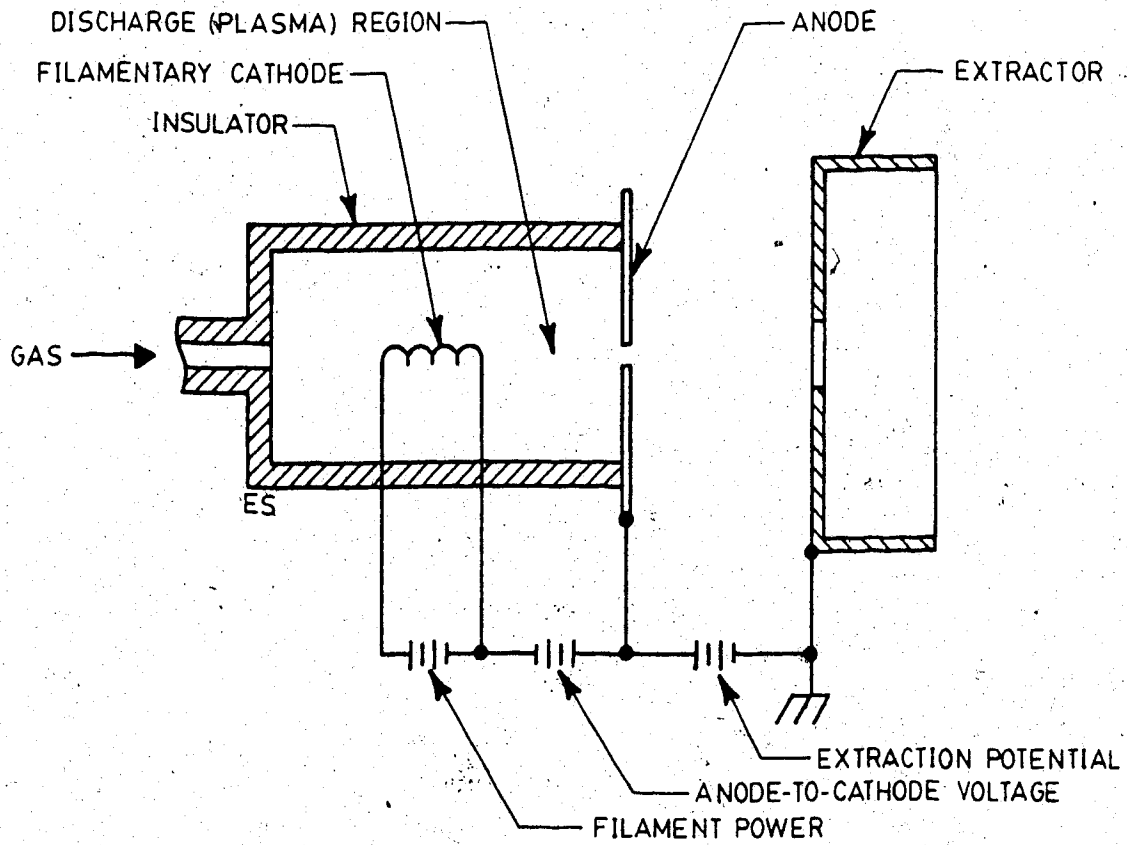


Figure 2.8 Ion Source Schematic

## Lens.

An adaptation of the Colutron Corporation lens system model 200 was used in this ion gun. It is a three cylinder electrostatic lens referred to as an einzel lens or saddle-field lens (El-Kareh and El-Kareh 1970, pp. 60-62; Klemperer and Barnett 1971, pp. 82-92). The first outer electrode is combined with the extraction electrode of the ion source (see Figs. 2.7 and 2.8). Both outer electrodes are maintained at the same potential, in this case, chassis ground. A diagram of the present lens appears in Fig. 2.9 along with the recommended power supply connections. The lens is operated in an initially decelerating mode (Klemperer and Barnett 1971, pp. 184-185 and p. 293), which means that, for ions, the center electrode voltage is positive with respect to the outer electrodes.

A theoretical determination of the potential contours around the lens and ion source was done using finite difference numerical methods (Weber 1967, p. 49; Ames 1977, p. 106, p. 124). The influence of space charge fields on the potential distribution was neglected. The result for an extraction voltage of 4 kV and a lens voltage of 3200 V is given in Fig. 2.10. Theoretical lens focal properties were also determined. The lens was modelled as having outer electrodes of infinite extent. A theoretical expression for the axial potential of such a model was used (Parks 1971) in conjunction with Timm's method (Galejs and Rose 1967, p. 317). The paraxial focal properties of the lens were inferred from the analysis for the case of a beam of singly charged ions extracted at a potential of 4 kV. The results are presented in Fig. 2.11. The accuracy of this method of analysis was verified by reproducing the experimental data of Liebmann (1949). Since the lens model is symmetric, the principal planes are equidistant from the midpoint of the lens. As well, the focal length in image and object space are the same.

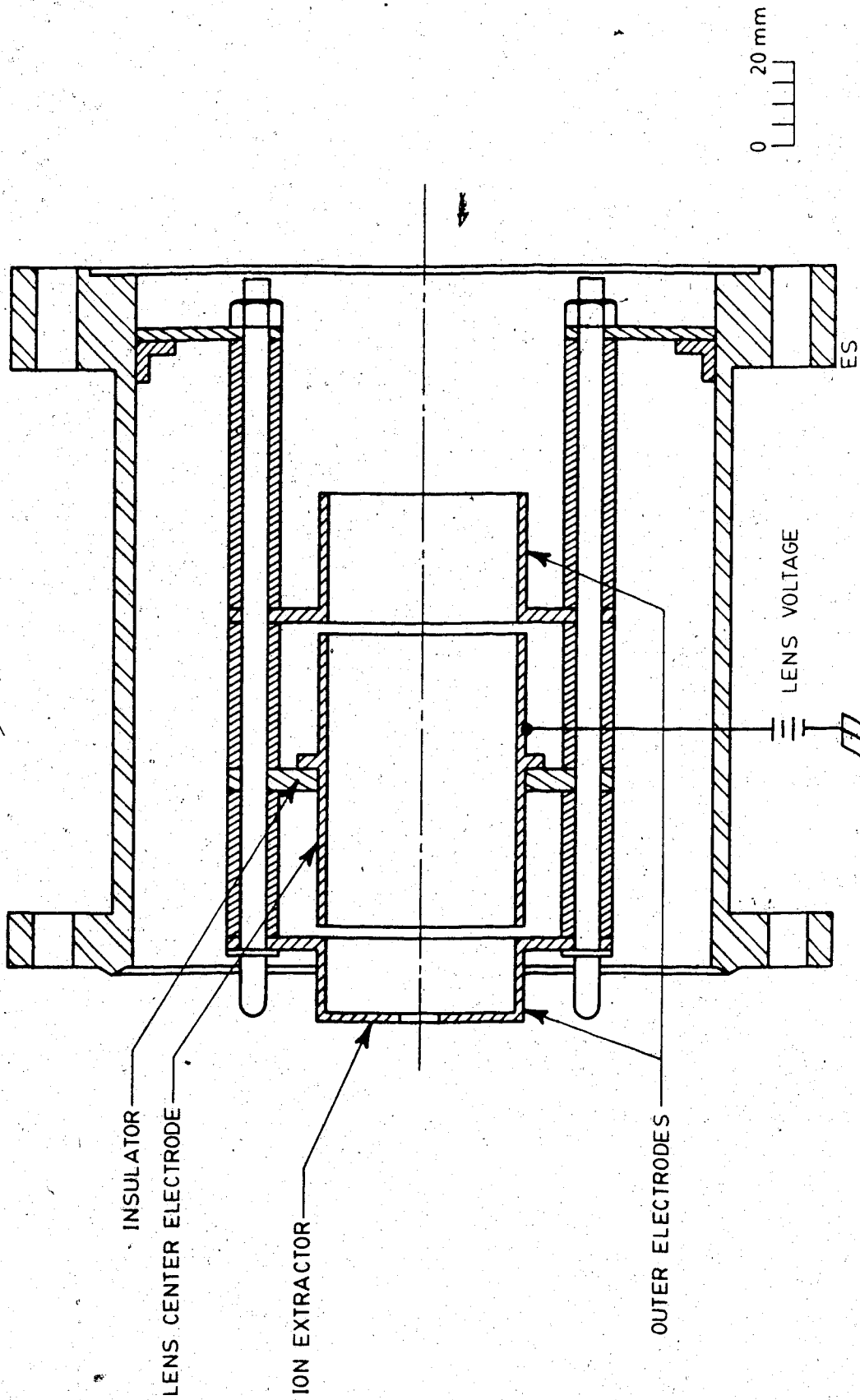


Figure 2.9 Lens Detail

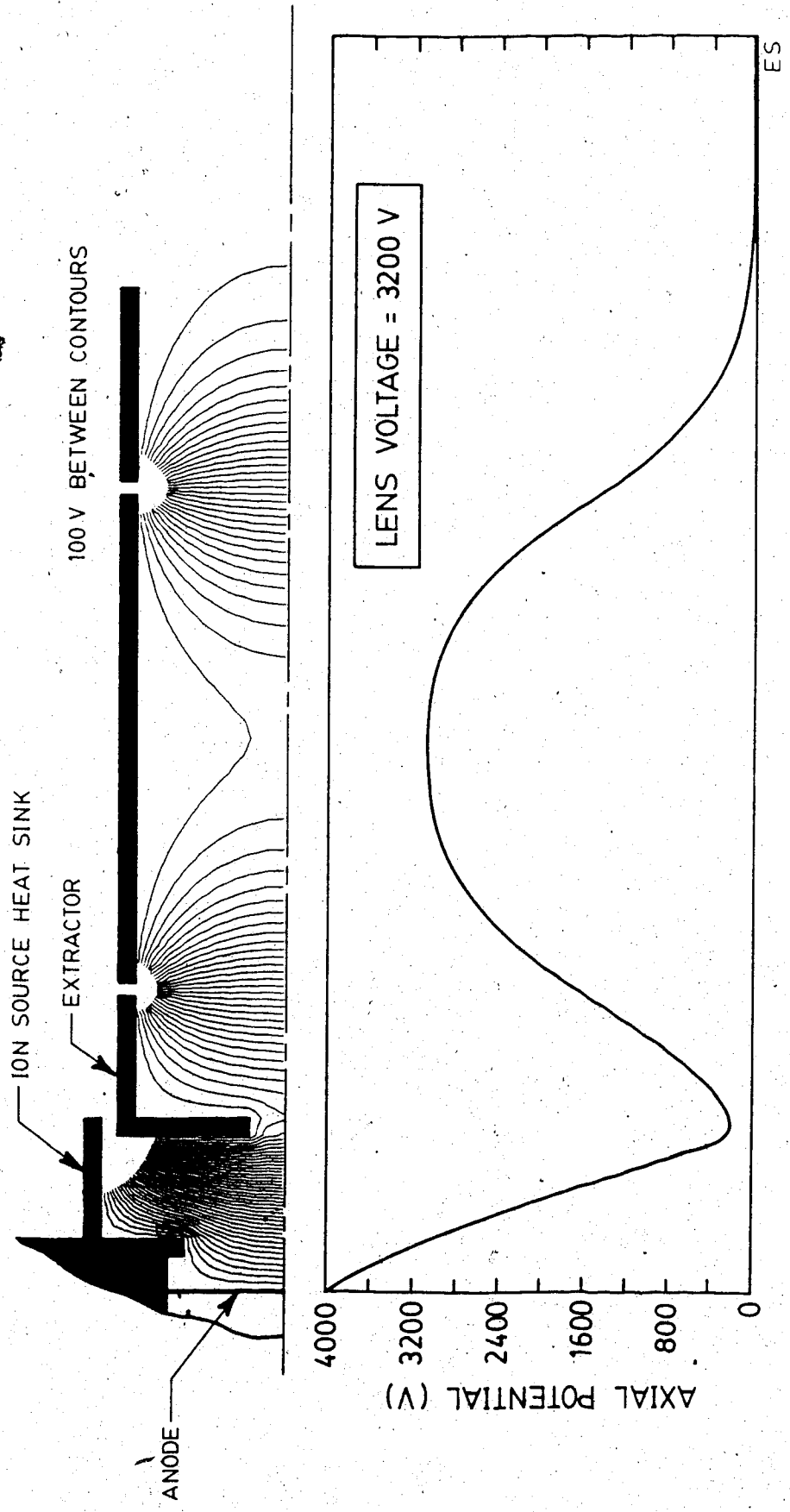


Figure 2.10 Lens Potential Contours

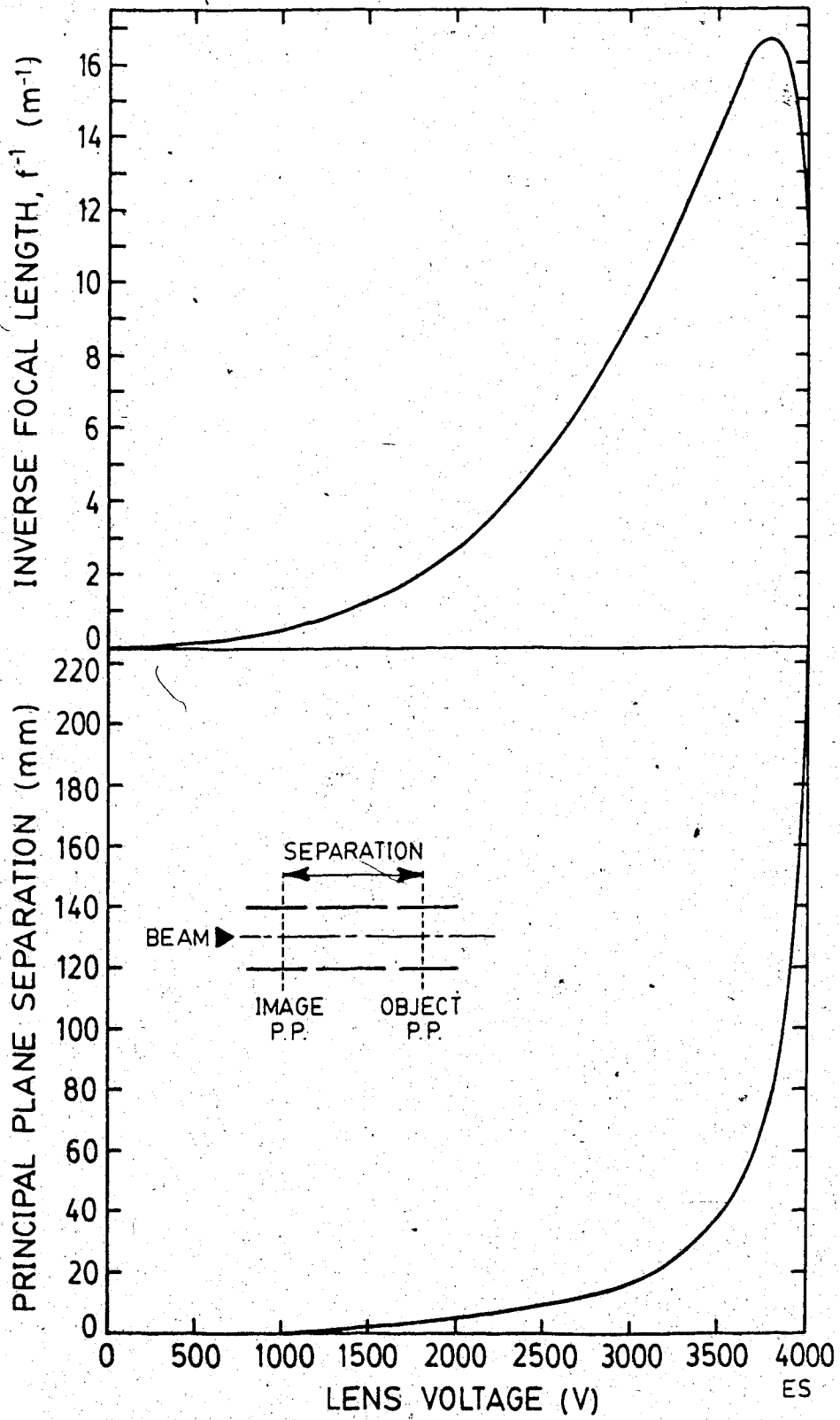


Figure 2.11 Lens Focal Properties

## Mass Filter

A Colutron Corporation model 600 Wein-type mass filter was purchased. A drawing of the device appears in Fig. 2.12. A simplified lateral cross section view showing the recommended power supply connections is given in Fig. 2.13.

The operation of the filter, called an E-cross-B or velocity filter, is outlined by Wählin (1964, 1965), Seliger (1972), and Wilson and Brewer (1973, pp. 213-227). In a filter where the electric and magnetic fields are uniform, the focussing action of the crossed fields is astigmatic. That is, an initially parallel incident beam converges to the beam axis only in the plane of the electric field under the influence of the magnetic field and simply drifts through the filter in the plane of the magnetic field. With proper voltages applied to the guard rings—which are not rings but rectangular strips made from shim stock—the electric field can be made stronger at the negative plate and weaker at the positive plate. This nonuniform electric field tends to counteract the focussing action of the magnetic force (Wählin 1964).

Regarding mass dispersion, the particle trajectory slope at the filter exit was determined for an astigmatic separator in a manner similar to that used by Seliger (1972). The result is

$$y' = \frac{(1-\eta)\sin\frac{L}{r_0}\eta}{1-(1-\eta)\cos\frac{L}{r_0}\eta}, \quad \eta = \sqrt{\frac{m_0}{m}}$$

where  $y'$  is the exit slope in rad;  $m$  is the mass of the deflected ion;  $m_0$  is the mass of the undeflected ion;  $r_0$  is the cyclotron radius given by  $2V_0/E_0$ , with  $V_0$  being the beam voltage and  $E_0$ , the electric field strength in the filter required to transmit  $m_0$ ; and  $L$  is the length of the filter, in the Colutron, 152 mm (6.0 in.). For weak separators, this expression gives the same result as that for a stigmatic filter (Seliger 1972). The separation  $\Delta y$  between  $m_0$  and  $m$  at a distance  $D$  from the exit of the filter is given by

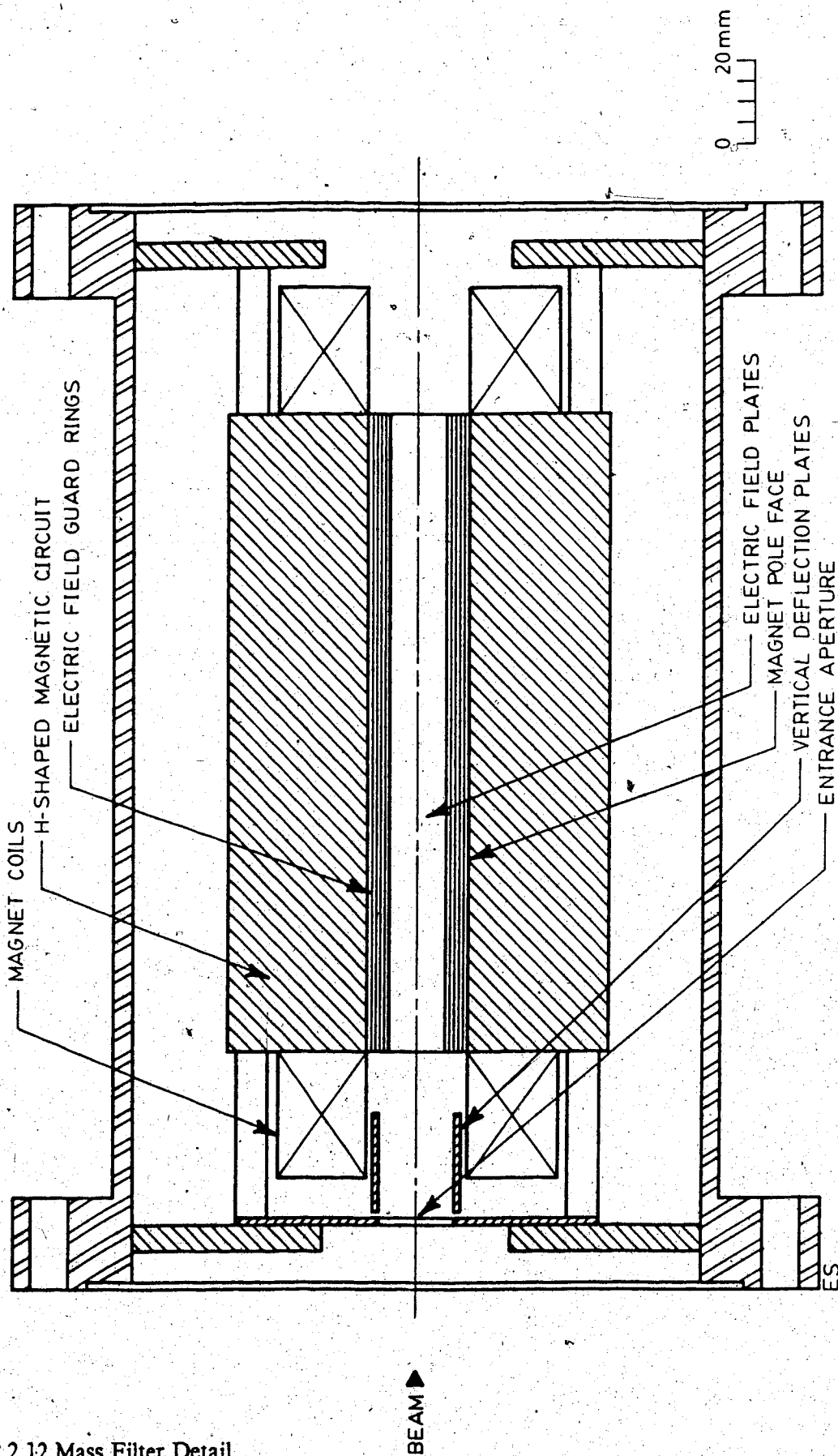


Figure 2.12 Mass Filter Detail



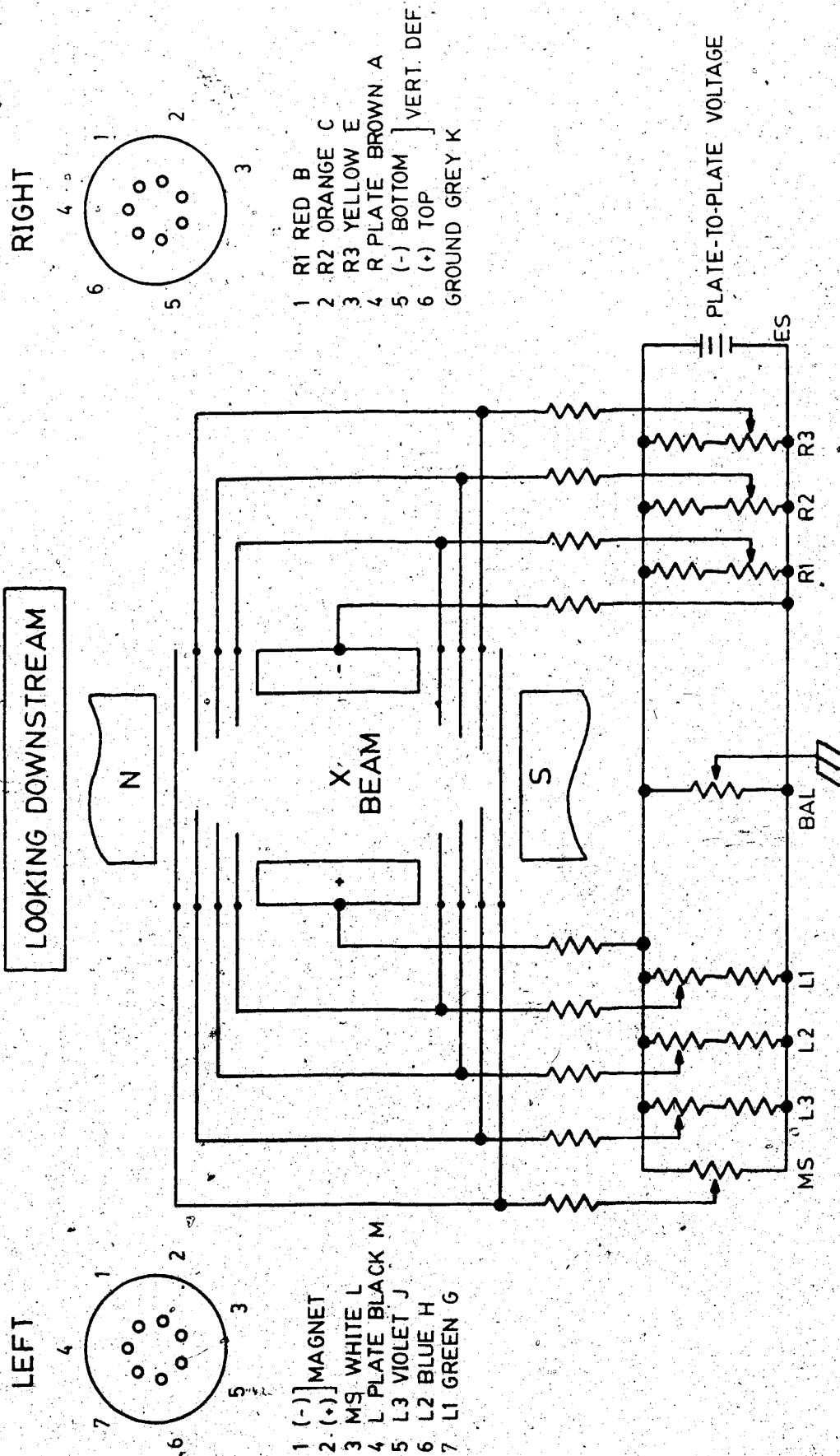


Figure 2.13 Mass Filter Schematic

the equation

$$\Delta y = y' \left( \frac{L}{2} + D \right)$$

The maximum operating parameters specified by Colutron Corporation for their filter are 1000 G for the magnetic field, 5 keV beam energy, 168 kV/m electric field strength (which is obtained with 300 V between the plates), and 400 V deflection plate voltage.

In this ion gun, the deflected ions are intercepted on a plate; see Fig. 2.14. The undeflected ions pass through an aperture before they enter the acceleration tube.

#### 2.2.1.4 Target Chamber

At the end of the acceleration tube opposite the ion gun is the target chamber. The only apparatus required in the target chamber is a beam collector. The arrangement of this apparatus inside the target chamber is shown in Fig. 2.15. The beam enters through a grounded shield electrode and is collected in a Faraday cup. Secondary electron emission from the cup is suppressed by an adjacent electrode that is biased negative with respect to the cup. In addition, the shield electrode is equipped with a manually operated shutter plate that can intercept portions of the incoming beam. On the shutter plate is mounted a ground quartz window that scintillates when struck by energetic ions, thereby allowing a visual observation of the beam cross section.

### 2.2.2 High Voltage Apparatus

#### 2.2.2.1 Introduction

There was a decision to make regarding how the acceleration voltage should be connected. That is, knowing the configuration of the beam line (Fig. 2.6), the acceleration voltage could be applied in two ways: (1) the ion gun at ground potential with the target raised to negative acceleration voltage or (2) the ion source at positive acceleration voltage

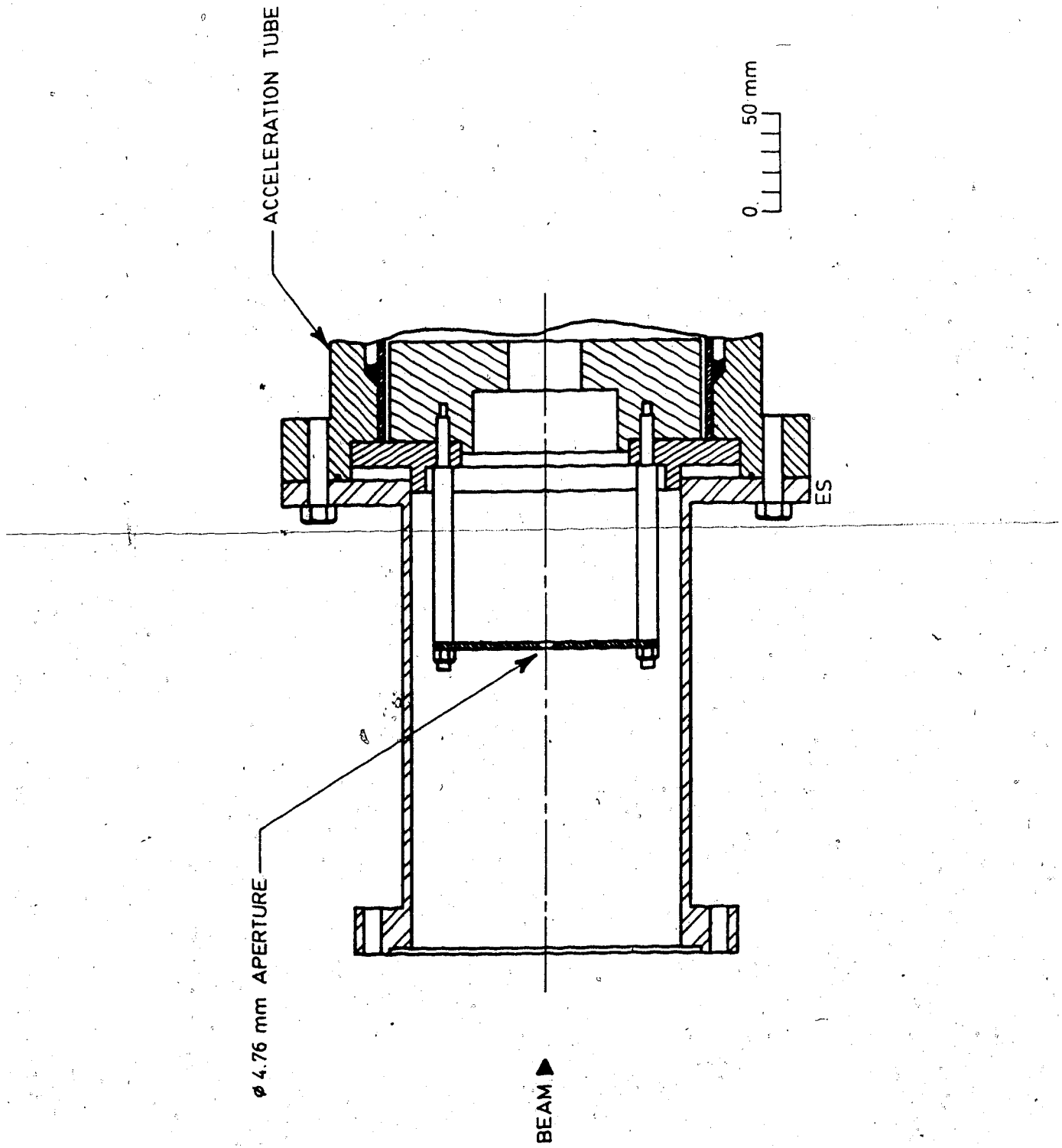


Figure 2.14 Mass Selection Aperture

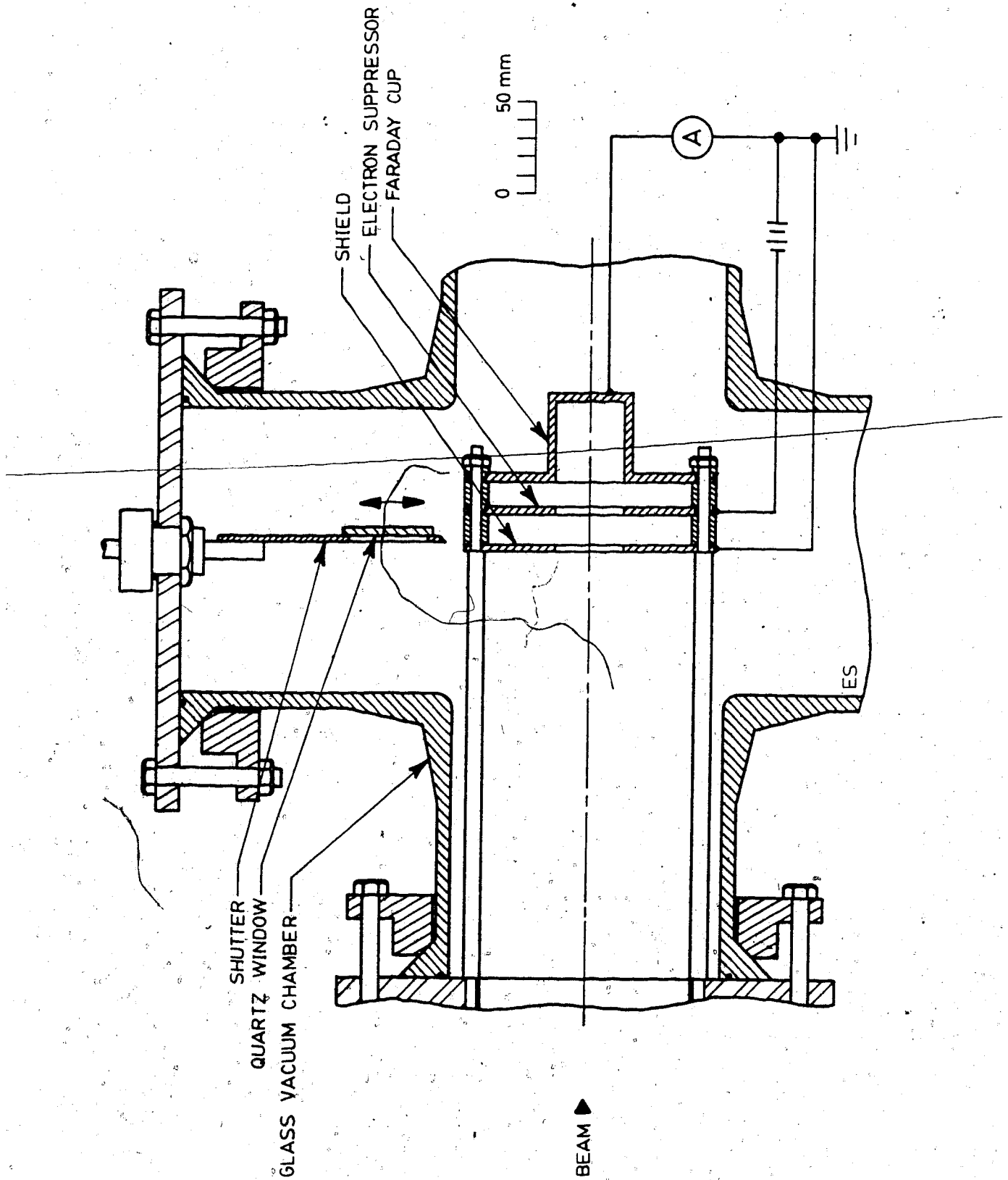


Figure 2.15 Target Detail

and the target at ground. If the accelerator is used in its intended applications as an RBS device or ion implanter it will require an elaborate postacceleration beam handling facility (see Sec. 3.5). Therefore, either of the two configurations would pose comparable problems in supplying electrical power to and controlling equipment in a high voltage region. In case (1), however, an inordinately long high voltage terminal would likely be required to shield a future postacceleration beam line; hence, the latter arrangement was selected. This array is depicted in Fig. 2.16 (compare Fig. 2.6).

With the mass filtering performed before acceleration, there is the advantage of a reduced ion current to be accelerated and, as a result, less severe space charge beam expansion in the acceleration tube (Wilson and Brewer 1973, p. 401; Bannenberg 1979). A mass filter in the ion gun does, however, increase the length of the low energy beam line and makes space charge a problem there.

In the following sections, the high voltage equipment will be described. There is a brief look at the voltage generator followed by a description of the layout of the high voltage terminal and its supports.

#### 2.2.2.2 High Voltage Power Supply

A Universal Voltronics Corporation model Bal-280-5.5 oil insulated voltage doubler that operates at 60 Hz was available to supply the acceleration potential for this accelerator. Connection between the generator and the high voltage terminal is made with a coaxial high voltage cable in a manner similar to that used by Laubert and Wotherspoon (1965). As mentioned in Chap. 1, this apparatus had been used previously in a different accelerator system. A simplified circuit diagram of the voltage generator appears in Fig. 2.17. The output of this particular circuit is continuously variable from 0 to 280 kV with a full load of 5.5 mA.

The voltage multiplier, or cascade rectifier, was first used in accelerator technology by Cockcroft and Walton (1932a). The circuit used here is referred to as a half-wave voltage doubler. The principle of circuit operation is outlined by Cockcroft and Walton

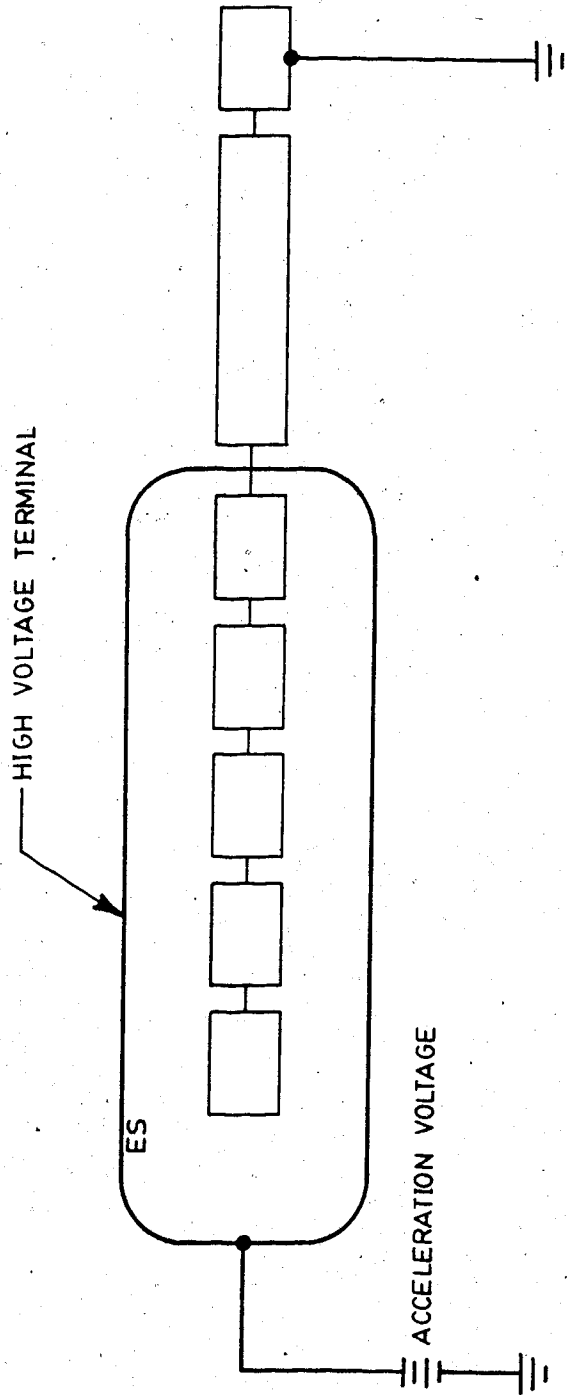


Figure 2.16 Block Diagram III

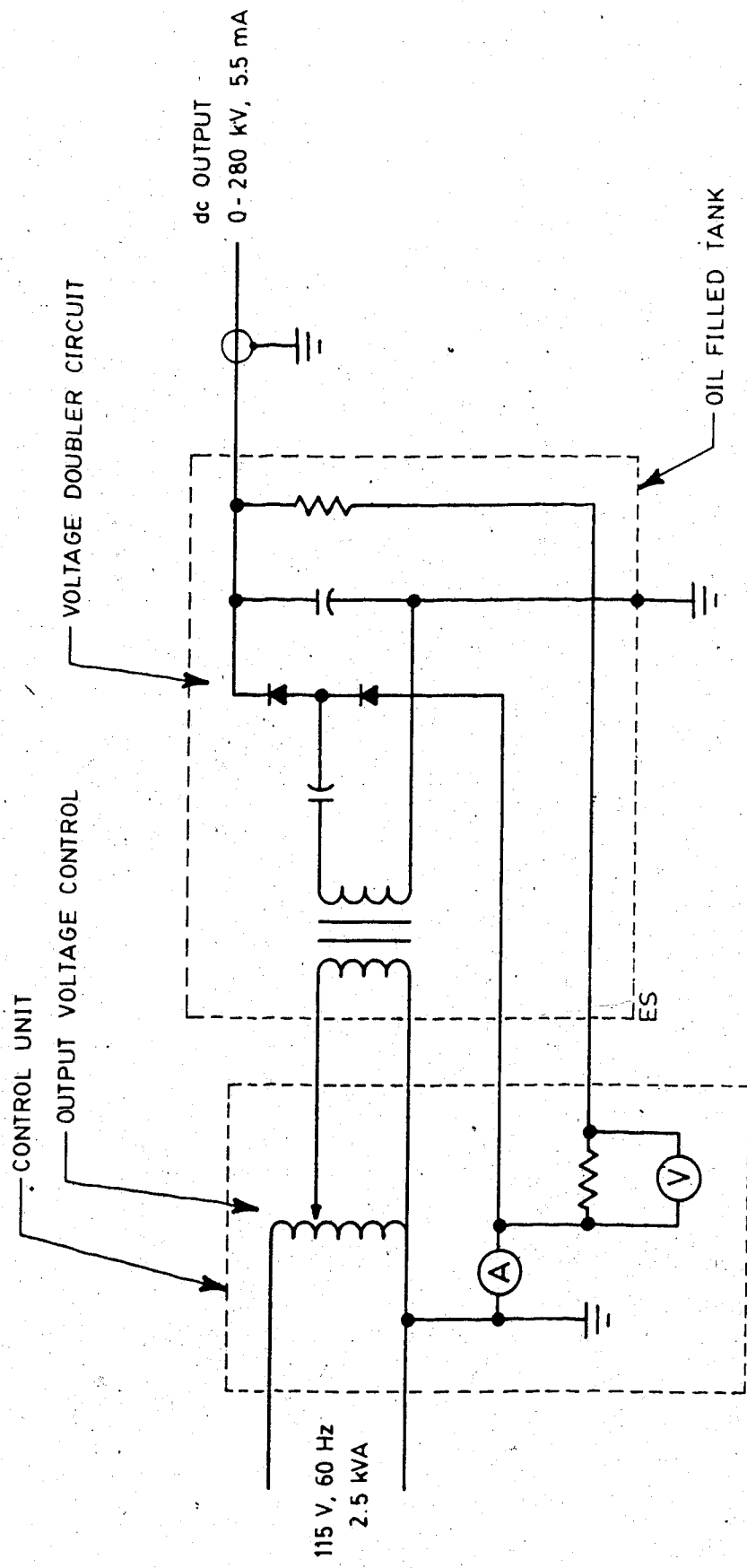


Figure 2.17 High Voltage Generator

(1932a), Waidelich and Gleason (1942), and Reich (1944, p. 566).

### 2.2.2.3 Structures

In Sec. 2.2.3.3 Power Source Inside the Terminal, it will be shown that an electrical generator must be housed in the high voltage terminal to supply power to the ion gun. This generator set, because of its size and mechanical vibration, is mounted in a mechanically isolated enclosure adjoining the main terminal. The layout of the terminals and their support is diagrammed in Fig. 2.18. In the figure is shown the manner in which the high voltage is connected to the terminal. Note that the beam line is horizontally oriented because this was the best way to utilize the existing support structures.

## 2.2.3 Beam Line Support Systems

### 2.2.3.1 Introduction

Here the ancillary equipment for the accelerator beam line is described. These systems were alluded to in Sec. 2.1. They include the vacuum system, electrical system, and ion source cooling system.

The beam line is first described in terms of its vacuum system characteristics. Mention will be made of the gas supply apparatus for the ion source (see Sec. 2.2.1.3 Ion Source). Following this is a description of the electrical systems, one of which is the electronic power supply and control scheme that energized the ion gun. Besides this, the electrical system also includes the apparatus that delivers ac power to these circuits. The subject of the second innovation in this accelerator design is the manner in which this power is transmitted from ground to the high voltage terminal. (The first innovation was an alternate acceleration tube construction described in Sec. 2.2.1.2.)

### 2.2.3.2 Vacuum Equipment

The beam line is evacuated by a single pump that is attached to the target chamber. A small gas handling plant supplies gas to the ion source from a reservoir through a needle



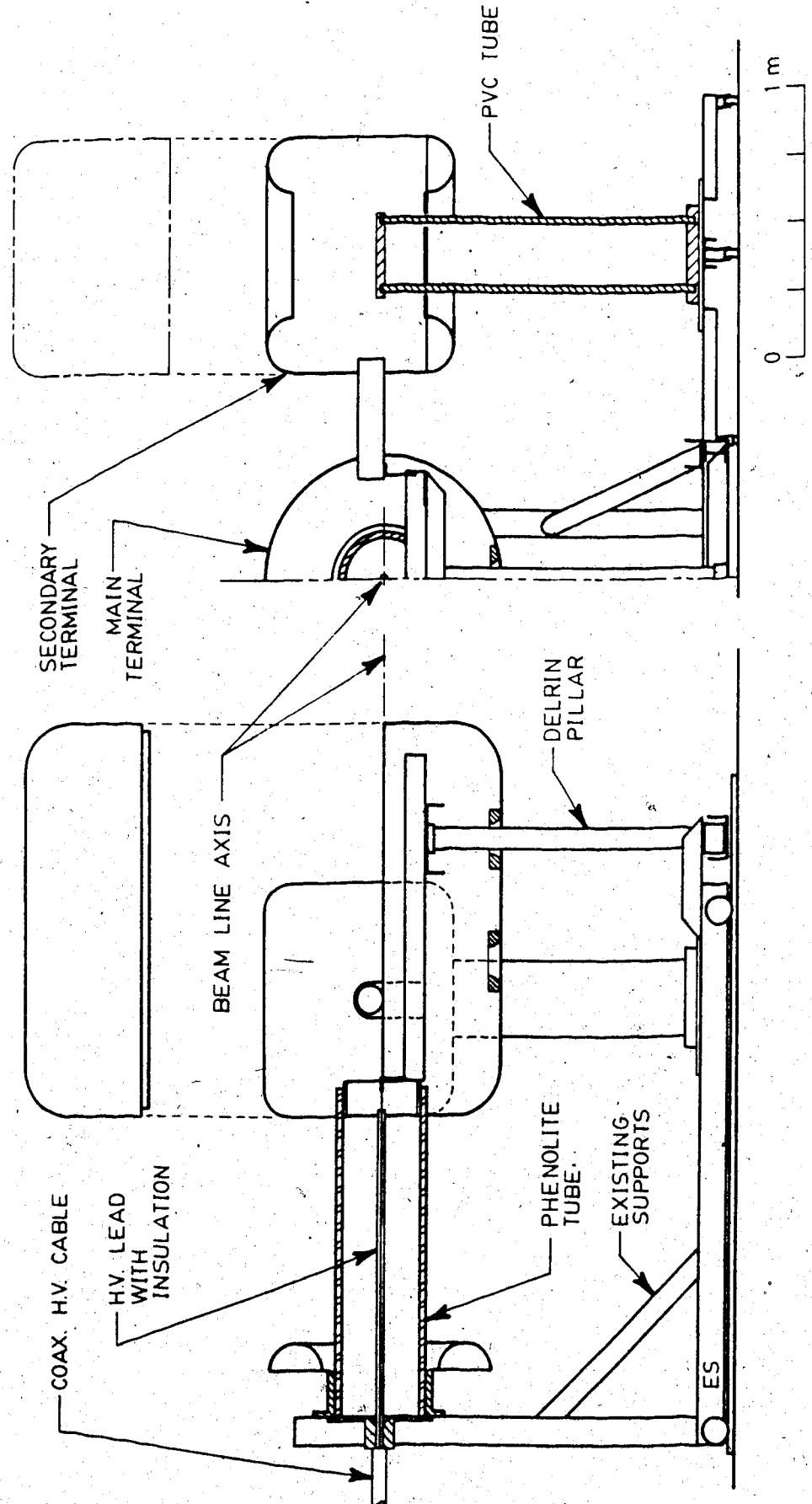


Figure 2.18 Terminal Supports

valve. With the addition of these components the block diagram of the accelerator system is as shown in Fig. 2.19 (compare Fig. 2.16).

A detailed schematic diagram of the vacuum system is given in Fig. 2.20. In it are shown the valves, gauges, and the beam line pump which is a Sargent-Welch model 3102-D 250 liter/s turbomolecular pump. The particular arrangement of valves allows the beam line above the target chamber to be isolated under vacuum, although not pumped, while the pump is shut down for target chamber servicing or any other reason. The pump must be vented through the target chamber. The ion source gas handling plant has a quick disconnect receptacle through which gases are removed from and admitted into the reservoir. The various electrical feedthroughs on the ion gun and target chambers together with the sliding feedthrough on the target are omitted from Fig. 2.20.

### 2.2.3.3 Electrical Systems

#### Electronic Power Supply and Control Scheme

Some of the electrical system requirements have already been described within the discussions presented in Sec. 2.2.1.3, regarding the beam line, and were illustrated in Figs. 2.8, 2.9, 2.13, and 2.15. These requirements along with a remotely located control unit are summarized in the block diagram of Fig. 2.21 (compare Fig. 2.19). A more detailed representation of the system, including monitor and control paths, is given in Fig. 2.22. This is a block diagram intended to show the connection of control, monitoring, and power units. There is a record of all the electronic circuit schematic diagrams, although they are not included in this dissertation.

In the high voltage terminal, the ion gun functions are monitored and controlled on two separate panels. One panel is assigned to the ion source and lens and the other, to the vertical deflection plates and mass filter. These controls are used for standby operation of the ion gun. Control of the ion gun during high voltage operation is accomplished through a glass fiber communication channel linking the ion gun

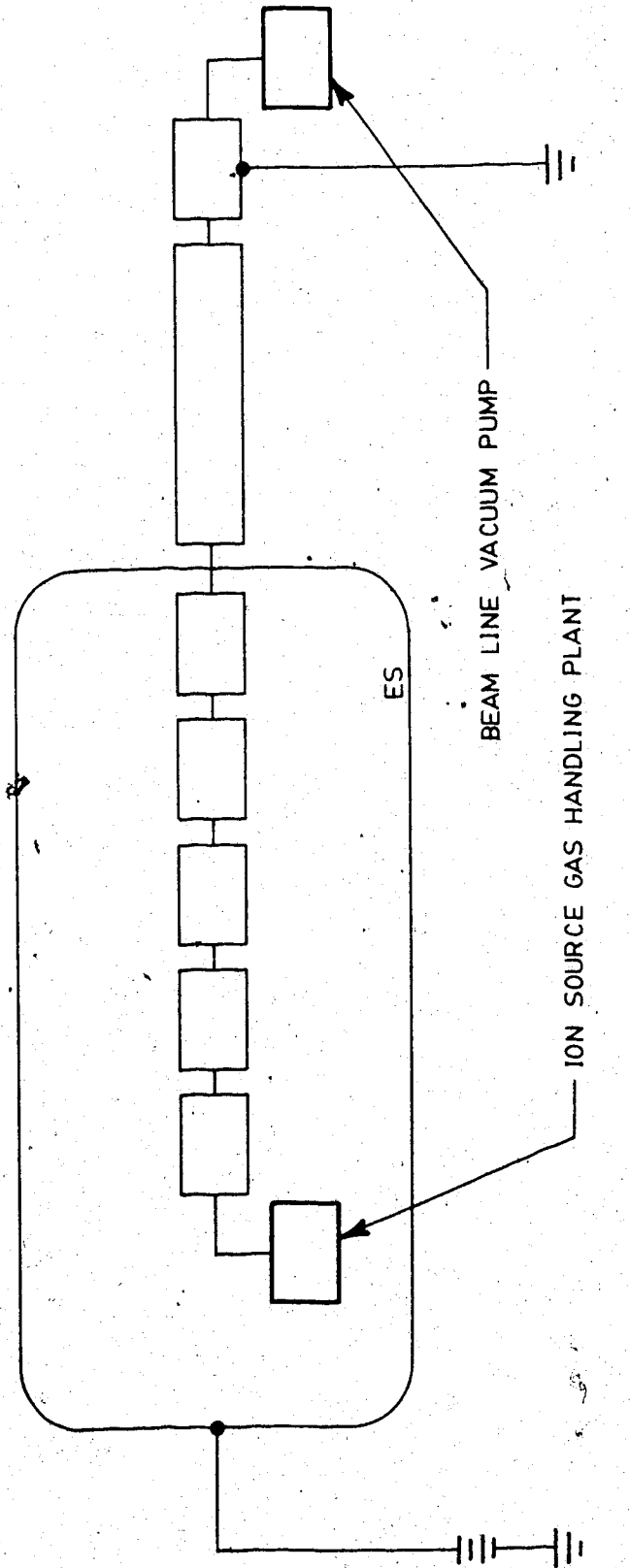


Figure 2.19 Block Diagram IV

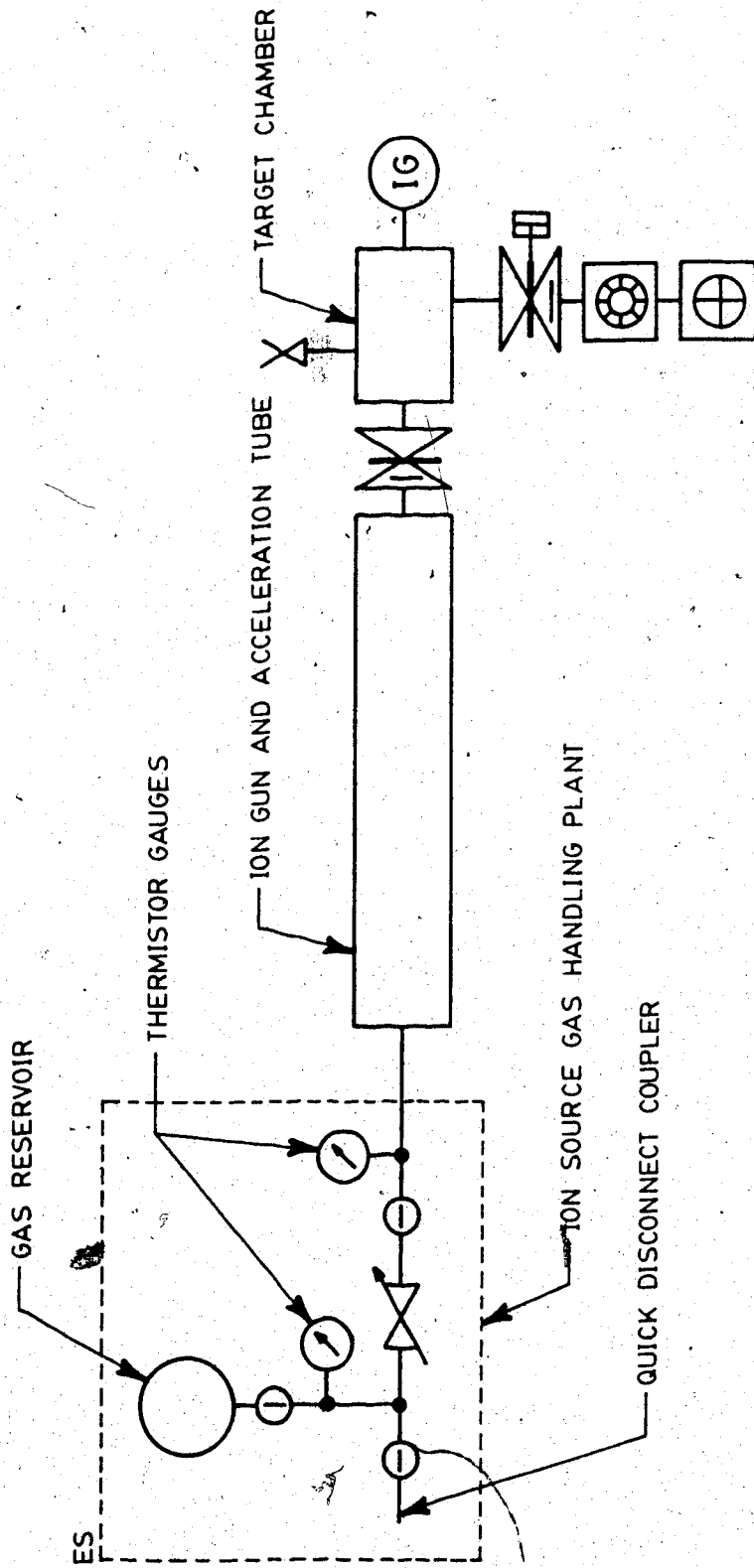


Figure 2.20 Vacuum System Schematic (AVS 7.1-1966)

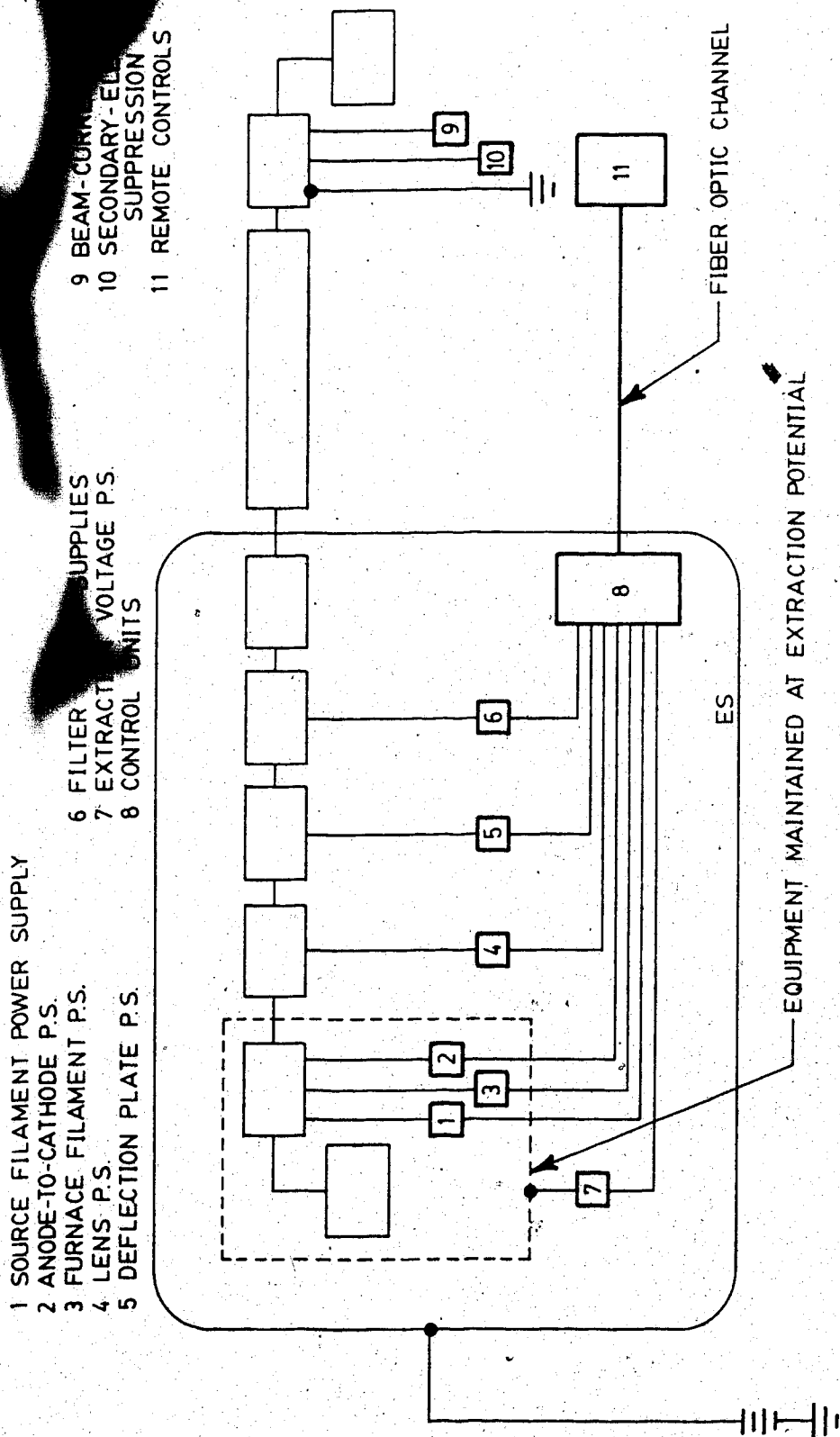


Figure 2.21 Block Diagram V

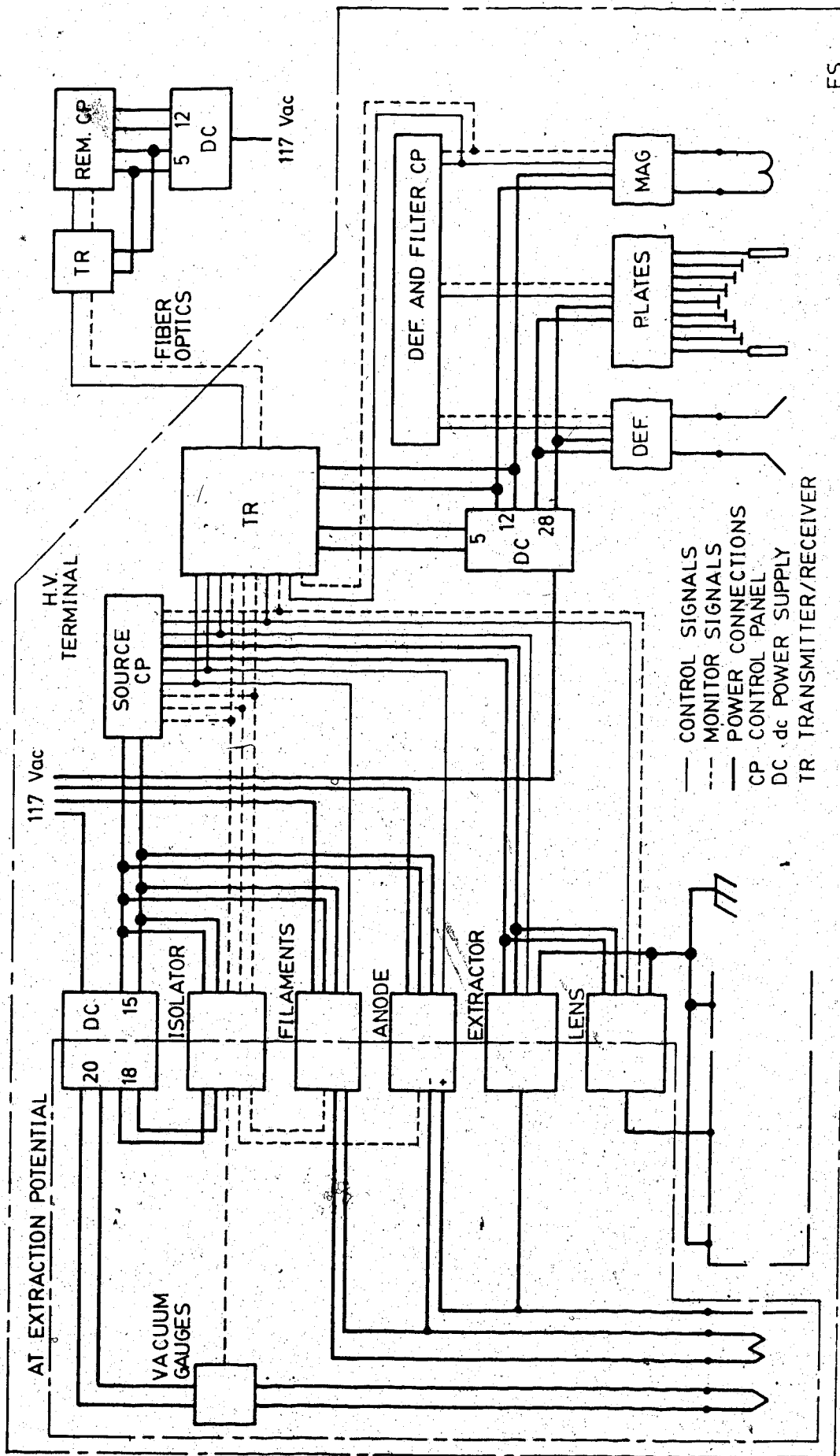


Figure 2.22 Control System

circuits to a ground-end control panel. Control and monitor signals are digitized and multiplexed for transmission on this channel. It is the function of the transmitter/receiver to decode and encode the various signals.

All of the electronic equipment in the high voltage terminal is powered by a 117 V ac source. During standby operation of the ion gun, this power is taken from a 15 A wall outlet. During high voltage operation, on the other hand, this power is generated inside the high voltage terminal. This topic is considered next.

#### Power Source Inside the Terminal

**Background.** In Cockcroft and Walton's first accelerator, the 300 kV transformer-rectifier, electrical power was supplied to the source in the high voltage terminal through an isolation, or insulation, transformer (Cockcroft and Walton 1930). This method of delivering power to a high potential region is convenient, but is practically limited by size and cost to low voltage applications. In their second machine, the cascade rectifier, which operated at 700 kV, Cockcroft and Walton installed an electric generator inside the high voltage terminal (Cockcroft and Walton 1932a). They coupled this terminal mounted alternator to an electric motor located at ground potential with a loop of cotton rope. Both of these techniques have been used in subsequent accelerators of the Cockcroft-Walton type; see, for example, Burkham (1947), Arnold (1950), and Peck and Eubank (1955). Lorrain et al. (1957) have built a machine in which the cascade rectifier circuit, which was energized at 32 kHz, provided power to operate an ion source. A variation on the belt coupling between motor and generator is a rigid insulating shaft (Reinhold and Minkner 1965; Laubert and Wotherspoon 1965; Bannenberg 1979).

**Present design.** The use of an isolation transformer was ruled out on the basis of cost. It was therefore intended to generate electrical power inside the high voltage terminal. The conventional methods of transferring power via a belt or shaft, however, were bypassed. To be innovative, a fluid power system has been designed.

the fluid being hydraulic oil.

A simplified block diagram of the power transfer system is given in Fig. 2.23 (compare Fig. 2.21). The generator unit is housed in a separate high voltage terminal to save space in the main terminal and to isolate vibration (see Sec. 2.2.2.3). In the system, pressurized oil circulates between the motor unit, which is at ground potential, and the generator unit through insulating hydraulic hose in an open loop fluid flow configuration (Hedges 1969, Vol. 3, p. 80).

A schematic diagram of the fluid flow circuit is given in Fig. 2.24 (the component specifications are the manufacturer's theoretical data). The valve shunting the pump pressure line is a bypass speed control device. An important feature that is not shown in the figure is a hydraulic-oil coolant system that moderates oil temperature in the reservoir. This facility was integrated with the ion source cooling system and, as such, is described separately (see the following section).

The advantage in using hydraulics to transfer power to the high voltage terminal lies in the flexibility of locating the fluid lines. Indeed, the motor unit can be located anywhere. It can be located outside the accelerator room or even outside the building, with very little pressure drop over long fluid lines. This could be of particular benefit in other accelerator installations where space inside a laboratory is limited.

**System details.** In the motor unit, the electric motor is coupled directly to the hydraulic pump. In the generator unit, on the other hand, the hydraulic motor and electric generator are linked through a jackshaft drive on pillow block bearings, as shown in Fig. 2.25. The generator is geared up so that its speed is twice that of the hydraulic motor. The output of the electric generator is electronically regulated.

All of the fluid power lines in the motor and generator units were plumbed with medium pressure hose. This hose has a synthetic rubber tube, is wire braid reinforced, and has a synthetic rubber cover. The hydraulic motor drain line is a low pressure textile-braid-reinforced hydraulic hose. For the insulating sections, a



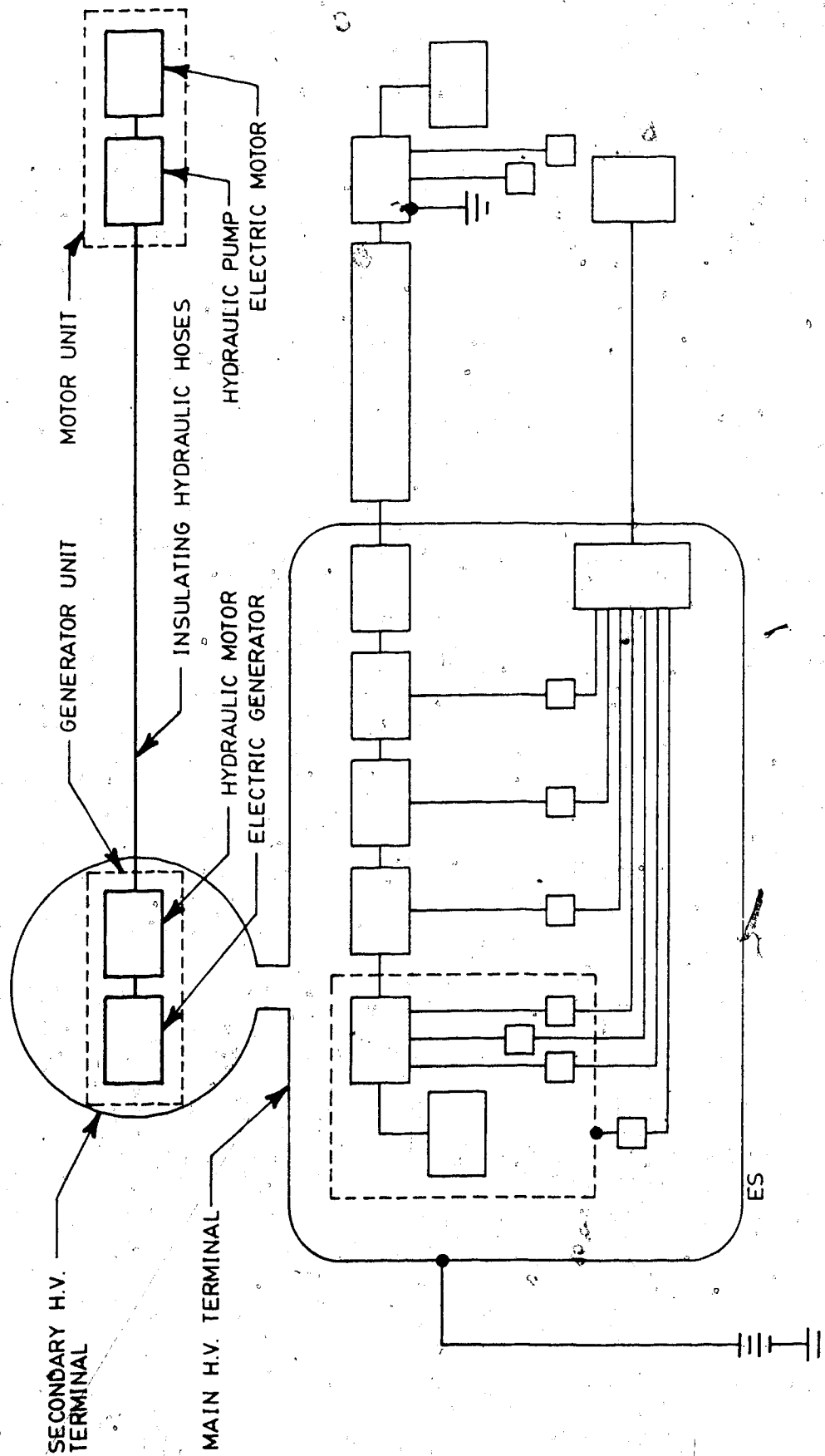


Figure 2.23 Block Diagram VI

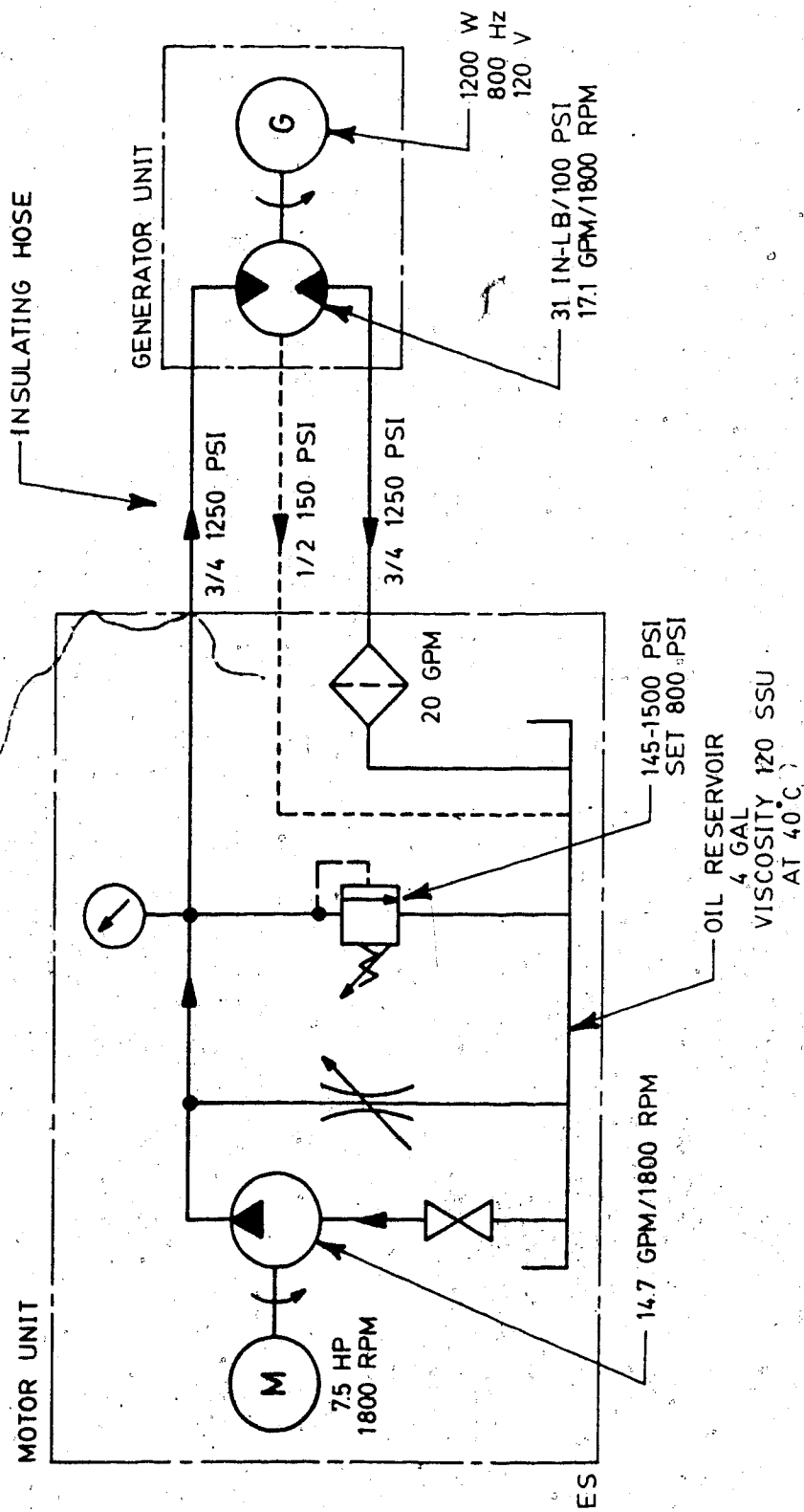


Figure 2.24 Hydraulic System Schematic (ANSI Y32.10-1967)

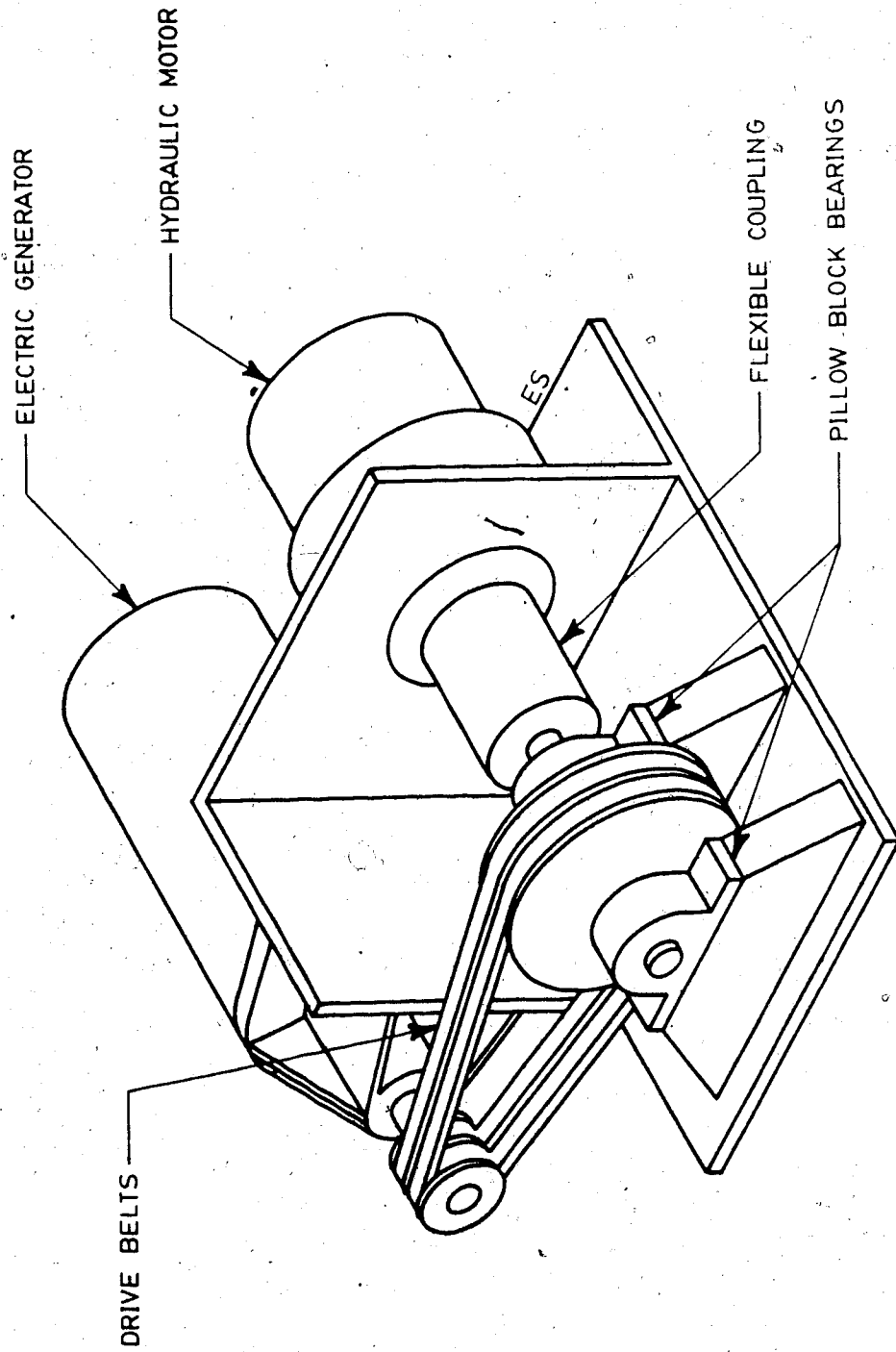


Figure 2.25 Generator Unit

nonconductive medium pressure hose with a nylon tube, nylon braid reinforcement, and a polyurethane cover was used for the power lines, and a low pressure nylon tubing, for the drain line. The nonconductive medium pressure hose is specified by the manufacturer to allow a maximum leakage current of  $50 \mu\text{A}$  for an applied voltage gradient of  $246 \text{ kV/m}$  ( $75 \text{ kV/ft}$ ) for five minutes. The path of hydraulic hose in the laboratory is illustrated in Fig. 2.26 (see Fig. 2.18).

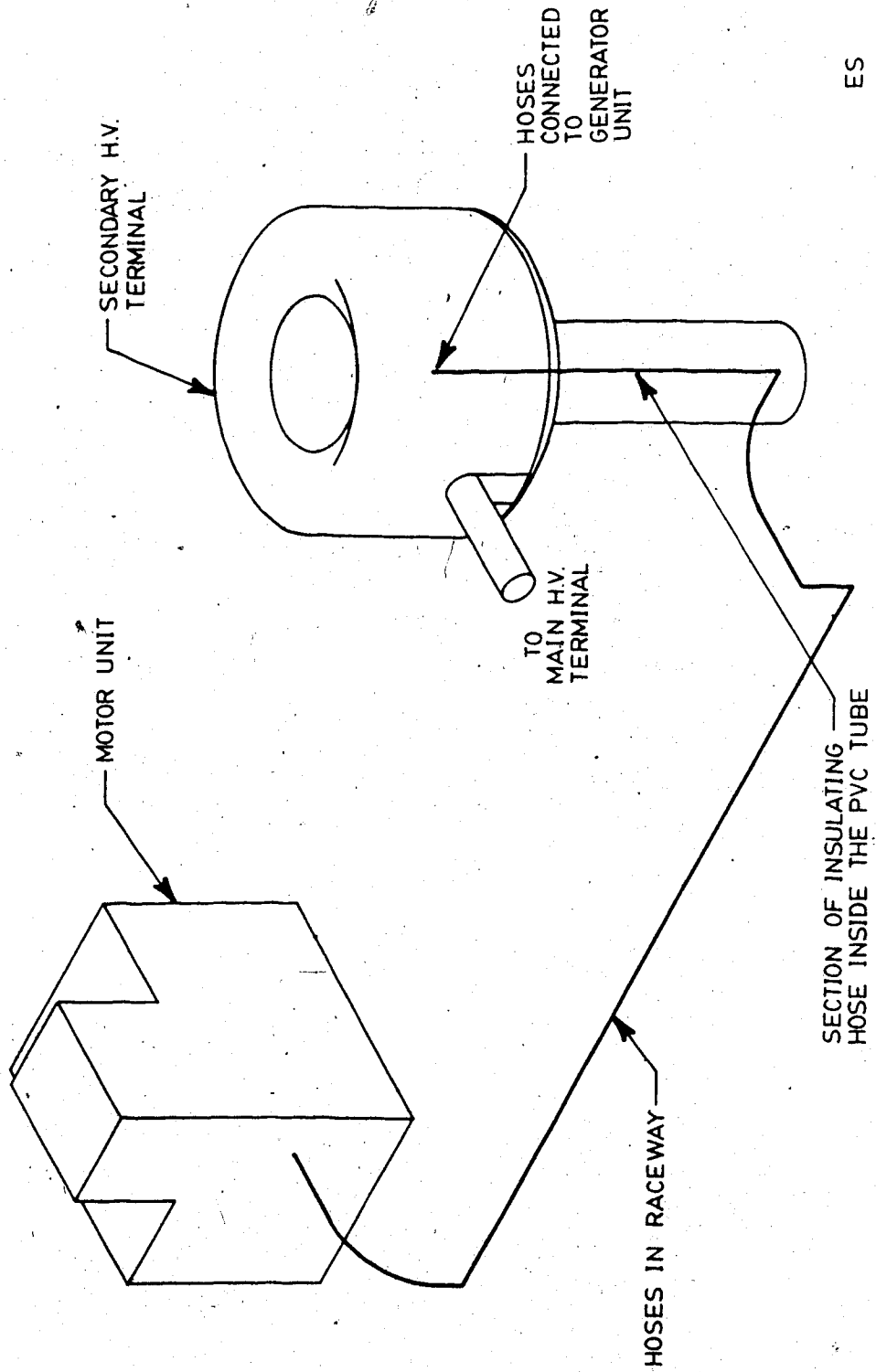
#### 2.2.3.4 Coolant Flow System

A separate oil circulation system moderates the temperature of the power hydraulic oil in the reservoir (see Sec. 2.2.3.3 Power Source Inside the Terminal) and also cools the ion source (see Sec. 2.2.1.3 Ion Source). The system was designed with a tube-and-shell heat exchanger. The same type of oil was used as in the power hydraulic system. A block diagram of the apparatus is given in Fig. 2.27 (compare Fig. 2.23); a schematic diagram appears in Fig. 2.28.

The pump unit is mounted on the same frame as the fluid power motor unit, and the two sets of fluid lines—power and coolant—follow the same path to the high voltage terminal (Fig. 2.26). Most of the coolant circuit was plumbed with low pressure hydraulic hose, but as in the fluid power system, lengths of nylon tubing provide an insulating path between ground and the high voltage terminal. The same nylon tubing was used to connect to the ion source since it is 4 kV above the terminal potential. The water flow to the heat exchanger was carried over ordinary garden hose from a cold water faucet.

#### 2.2.4 Radiation Shielding

Radiation shielding, in the form of stacked bricks, 292 mm (11.5 in.) thick, surrounds the accelerator on two sides. The concrete walls, ceiling, and floor of the building act as the shield for the remainder of the installation. The accelerator room is about 75% below ground level.



ES

Figure 2.26 Hose Layout in the Lab

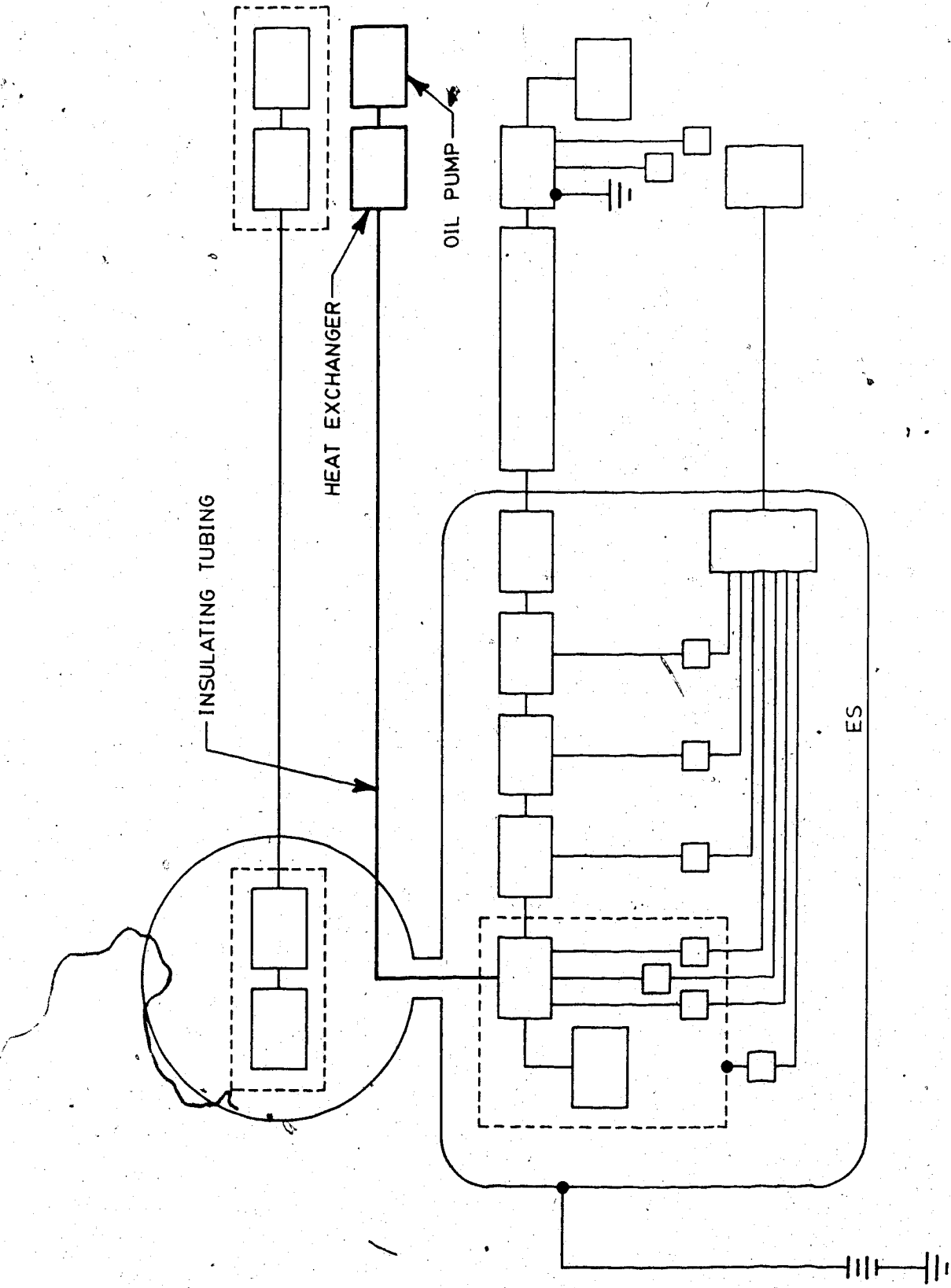


Figure 2.27 Block Diagram VII

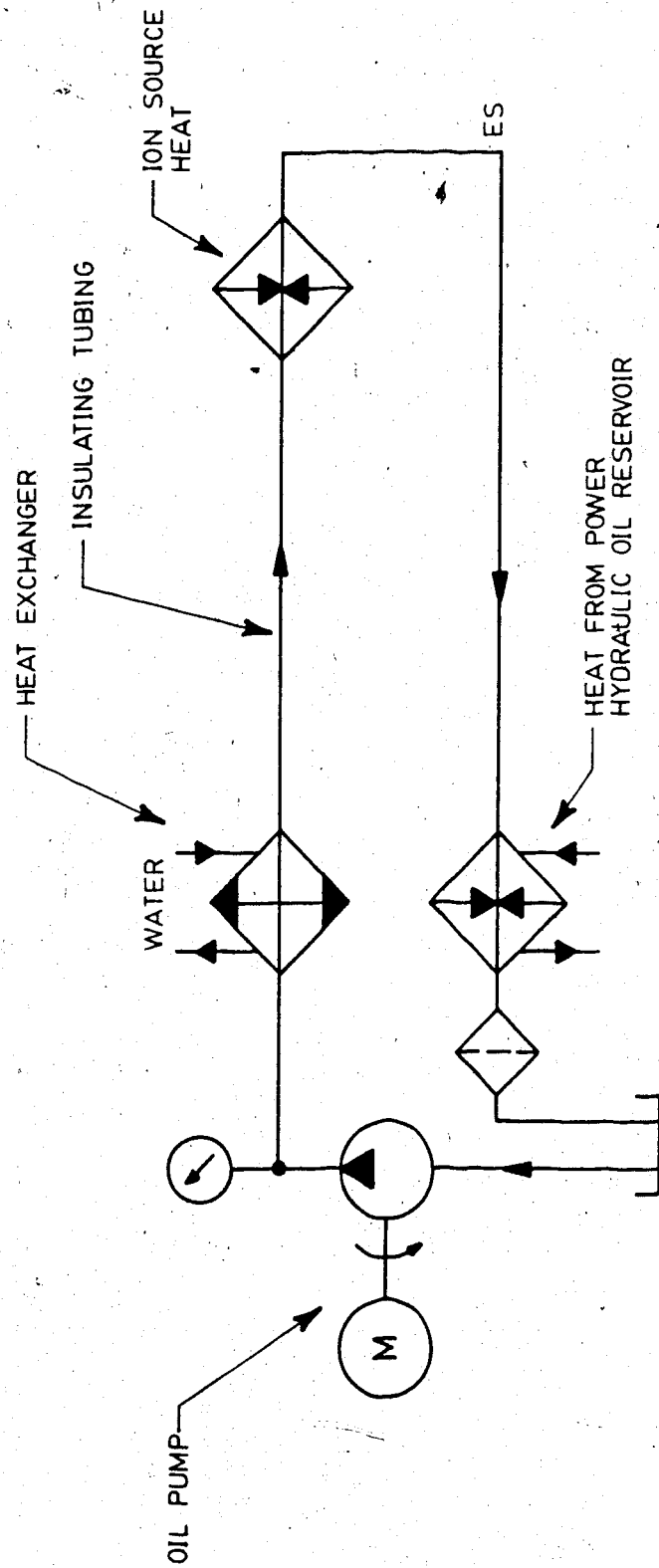


Figure 2.28 Coolant System Schematic (ANSI Y32.10-1967)

In block diagram form, the radiation shielding is as shown in Fig. 2.29 (compare Fig. 2.27). A plan view of the shielding scheme appears in Fig. 2.30. This arrangement was held over from a previous accelerator structure, as mentioned in Chap. 1, General Introduction.

## 2.3 Component Testing and Evaluation

### 2.3.1 Introduction

Several accelerator components were tested to determine their true performance characteristics. Coincidentally, the experience which was gained in the operation of these components aided in the design of an accelerator operating procedure. In addition, the results of these equipment trials support arguments presented in Chap. 3 regarding the analysis of accelerator performance. As the characteristics of each component became more familiar, shortcomings in design and performance became evident. These are indicated here and are included in Sec. 3.5, which deals with recommendations for improvement.

Elements of the beam line are considered first. Being one of the two accelerator design innovations, the accelerator tube is given particular attention. Electrical characteristics for the individual spacer-resistors and the acceleration tube as a whole were obtained to ascertain the voltage holding limit and whether or not a constant voltage gradient along the tube has been obtained. As well, the ability of the vacuum mounted resistors to dissipate heat during high voltage operation is evaluated. The upper voltage limit for the acceleration tube was not determined because of a lack of higher voltage equipment.

Following this is a review of ion gun performance. The ion gun components were tested in three configurations: ion source alone, ion source with the lens, and ion source with lens and mass filter. Ion currents were collected and beam profiles were observed to determine ion gun performance under recommended operating conditions.

Finally, the performance of the second accelerator design innovation, the fluid power transfer system, is outlined. The results of a load test are presented, showing that an adequate



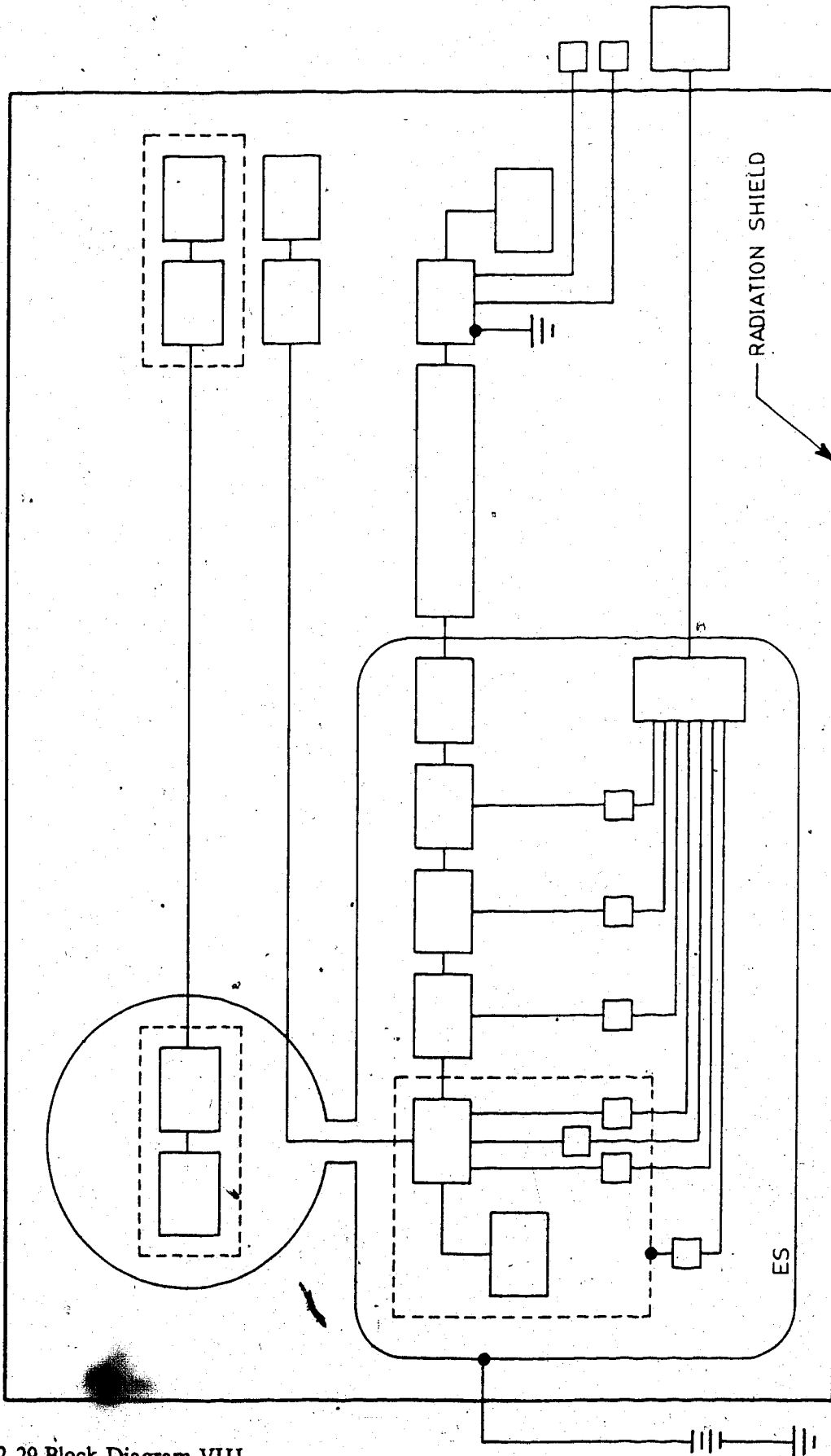


Figure 2.29 Block Diagram VIII

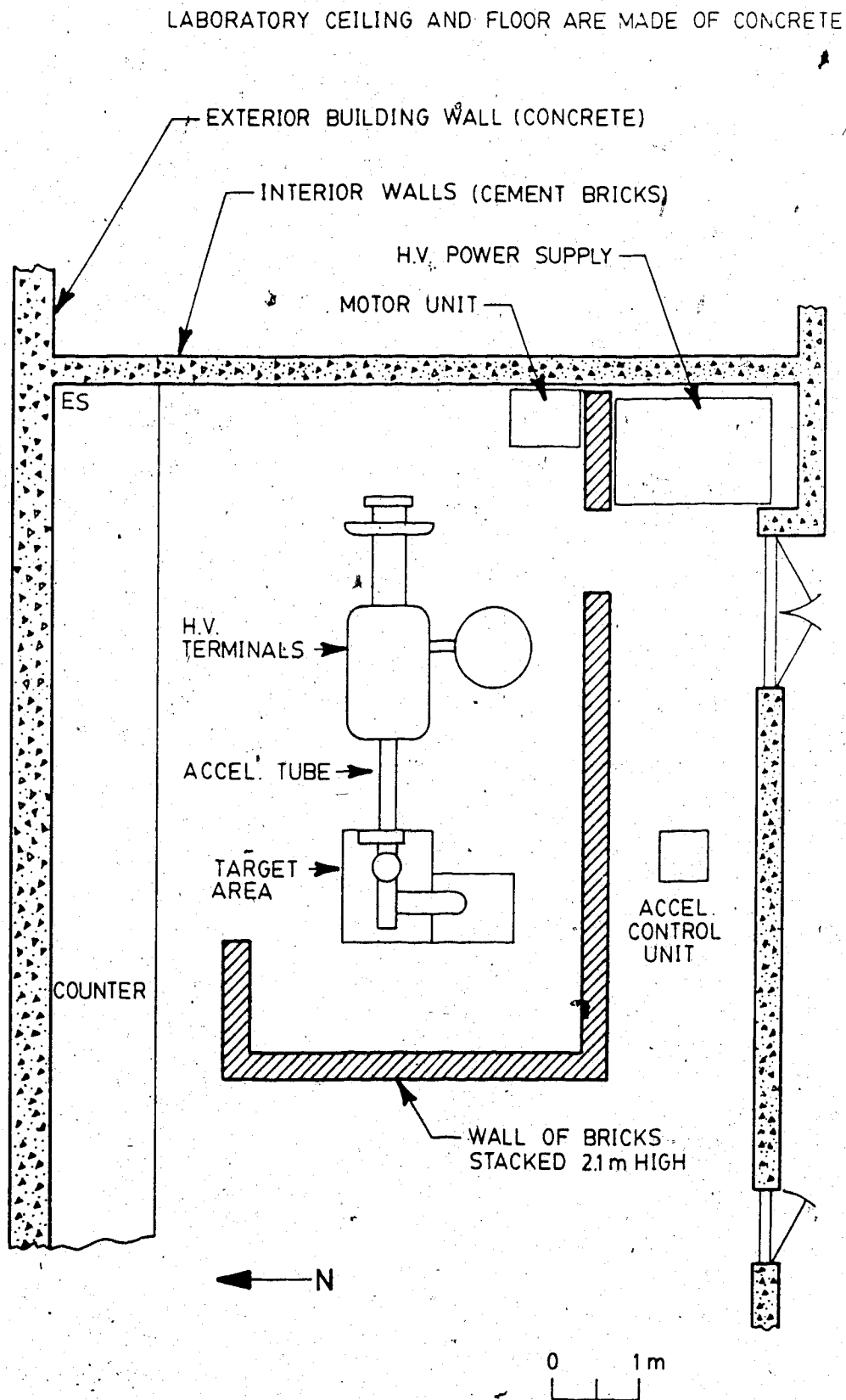


Figure 2.30 Accelerator Room Plan View

supply of electric power is generated. In addition, to show that leakage currents down the insulating sections of hydraulic hose are within acceptable limits, the results of high voltage endurance trials are given.

### 2.3.2 Acceleration Tube

**Spacer-resistors.** The resistance of each of the 188 spacer-resistors was measured with a megger. The average was  $2900\text{ M}\Omega$ , which compares favourably with the expected value of  $2800\text{ M}\Omega$ , assuming two coats of resistance paint behave like two resistors in parallel. The standard deviation of the measurements about the mean was approximately  $1700\text{ M}\Omega$ , likely a result of nonuniformity in resistance paint thickness among the spacer-resistors.

The voltage-versus-current characteristic was determined for each of the 47 spacer-resistor groups in the acceleration tube electrode structure. The four spacer-resistors from each group were stood on a 203-mm (8.0-in.) diameter 13-mm (0.5-in.) thick aluminum plate in a roughly equal spacing. A 127-mm (5.0-in.) diameter 51-mm (2.0-in.) thick aluminum plate was placed on top. A voltage was applied between the two electrodes, and the current was monitored. The voltage was recorded for a set of fixed current levels ranging from 0 to  $40\text{ }\mu\text{A}$ . This required a maximum voltage of about 6 kV. (The maximum voltage per electrode section is expected to be 5.95 kV at an acceleration potential of 280 kV.) The average voltage among the groups at each fixed current is plotted in Fig. 2.31 along with the standard deviation in the measurement sample, the average static resistance, and the average power dissipated by an individual spacer-resistor.

Using the same test apparatus, a spacer-resistor group, selected at random, was subjected to excessive voltages in order to determine the voltage holding limit of an interelectrode gap. The test was performed in air. An electrical breakdown was induced at a recorded current being  $236\text{ }\mu\text{A}$ . There was no apparent damage to the electrodes. A flashover between the two electrodes occurred down the bore of one of the electrodes. The presence of resistance paint flakes in the bore of the plastic cylinder

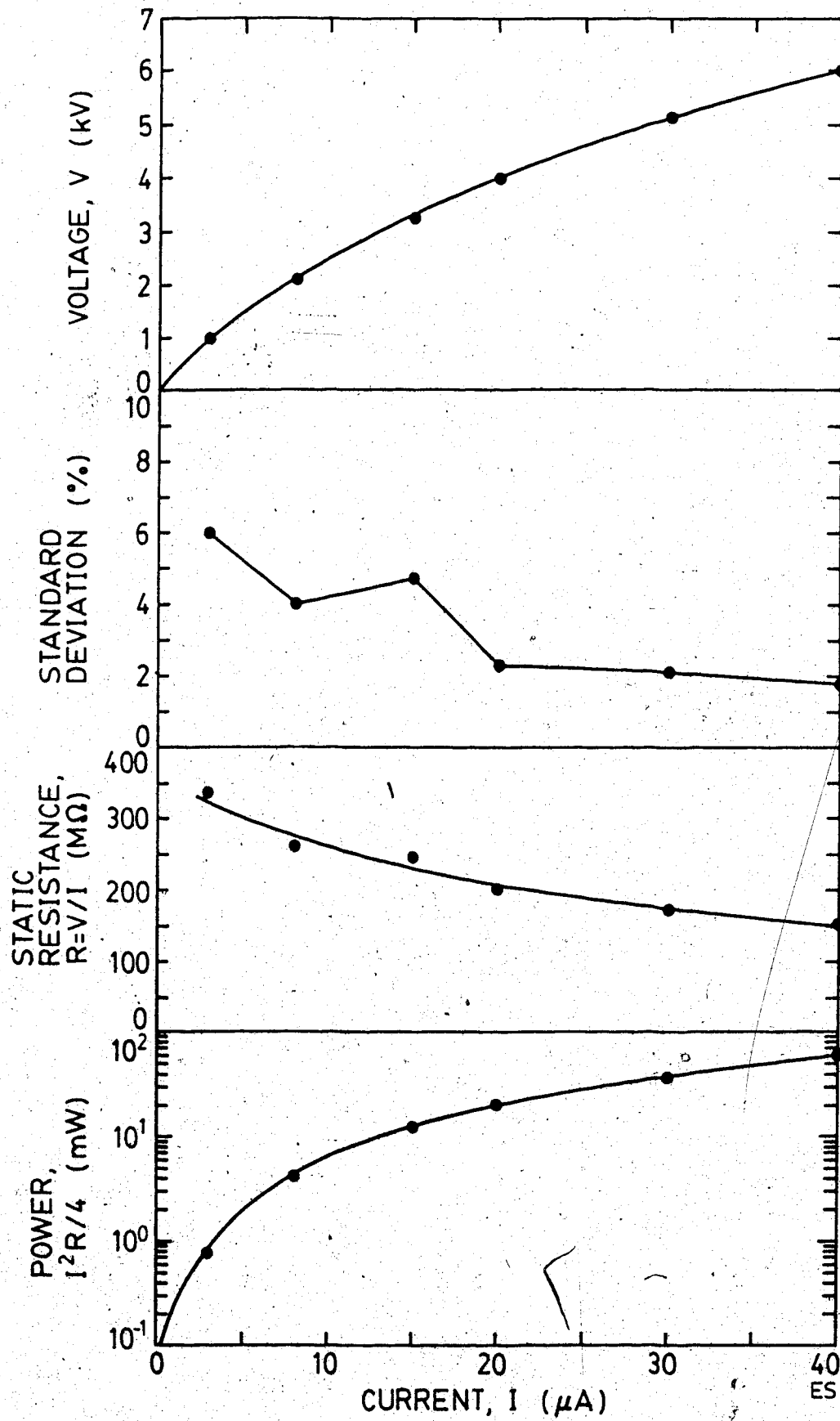


Figure 2.31 Spacer-Resistor Performance Data

part of the spacer-resistor likely precipitated breakdown. During previous attempts to produce satisfactory spacer-resistors, the plastic cylinders were painted, soaked in paint solvent, and repainted several times, and since it was impractical to clean each cylinder thoroughly, flakes of resistance paint accumulated on the cylinder bore. Intensification of the electric field at the paint flakes promoted a low value of breakdown voltage. Spacer-resistors made from clean Delrin cylinders may hold a higher voltage. If the tube were to be used for higher voltage applications this would be important.

**Acceleration tube.** The entire beam line—that is, ion gun, acceleration tube, and target chamber—was assembled and mounted on the accelerator supports (see Fig. 2.18 and Sec. 3.1). A representative current-versus-voltage characteristic for the tube, obtained under vacuum conditions, appears in Fig. 2.32. Before the data for the figure was collected, gas pressure at the ground end of the tube was 0.21 mPa ( $1.6 \cdot 10^{-6}$  Torr) and at the high voltage end, 2.1 mPa ( $1.6 \cdot 10^{-5}$  Torr) (see Fig. 2.20).

The average interelectrode voltage in the tube can be estimated from Fig. 2.32 by dividing the horizontal scale by 47, the number of electrode sections. For a particular current, the interelectrode voltages obtained in this way correspond with the average spacer-resistor group voltage in Fig. 2.31. This means that the deviation of the voltage distribution in the tube can be inferred from the data for the individual spacer-resistors, that is, Fig. 2.31. Accordingly, from Fig. 2.31, the maximum voltage deviation was 6% at 3  $\mu$ A, which corresponds to a tube voltage of 50 kV, as seen in Fig. 2.32. Beyond 20  $\mu$ A, that is, for potentials greater than 200 kV, the deviation was less than 2%. Deviations of less than 6% are considered acceptable; the data, therefore, indicates satisfactory performance.

Gas pressure at the ground end of the tube was monitored during high voltage tests. As mentioned, before the start of the tests, the pressure was 0.21 mPa ( $1.6 \cdot 10^{-6}$  Torr). There was no pressure change as the voltage was raised to 200 kV. At 250 kV, the pressure rose to 0.23 mPa ( $1.7 \cdot 10^{-6}$  Torr). Increasing the voltage to 280 kV caused the pressure to rise and plateau at 0.24 mPa ( $1.8 \cdot 10^{-6}$  Torr) within five minutes. This voltage level was maintained for

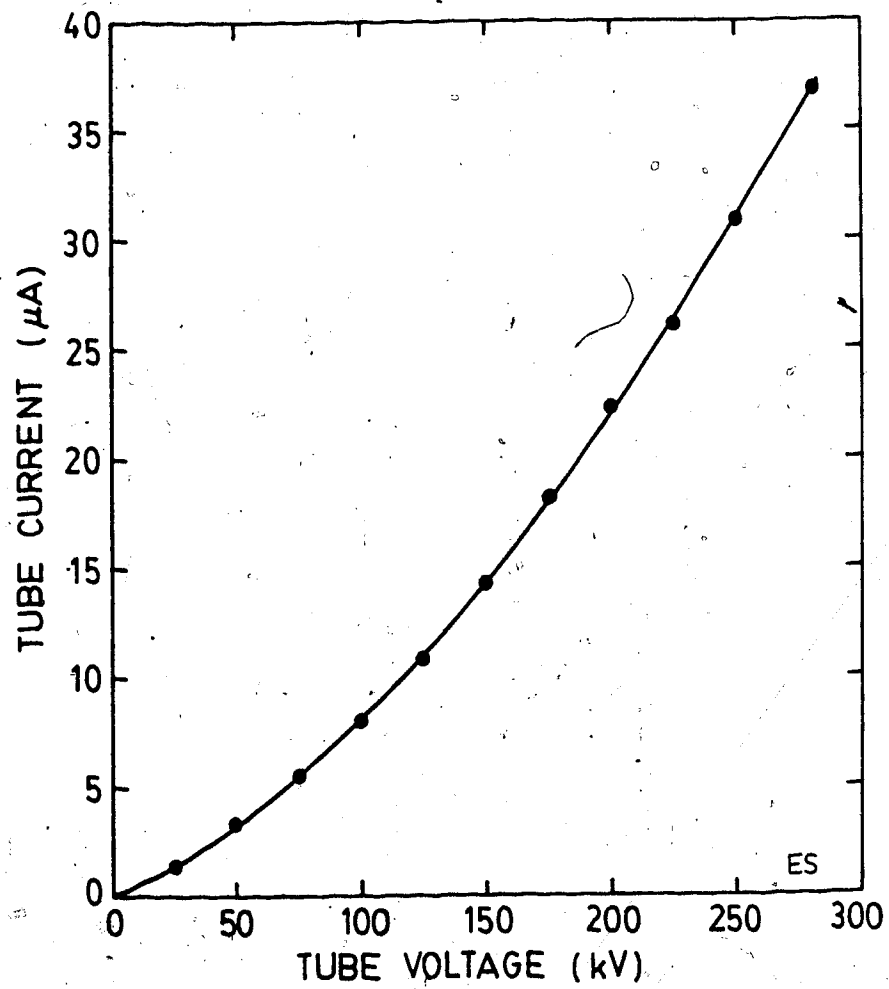


Figure 2.32 Acceleration Tube Column Current

10 minutes during which time the pressure stayed the same. Six minutes after the voltage was reduced to zero, gas pressure recovered to 0.22 mPa ( $1.65 \cdot 10^{-6}$  Torr). Apparently, resistive heating of the spacer-resistors did not cause a significant outgassing load in the acceleration tube. In other words, heat dissipation by radiation was adequate to maintain spacer-resistor temperature at acceptable levels. Moreover, no changes in the electrical characteristics of the tube were evident during subsequent high voltage tests, indicating that the properties of the spacer-resistors do not change when operated under vacuum in this way.

### 2.3.3 Ion Gun

#### 2.3.3.1 Ion Source

A test stand was arranged in which a stainless steel beam collector plate was located 65 mm (2.56 in.) from the ion source exit. A secondary electron suppression electrode was located close to the beam collector. With air in the ion source gas reservoir, the recommended starting procedure was followed (see Sec. 2.2.1.3 Ion Source), and an arc current of 0.5 A was successfully obtained. Arc voltage, which was established by a current regulated supply, ranged from 60 to 80 V during a number of trials. Gas pressure readings for the discharge chamber were uncalibrated at the time and consequently, are not given. Pressure on the extractor side of the ion source, however, was near 3 mPa ( $2 \cdot 10^{-5}$  Torr) during ion source operation. (The pressure was 30  $\mu$ Pa, or  $2 \cdot 10^{-7}$  Torr, with the ion source filament idling at 10 A and no gas flow from the reservoir.) Figure 2.33 shows the ion currents that were collected for various extraction potentials. The secondary electron suppressor was set between -50 and -70 V with respect to the collector to obtain true currents on the collector. Similar ion source performance was obtained with argon in the ion source gas reservoir.

On dismantling this apparatus, discolourations were noted on some of the electrodes. The collector had a well defined central white region about 8.9 mm (0.35 in.) in diameter surrounded by a dark grey strip that was approximately 5 mm (0.2 in.) wide.

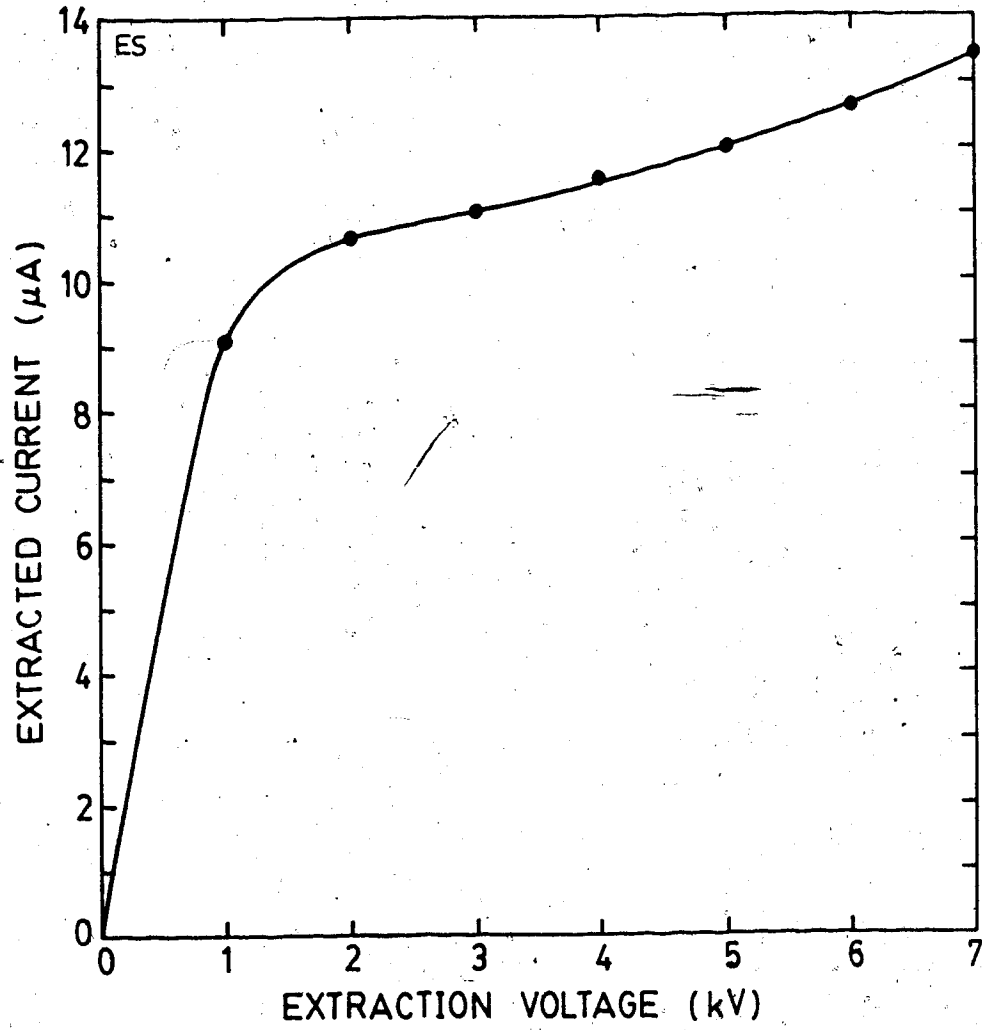


Figure 2.33 Ion Source Performance



Surrounding the beam hole in the extraction electrode, there was a dark grey border, about 13 mm (0.5 in.) in diameter, on the side of the electrode facing the ion source anode. The patterns of discolouration can be explained by considering the divergence of an ion beam emanating from the anode hole using the theoretical expressions of Chavet and Bernas (1967) for a circular emitting area. The geometry of the test apparatus is indicated in Fig. 2.34. Assuming that there is enough tungsten being sputtered off the cathode inside the ion source discharge chamber and subsequently ionized so as to contribute  $0.2 \mu\text{A}$  of beam current with an extraction voltage of 1 kV—the lowest extraction voltage that was used during the tests—the angle of dispersion of the envelope of a tungsten beam would be  $645 \text{ mrad}$  ( $37.0^\circ$ ). This is consistent with the pattern of dark grey regions on the extraction electrode and collector plate. At higher voltages, even though a slightly higher tungsten ion current would likely be drawn, the divergence angle would be smaller. The dark regions may therefore be deposited tungsten. As for the central white spot, it is accounted for by realizing that the current of gas ions would likely have sputtered the deposited tungsten off the collector. An extraction voltage of 1 kV produces  $9 \mu\text{A}$  of beam current (see Fig. 2.33). If the main constituent of this current is  $5 \mu\text{A}$  of  $\text{N}_2^+$ —an assumption that is verified in Sec. 2.3.3.3—the divergence angle of the gas ions would be  $122 \text{ mrad}$  ( $7.0^\circ$ ), which corresponds well with the observations. Again, at higher extraction potentials, the divergence angle would be smaller. (Incidentally, the technique of Chavet and Bernas suggests that the shape of the plasma boundary under the operating conditions of this ion source is convex, that is, it bulges out of the discharge chamber towards the extractor.)

#### 2.3.3.2 Ion Source with Lens

With argon in the ion source gas reservoir and an extraction voltage of 4 kV, ion beam cross sections were observed on a phosphor coated collector plate that was moveable along the beam axis. The location of the collector was measured from the midpoint of the lens center electrode. For distances less than 150 mm (5.9 in.) but greater than 130 mm (5.1 in.), the lens produced a minimum spot size that was approximately 1 mm (0.04 in.)

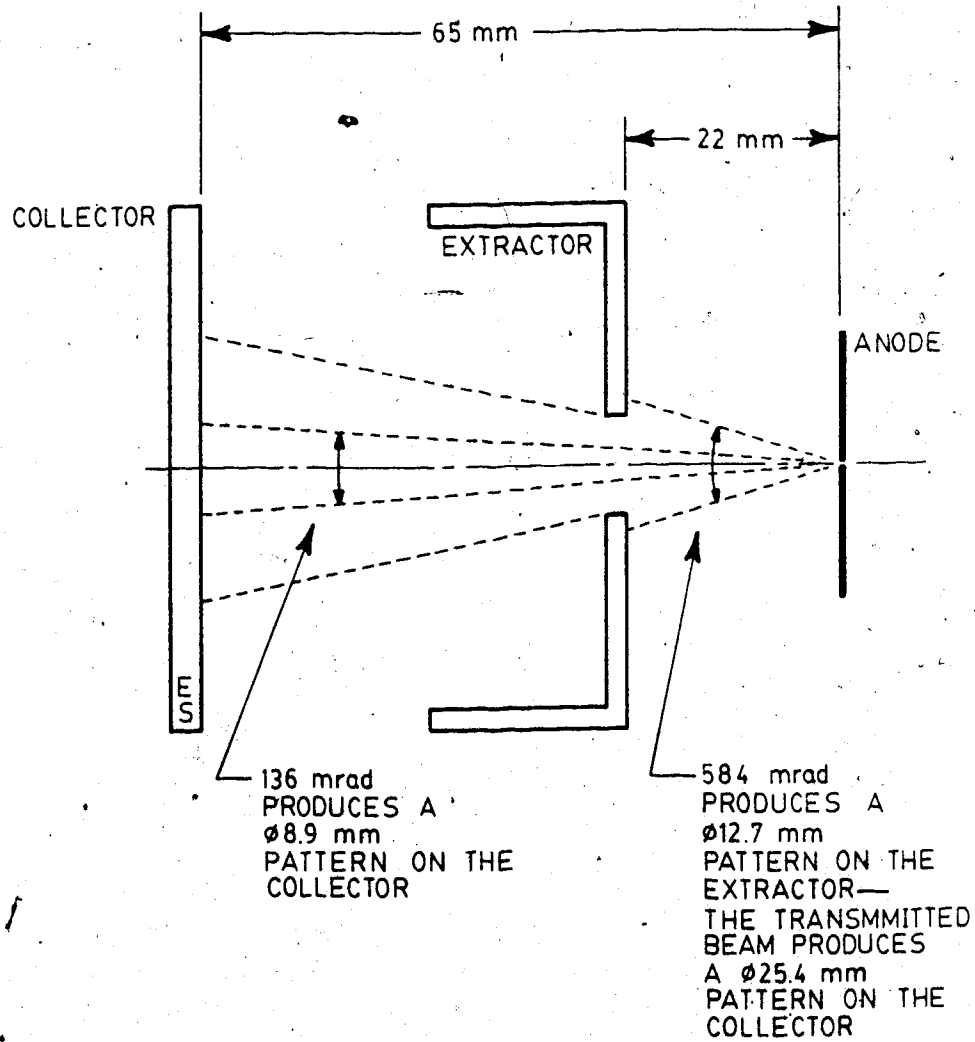


Figure 2.34 Collector Geometry

in diameter. Between 150 and 300 mm (5.9 and 11.8 in.), the spot was about 3 mm (0.1 in.) in diameter. Beyond 300 mm, the image on the phosphor became roughly elliptical, 3 mm by 6 mm (0.1 in. by 0.2 in.). A current of between 8 and 10  $\mu\text{A}$  was recorded from the coated collector at all collector positions, which corresponds to the output current of the ion source alone. (The phosphor coated collector, therefore, allows a good approximation to the true beam current to be measured, assuming no current is lost as the beam traverses the lens.)

Only slight variation of the lens voltage near 3600 V produced the minimum spot size for collector locations less than 300 mm (5.9 in.). Consider the focal properties of the idealized lens (see Sec. 2.2.1.3 Lens) as given in Fig. 2.11. Using standard expressions from Gaussian optics (Galejs and Rose 1967, pp. 312-313; El-Kareh and El-Kareh 1970, pp. 56-59), with a point-source object, that is, the anode hole, located 79.0 mm (3.11 in.) from the midpoint of the lens, the image position can be expressed as a function of lens voltage. The result is plotted in Fig. 2.35. Accordingly, the image is 134.1 mm (5.28 in.) from the lens center for a lens voltage of 3640 V. At 3480 V, the lens would theoretically image the beam at 260.0 mm (10.23 in.). For the idealized lens, therefore, a swing of 160 V would account for the range of image locations that were considered.

The transverse expansion of the beam due to space charge forces, however, changes this view. In part, it accounts for the nonzero spot sizes. Again, from the method of Chavet and Bernas (1967), assuming an ion current of 10  $\mu\text{A}$ , the divergence of an argon beam at the anode hole with an extraction potential of 4 kV is approximately 82.0 mrad (4.70°). Assuming an analysis based on point source optics is valid, there is an angular magnification of 0.65 at 3640 V lens voltage (see Fig. 2.35), which means the beam envelope initially converges to an image point at an angle of 26.6 mrad (1.53°) to the beam line axis. Furthermore, to facilitate calculations, assume the space charge forces begin to act after the beam passes the center electrode of the lens. Under these conditions, the laminar space charge effect produces a waist position that is beyond the theoretical image

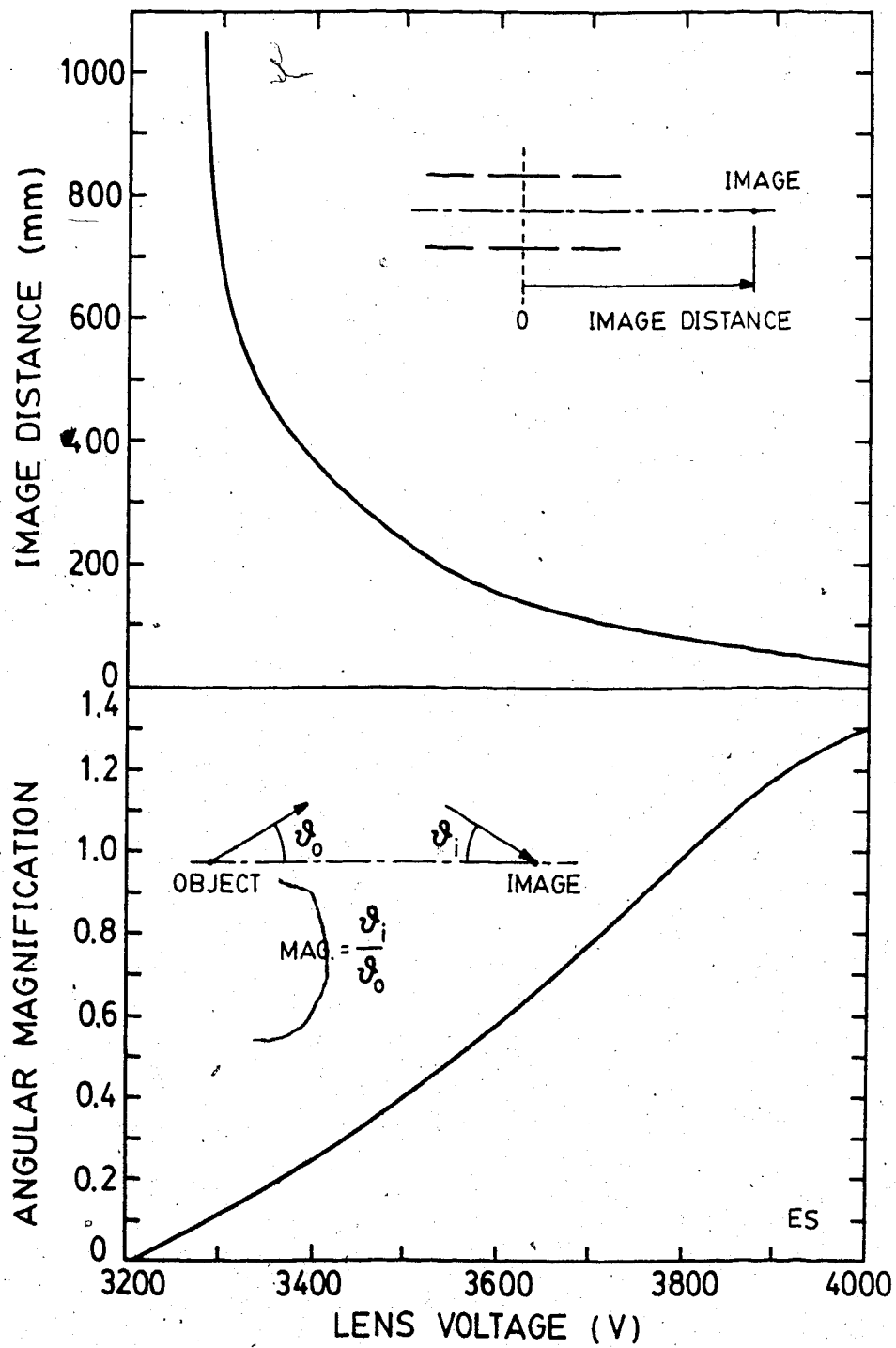


Figure 2.35 Lens Imaging Characteristics

distance at 162.8 mm (6.40 in.) (Dahl 1973, p. 114, Fig. 26.2). Therefore, it would take a higher lens voltage, 3680 V, to establish a waist position as close as 140.6 mm (5.54 in.) and, 3500 V to establish a waist at 234.9 mm (9.26 in.). But, at a particular collector location, the waist will not be the minimum spot size. To establish a minimum spot size at a particular collector location, the beam waist must be formed upstream of the collector (Thompson and Headrick 1940; Hollway 1952). Consequently, 3680 V produces the minimum spot diameter at 149.7 mm (5.90 in.) not 140.6 mm.

Notwithstanding, the difference in the size of the minimum spot and waist is slight. The error in visually estimating the spot sizes from the image on the phosphor coated collector is greater than the expected difference in size between minimum spot and waist. As a result, a minimum spot size would be detected over a range of collector locations for one setting of lens voltage. For example, at 3600 V the location of the minimum spot is calculated to be 217.8 mm (8.56 in.). At that distance, the best estimate of the spot size was 3.2 mm (0.13 in.). The waist position and diameter are then calculated to be 183.8 mm (7.24 in.) and 2.3 mm (0.09 in.) respectively. Since the error in estimating image diameter was the order of  $\pm 0.5$  mm (0.02 in.), a minimum spot would be observed over the 40 mm distance between waist and minimum spot size for the same voltage, 3600 V. Moreover, the beam is symmetric about the waist; hence, the range would extend from about 140 to 220 mm. This is likely what happens for the range of collector locations from 130 to 300 mm over which imperceptible variations in lens voltage in the vicinity of 3600 V produced the minimum beam spot. At greater distances, lower lens voltages were used. Then, because the distinction between waist diameter and minimum spot size becomes apparent, lens voltage had to be adjusted. Whereas Gaussian optics predicts a swing in lens voltage of 160 V to establish a focus over the range of collector locations investigated, only very small lens voltage adjustments had to be made. Note that, in the preceding analysis, the ion source was assumed to behave like a point-source emitter, that is, the initial thermal velocities of the ions and the aberrations introduced by the extraction system were

neglected. Furthermore, nonlaminar space charge effects were ignored, as were lens aberrations.

### 2.3.3.3 Ion Source with Lens and Filter

The relationship between the magnetic flux density and the magnet coil current and magnet coil voltage in the mass filter were experimentally determined; see Fig. 2.36. A semi-empirical mass selection law for the filter can be subsequently derived from the filter balance equation,  $v_0 = E_0 / B_0$ . Consider the following.

$$\text{kinetic energy} = qV_0 = \frac{1}{2} m_0 v_0^2, \quad q = Ze \text{ and } m_0 = nM$$

Whence,

$$v_0 = \sqrt{\frac{2qV_0}{m_0}}$$

where  $v_0$  is the ion velocity in m/s;  $V_0$  is the beam voltage, 4 kV in the present system;  $e$  is the electronic charge,  $1.60 \cdot 10^{-19}$  C;  $Z$  is the charge state of the ion;  $m_0$  is the ion mass in kg;  $n$  is the (unified) atomic mass unit, that is,  $1.66 \cdot 10^{-27}$  kg; and  $M$  is the ion mass in atomic mass units. Assuming a uniform electric field in the gap between filter plates, with plate separation equal to 18.3 mm (0.72 in.),  $E_0 = V/0.0183$ , with  $V$  being the plate-to-plate voltage. Substituting the above expression for  $v_0$  into the filter balance equation and solving for  $B_0$  yields

$$B_0 = 0.62V \sqrt{\frac{M}{Z}} 10^{-4}$$

From Fig. 2.36

$$B_0 = (320I + 30) 10^{-4}$$

Hence,

$$\frac{M}{Z} = \left( \frac{320I + 30}{0.62V} \right)^2$$

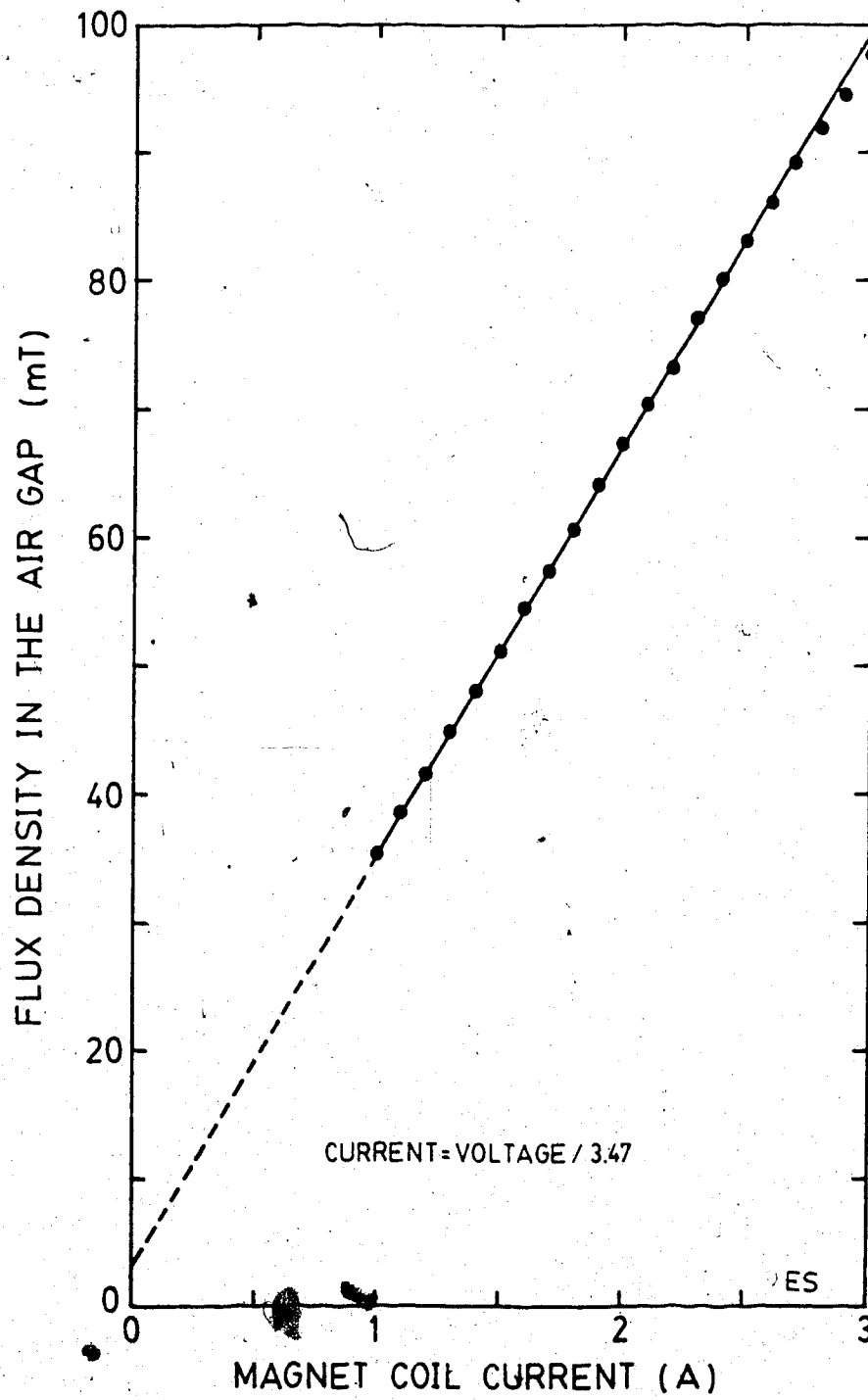


Figure 2.36 Magnet Characteristics

or, with  $I=U/3.47$ ,

$$\frac{M}{Z} = \left( \frac{92.2U+30}{0.62V} \right)^2$$

where  $I$  is the magnet coil current, and  $U$ , the magnet coil voltage.

The ion beam generated by the source was collected on a phosphor coated plate that was located approximately 420 mm (16.5 in.) away from the exit of the filter chamber. In addition, an uncoated collector with a secondary electron suppressor and a grounded shield electrode with a 25.4 mm (1.00 in.) square aperture was used.

Five images were observed on the phosphor covered collector for a filtered beam that was generated with air as the source gas. While the largest of the images was centered on the collector with a magnet current of 2.4 A, the following filter voltages, measured with respect to chassis ground (refer to Fig. 2.13), produced an approximately circular 13 mm (0.5 in.) diameter spot size. (The units are volts.)

L1 = +80	R1 = +2
L2 = +80	R2 = -74
L3 = +60	R3 = +10
MS = -90	
LP = +152	RP = -90

The lens voltage used was 3290 V. The vertical deflection voltage was 75 V, and the deflection voltage balance control was central.

With a plate-to-plate voltage of 242 V and a magnet current of 2.4 A, the mass-to-charge ratio of the ions in the centered image is calculated from the mass selection formula to be 28.3. (The units of mass-to-charge ratio, that is,  $M/Z$ , are atomic mass units per charge state.) The image was centered at a variety of other plate voltage and magnet current combinations, corresponding to mass-to-charge ratios in the range 27 to 32. This image could therefore represent either  $N_2^+$ ,  $O_2^+$ , or a mixture of both. The average



$M/Z$  ratio is 29.6, which favours  $N_2^+$ . Moreover, the separation of  $N_2^+$  and  $O_2^+$  at the collector location with a filter voltage of 242 V is predicted to be approximately 9.9 mm (0.39 in.) (see Sec. 2.2.1.3 Mass Filter), but there was no indication that there were two distinct images on the collector. In addition, when  $N_2$  gas was used in the source instead of air the same image shape was obtained at the same filter settings. Therefore, the main image on the collector was likely that of an  $N_2^+$  beam.

The second largest image was also centered on the collector for a variety of filter settings. The range of corresponding  $M/Z$  ratios suggests that the image is either that of an  $N^+$  or  $H_2O^+$  beam. The average, however, is 14.6, and it is therefore concluded that the secondary image represents  $N^+$ .

With the  $N_2^+$  image centered at a plate-to-plate voltage of 135 V and a magnet current of 1.35 A, the  $N^+$  image was separated by approximately 41 mm (1.6 in.). The value of image separation predicted by the expression in Sec. 2.2.1.3 Mass Filter, is 31 mm (1.2 in.). A source of error that may contribute to both mass selection and dispersion calculations, besides the error in visually estimating image position, is the effect of fringe fields. Wilson and Brewer (1973, p. 227) indicate that the magnetic field extends beyond the limits of the electric field. The net effect of this uncompensated magnetic fringe field is to deflect the beam in the direction of the positive plate of the filter. In the case of an  $N^+$  beam—which is dispersed by filter action towards the positive plate and, hence, is diverging at the filter exit—the magnetic fringe field imposes an additional force that enhances filter dispersion. As a consequence, the observed and calculated values for separation do not agree.

The total beam current, contributed by all the mass components in the beam, as measured from the phosphor collector, was 9.5  $\mu A$ . With the apertured collector, the  $N_2^+$  beam was measured to be 5  $\mu A$ . A 5  $\mu A$  beam of  $N_2^+$  diverges from the anode hole with an angle of 40.0 mrad (2.28°) (Chavet and Bernas 1967). The lens voltage of 3290 V would, theoretically, focus that beam to a point 794.5 mm (31.29 in.) from the lens center (see

Sec. 2.3.3.2 and Fig. 2.35). This is consistent with the location of the beam collector, which is 786 mm (31.0 in.). Were it not for the influence of space charge, the beam would converge with an angle of 2.3 mrad (0.13°) to the beam line axis. But, upon considering the laminar space charge forces, the result is obtained that a waist is formed 90.9 mm (3.58 in.) from the lens center or 695.3 mm (27.40 in.) upstream of the collector (Dahl 1973, p. 114, Fig. 26.2). The beam cross section on the collector was observed to be 13 mm (0.5 in.). If the filter is assumed to behave like a drift space, a  $5 \mu\text{A N}_2^+$  beam would be expected to expand much more than that (Dahl 1973, p. 114, Fig. 26.3). The focussing power of this particular filter is weak, with a maximum focal length of 1520 mm (Seliger 1972), but when the focussing power of the magnet fringe field is added, the total effect may be sufficient to counteract the space charge expansion of the beam as it traverses the filter. Consider the following analysis and refer to Fig. 2.37.

When the  $5 \mu\text{A N}_2^+$  cone of ions that emanates from the anode with an angle of 40.0 mrad (2.28°) is projected to the entrance boundary of the lens center electrode, a 1.77 mm (0.070 in.) diameter is obtained. For the lens in Sec. 2.3.3.2, the observed beam diameter at 3600 V can be used to extrapolate the beam diameter to the exit of the lens center electrode. The result is that the beam diameter at the exit of the center electrodes is 3.6 times the input diameter. If this same factor is used here, the exit beam diameter is estimated to be 6.4 mm (0.25 in.). Consequently, the waist diameter would be 6.1 mm (0.24 in.). On the unverified assumption that the effect of the filter is to exactly transfer the radial and axial velocity components of each ion in the beam from filter entrance to filter exit, the beam diameter is predicted to be 13.9 mm (0.55 in.) at the collector (Klemperer and Barnett 1971, p. 274, Fig. 8.2). This is in good agreement with observations. As in Sec. 2.3.3.2, the analysis was performed for idealized ion optical circumstances. The focal properties of the filter are likely more complex than what has been assumed, but this approach gives satisfactory results and will be useful in Sec. 3.3.

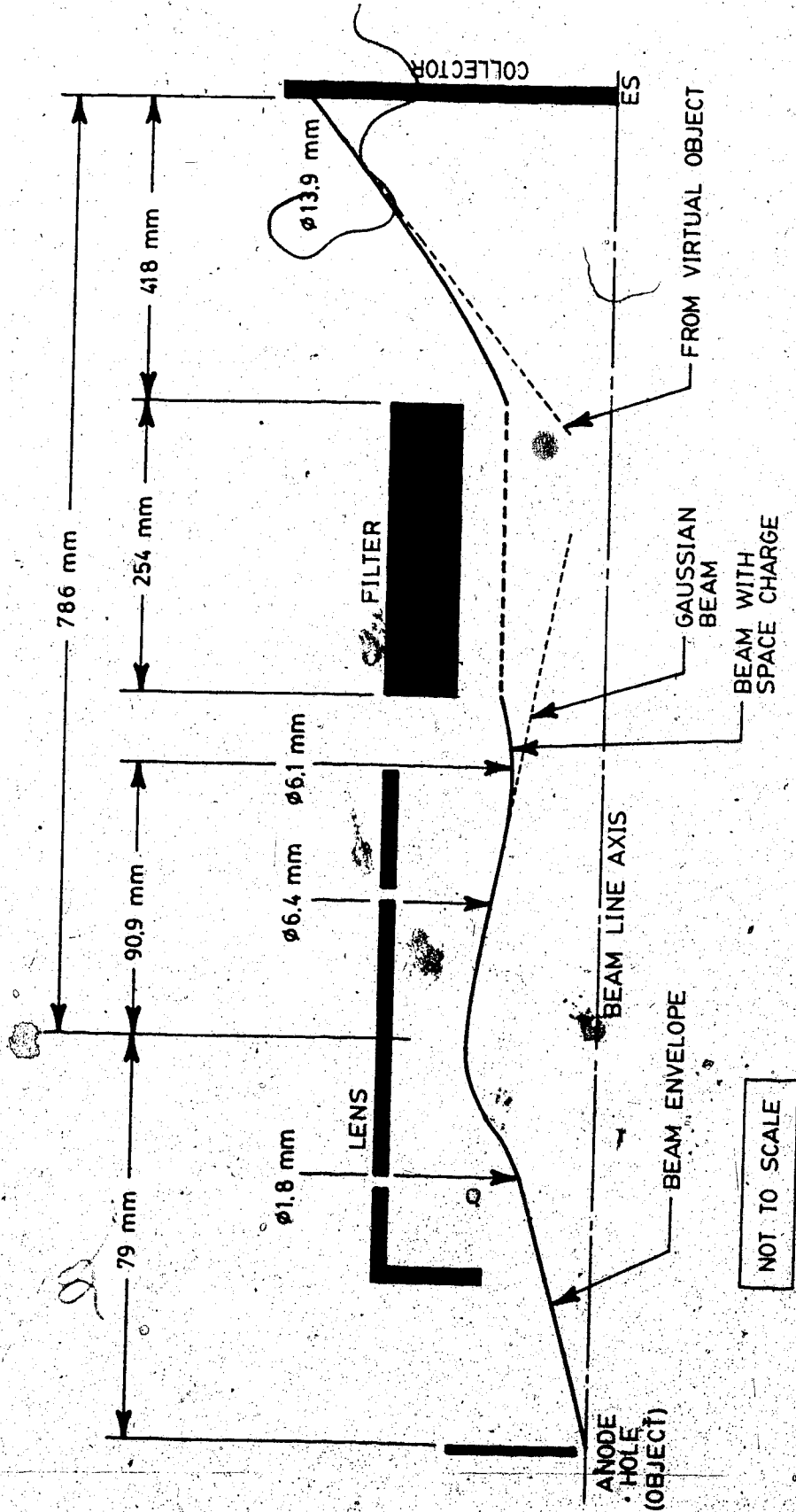


Figure 2.37 Ion Beam Envelope

Operating characteristics of an earlier version of the Colutron ion gun that used a 600 G filter are reported by Wilson and Jamba (1971). They studied the device with 4.5  $\mu\text{A}$  total beam current. The spot size they obtained for  $\text{N}_2^+$  was 7.5 mm (0.30 in.) diameter on a collector that was located 440 mm (17.3 in.) from the filter exit. Their filtered beam was slightly divergent. Both of these results support the observations from the present system.

### 2.3.4 Terminal Mounted Power Supply

A resistive load was connected to the electric generator of the system that was described in Sec. 2.2.3.3 Power Source Inside the Terminal. The results of a loading test appear in Fig. 2.38. Whenever the power hydraulics ran for more than 15 minutes, the coolant system was run. It kept the oil in the reservoir at 55°C (131°F) (without coolant flow, oil temperature was 85°C, or 185°F).

The power circuit of Fig. 2.24 may be analyzed using standard formulae from Hedges (1969, Vol. 1, p. 126; Vol. 3, p. 17). When driven at 189 rad/s (1800 rev/min), the hydraulic pump displaces 3.339  $\text{m}^3/\text{h}$  (14.7 gal/min). The maximum pressure that the pump can develop is then 4.9 MPa (700 lbf/in<sup>2</sup>), assuming a pump efficiency of 80%. Subtracting the pressure drop across the entire length of hose and across the quick disconnectors, the maximum pressure at the hydraulic motor would be about 4.3 MPa (630 lbf/in<sup>2</sup>). A hydraulic motor experiences a slip of 0.023  $\text{m}^3/\text{h}$  (0.1 gal/min) for each 0.7 MPa (100 lbf/in<sup>2</sup>) of oil pressure. As a consequence, the effective fluid input to the hydraulic motor is about 3.180  $\text{m}^3/\text{h}$  (14.0 gal/min) at 4.3 MPa (630 lbf/in<sup>2</sup>). Theoretically, the system should be able to deliver a maximum of 3.84 kW (5.15 HP) of mechanical power at the hydraulic motor shaft—an efficiency of 68.5% from electric motor shaft to hydraulic motor shaft. The speed of hydraulic motor shaft rotation should be 162 rad/s (1540 rev/min) and 323 rad/s (3080 rev/min) for the generator.

In a preliminary load test of a prototype hydraulic system, a dc generator, rotating at 294 rad/s (2800 rev/min), delivered 55 A at 25 V, or 1375 W, with a pump pressure of 5.6 MPa

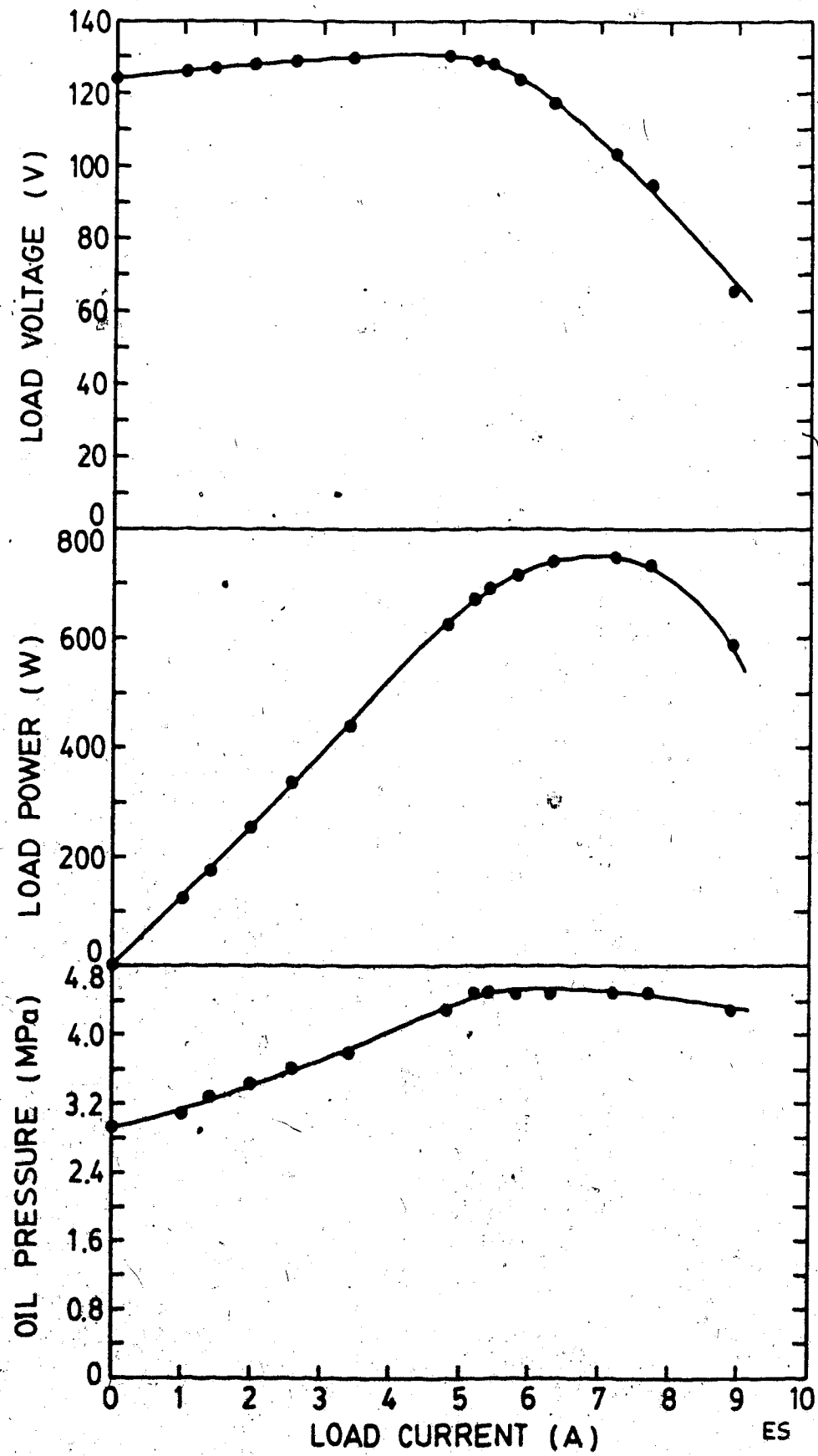


Figure 2.38 Hydraulic System Load-Test Data

(660 lbf/in<sup>2</sup>). The performance of the system has deteriorated since then. A probable cause for this may be that the hydraulic motor was operated for several hundred hours without a drain line. In fact, the drain port had been plugged. Damage may be manifesting itself in an excessive slip so that the hydraulic motor speed is lower. Furthermore, the ac generator does not supply its rated output. The present overall efficiency of the system, from electric motor shaft to electric generator load, is 13.2% at 127 V and 5.4 A (Fig. 2.38). Replacing the present asynchronous-type ac generator with an alternator and servicing the hydraulic motor may improve the performance of the system.

A high voltage test of the five insulating lengths of hydraulic line was conducted. The total current generated by the high voltage power supply (see Fig. 2.17) was recorded as a function of time with 280 kV applied, both fluid systems circulating oil, and no load on the electric generator. The result is presented in Fig. 2.39. After subtracting 40  $\mu$ A for acceleration tube current and 50  $\mu$ A for leakage current through the voltage doubler circuit, Fig. 2.39 shows that the hoses and tubes behaved as specified. That is, no more than 50  $\mu$ A was expected to flow down each of the five lengths of hose at 280 kV for five minutes (Sec. 2.2.3.3 Power Source Inside the Terminal). Beyond five minutes the current rose but the trend was a slower rate of increase as time progressed.

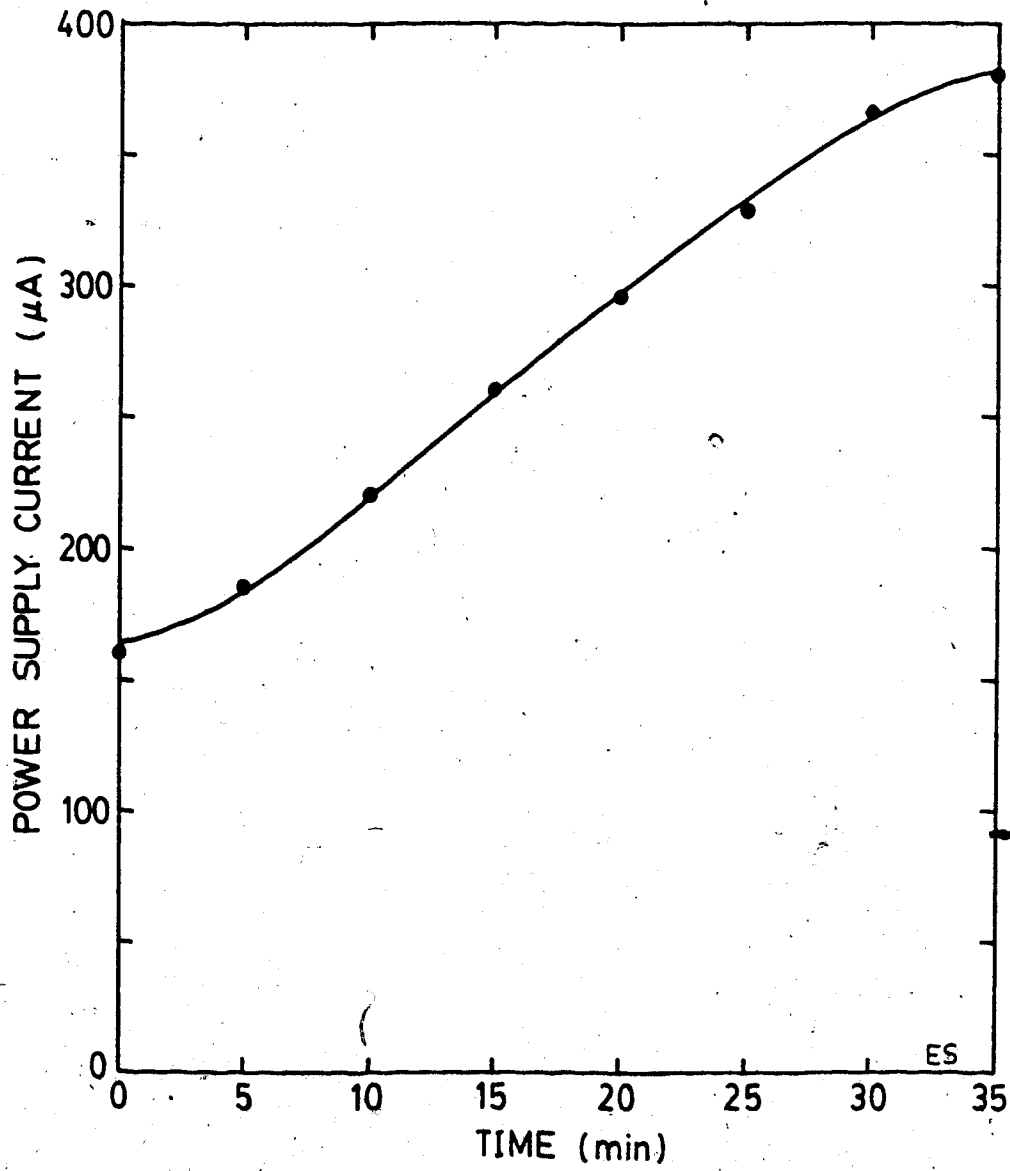


Figure 2.39 Hydraulic Hose Insulation-Test Results

### 3. Accelerator Performance and Analysis

#### 3.1 Introduction

Once all of the individual system components demonstrated satisfactory performance, the parts were assembled into a whole. The layout of the facility is shown in Fig. 2.30. A line drawing of the accelerator is given in Fig. 3.1 (see also Fig. 2.18), and the control equipment appears in Figs. 3.2, 3.3, and 3.4. Following assembly, a commissioning procedure verified that all the interdependent equipment functioned properly. That is, during high voltage tests, the remote control system was used to successfully manipulate the ion gun power supplies which were being energized from the ac power generating system in the high voltage terminal. Beam trials were then begun.

In the following chapters, the results of two accelerator tests performed with an  $N_2^+$  beam are outlined. One test was done to evaluate the current distribution in the beam at the fixed target location for a variety of accelerator potentials, from 50 to 280 kV. These results are then discussed and compared to expected performance. The other test was an observation of the radiation pattern that was generated at maximum acceleration voltage. In the final section, 3.5, some recommendations are suggested that may, if implemented, improve the reliability of the accelerator and make it easier to operate. As well, an introduction is given regarding the adaptation of this machine to its intended future uses, that is, RBS analysis and ion implantation.

#### 3.2 Performance Data

The accelerator system was run several times following the procedures outlined in the Appendix. Air was the source gas, and the objective was to accelerate  $N_2^+$ . The highest beam current,  $1.5 \mu A$ , was recorded at 280 kV.

Maximum beam currents were obtained for ion gun lens voltages between 3200 and 3300 V. Optimum values for lens voltage drifted upward as a particular beam trial progressed.



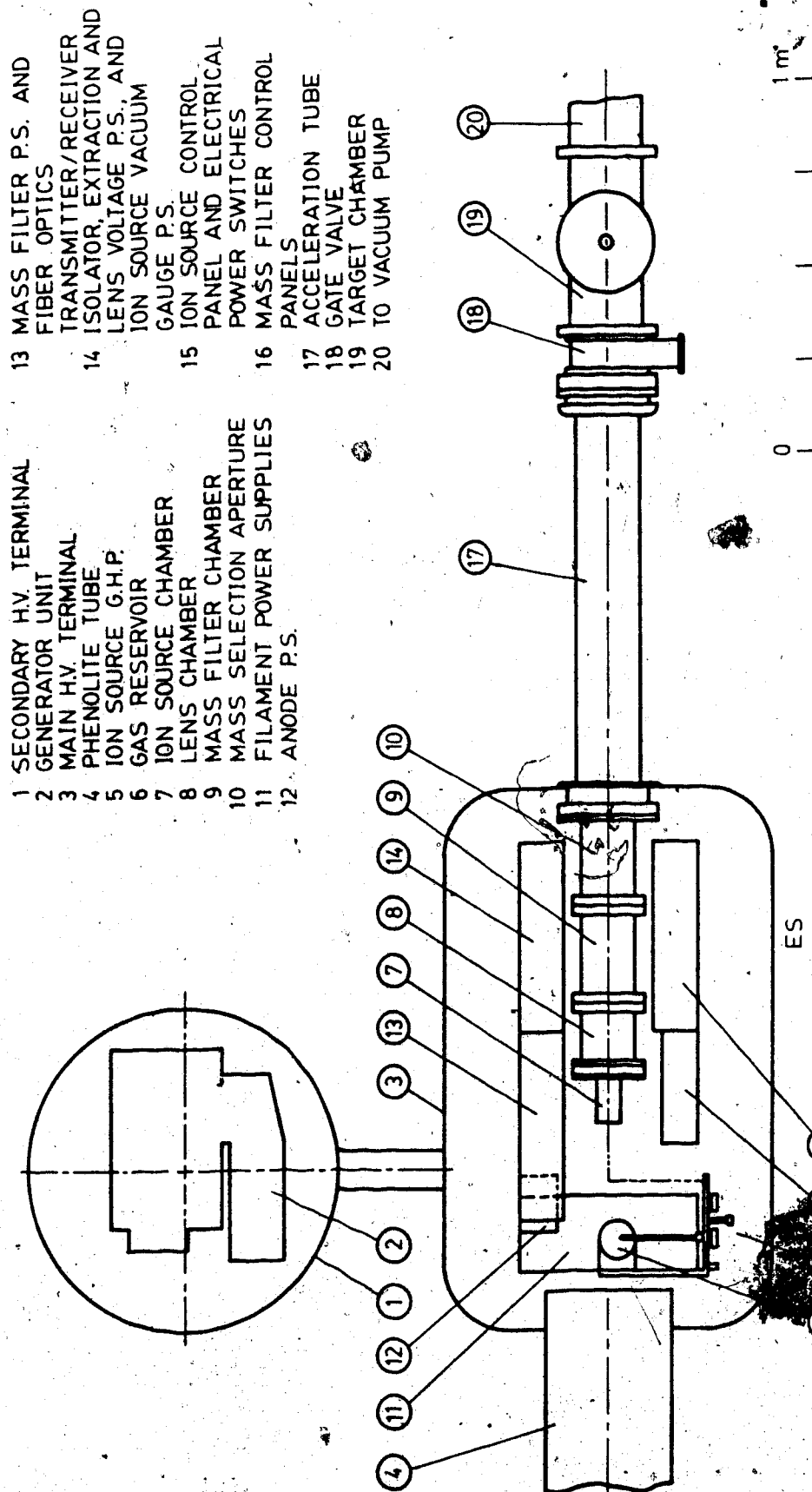


Figure 3.1 Plan View of the Accelerator Beam Line

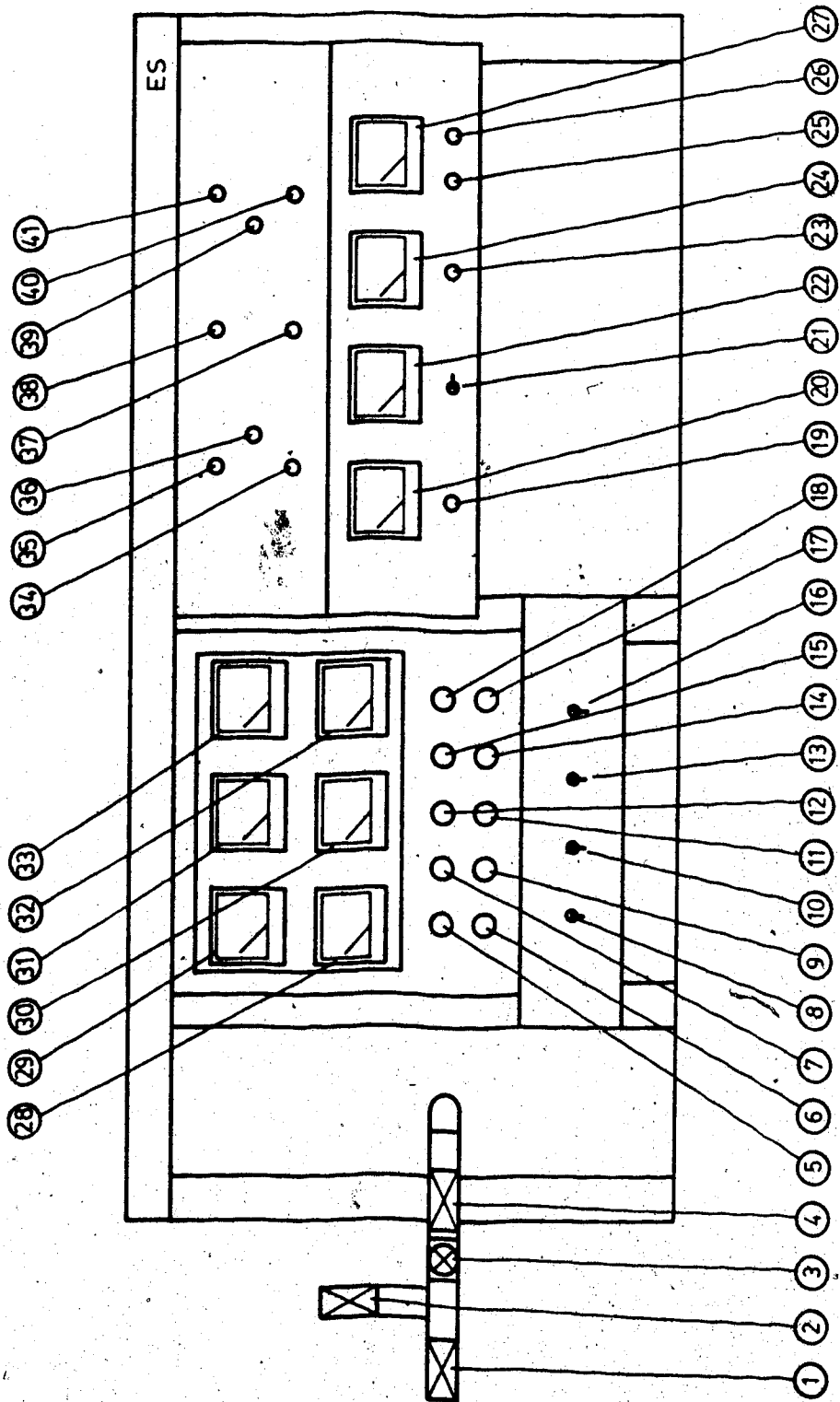


Figure 3.2 Control Panels Inside the High Voltage Terminal

- |    |   |    |   |
|----|---|----|---|
| 1  | ION SOURCE G.H.P. VALVE C                                     | 28 | FURNACE FILAMENT MONITOR                      |
| 2  | VALVE D   | 29 | ION SOURCE GAS RESERVOIR PRESSURE MONITOR     |
| 3  | NEEDLE VALVE--VALVE B   | 30 | SOURCE FIL. MONITOR                           |
| 4  | VALVE A   | 31 | ION SOURCE DISCHARGE CHAMBER PRESSURE MONITOR |
| 5  | ION SOURCE FILAMENT SELECTOR SWITCH                           | 32 | ANODE MONITOR                                 |
| 6  | 4 KV ENABLE/DISABLE SWITCH                                    | 33 | LENS VOLTAGE MONITOR                          |
| 7  | FURNACE FILAMENT CONTROL                                      | 34 | L1 FILTER GUARD RING CONTROL                  |
| 8  | MASTER POWER SWITCH   | 35 | R1 CONTROL                                    |
| 9  | FURN. FIL. MONITOR AND REMOTE SWITCH                          | 36 | FILTER PLATE-TO-PLATE VOLTAGE BALANCE CONTROL |
| 10 | FILAMENT SUPPLY POWER SWITCH                                  | 37 | L2 CONTROL                                    |
| 11 | SOURCE FIL. MONITOR AND REMOTE SWITCH                         | 38 | R2 CONTROL                                    |
| 12 | SOURCE FIL. CONTROL   | 39 | MIDDLE GUARD RING CONTROL                     |
| 13 | ANODE SUPPLY POWER SWITCH                                     | 40 | L3 CONTROL                                    |
| 14 | ANODE MONITOR AND REMOTE SWITCH                               | 41 | R3 CONTROL                                    |
| 15 | ANODE SWITCH AND CONTROL                                      |    | ES  |
| 16 | FILTER PLATE AND MAGNET AND FIBER OPTIC SUPPLIES POWER SWITCH |    |   |
| 17 | 4 KV ON/OFF AND REMOTE SWITCH                                 |    |   |
| 18 | LENS VOLTAGE CONTROL  |    |   |
| 19 | FILTER MAGNET CONTROL   |    |   |
| 20 | FILTER MAGNET VOLTAGE MONITOR                                 |    |   |
| 21 | FILTER MAGNET REMOTE SWITCH                                   |    |   |
| 22 | FILTER MAGNET CURRENT MONITOR                                 |    |   |
| 23 | FILTER PLATE VOLTAGE CONTROL                                  |    |   |
| 24 | FILTER PLATE-TO-PLATE VOLTAGE MONITOR                         |    |   |
| 25 | VERTICAL DEFLECTION PLATE VOLTAGE CONTROL                     |    |   |
| 26 | DEFLECTION PLATE VOLTAGE BALANCE CONTROL                      |    |   |
| 27 | DEFLECTION PLATE VOLTAGE MONITOR                              |    |   |

Figure 3.3 Legend for Fig. 3.2

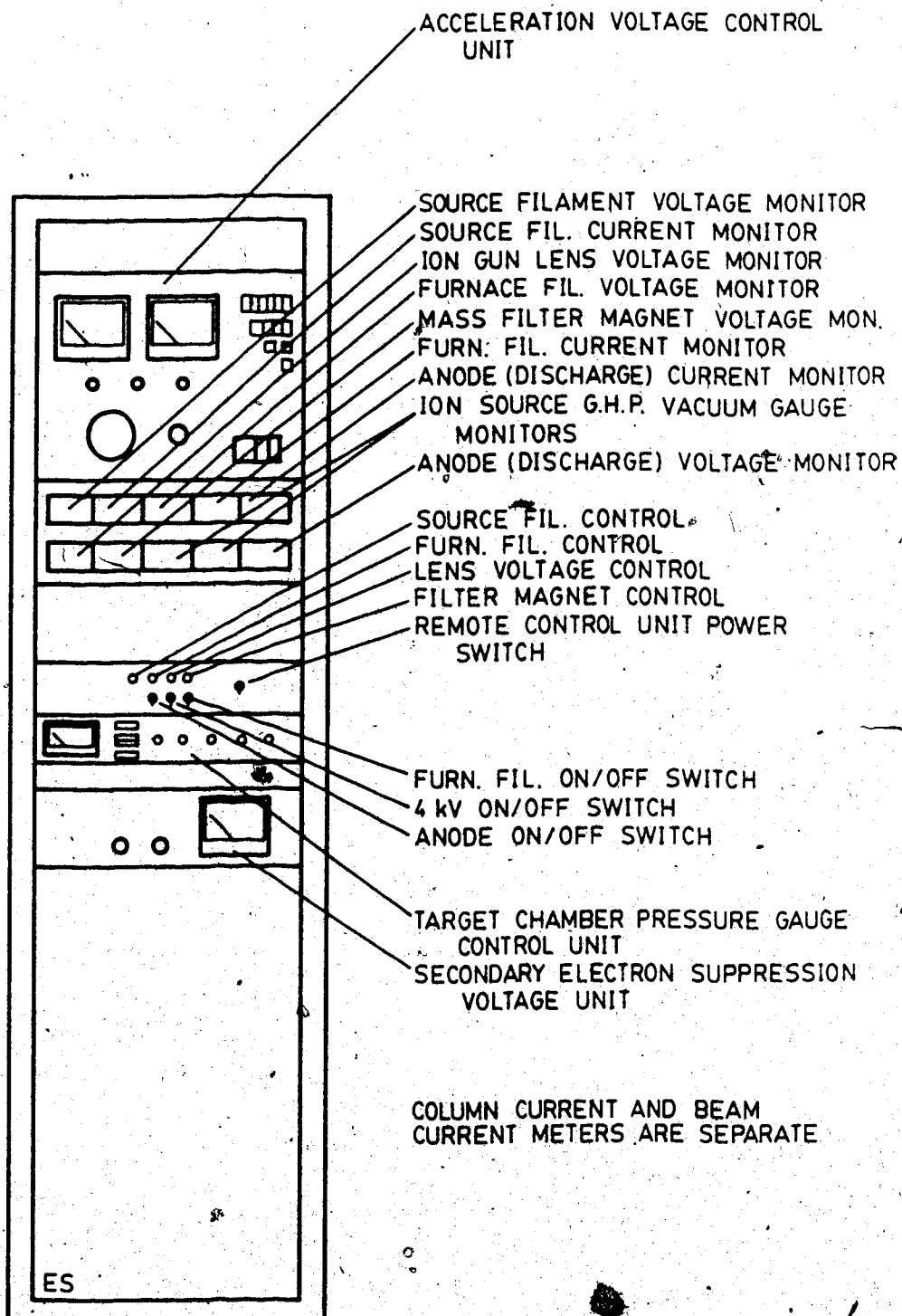


Figure 3.4 Remote Control Unit

A similar trend was observed with magnet current. At the beginning of a run, maximum beam current was obtained with 7.8 to 8.0 V magnet voltage. Magnet voltage had to be gradually increased during the run to maintain a constant beam current. After about one hour, the voltage was in the range 8.2 to 8.6 V. Also, during the time when maximum beam current was being collected in the target chamber, column current was approximately  $1 \mu\text{A}$  higher than its expected value.

Figure 3.5 shows how  $\text{N}_1^+$  beam current varied as the target-apparatus shutter was moved in front of the beam. As viewed on the quartz window, the beam was concentrated in an approximately circular spot. There was a less intense pattern of scintillation surrounding the main spot which varied in size and shape as the beam voltage was changed. The size of the main spot, however, remained constant at about 2 to 3 mm (0.08 to 0.1 in.) diameter regardless of acceleration potential or beam current; see Fig. 3.6. The main image was centered laterally on the screen, but was shifted slightly upward. It always remained stationary.

### 3.3 Analysis of Performance Data

From the filter mass selection formula in Sec. 2.3.3.3, an  $\text{N}_1^+$  beam should have appeared for a magnet voltage of 8.3 V. During the beam trials, however, magnet voltage had to be varied. As such, maximum accelerator beam currents were obtained for magnet voltages representing  $M/Z$  ratios that ranged from 25 through 30. On the basis of the experimental data on mass filter performance given in Sec. 2.3.3.3, there could only be one ion species that was injected into the acceleration tube, namely,  $\text{N}_1^+$ .

Lens voltages in the range 3200 to 3300 V produced maximum accelerator beam current. For example, a lens voltage of 3280 V was used during one of the many trials. Theoretically, at 3280 V, the lens would image the beam 1025 mm (41.0 in.) away from the lens (see Sec. 2.3.3.2 and Fig. 2.35). The distance from the lens to the mass selection aperture is 495 mm (19.5 in.). A 4 kV  $5 \mu\text{A}$  beam of  $\text{N}_1^+$  diverges from the anode with an angle of 40.0 mrad ( $2.28^\circ$ ) (Chavet and Bernas 1967). The lens causes the beam to, initially, converge to a point image at an angle

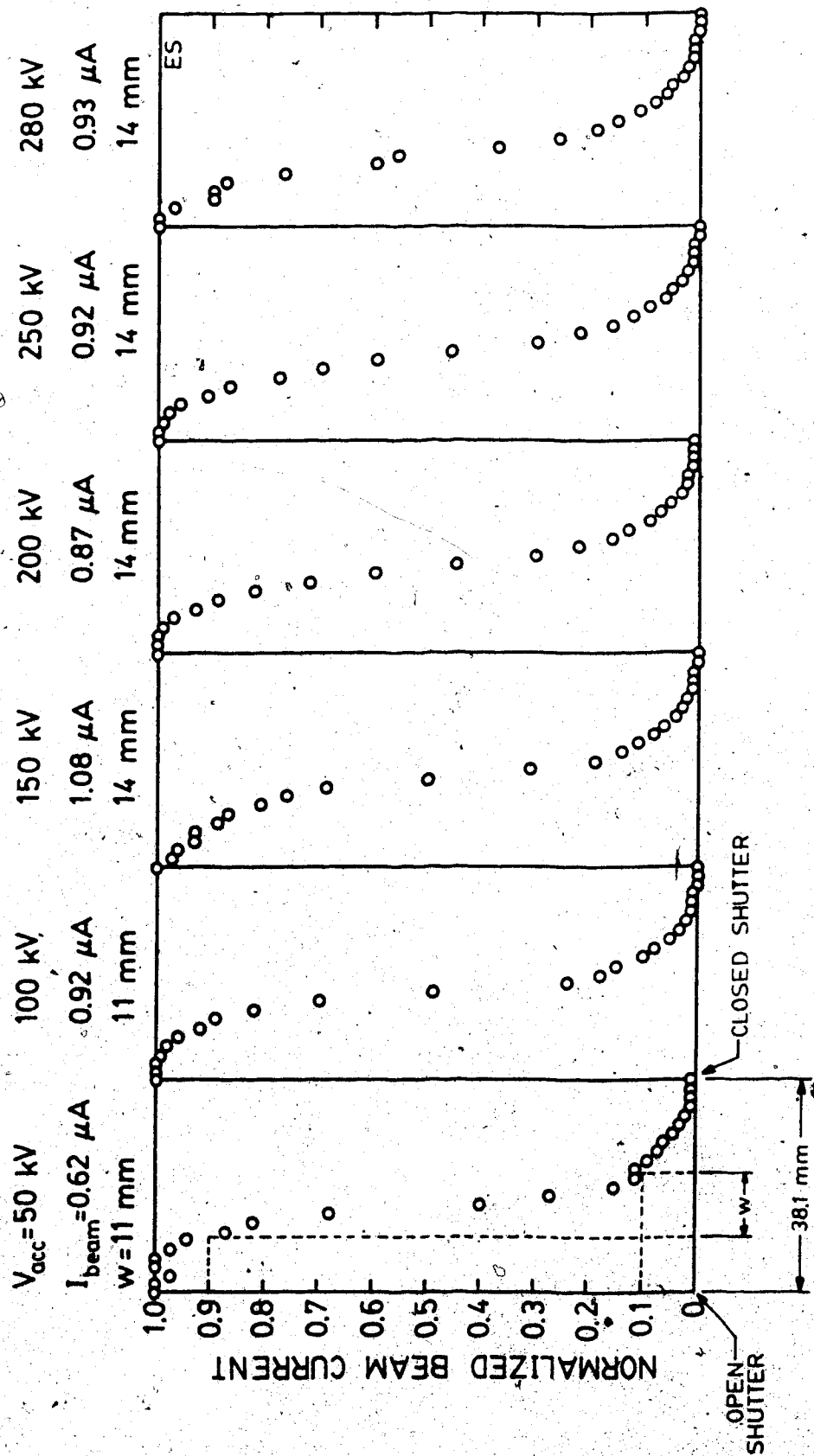
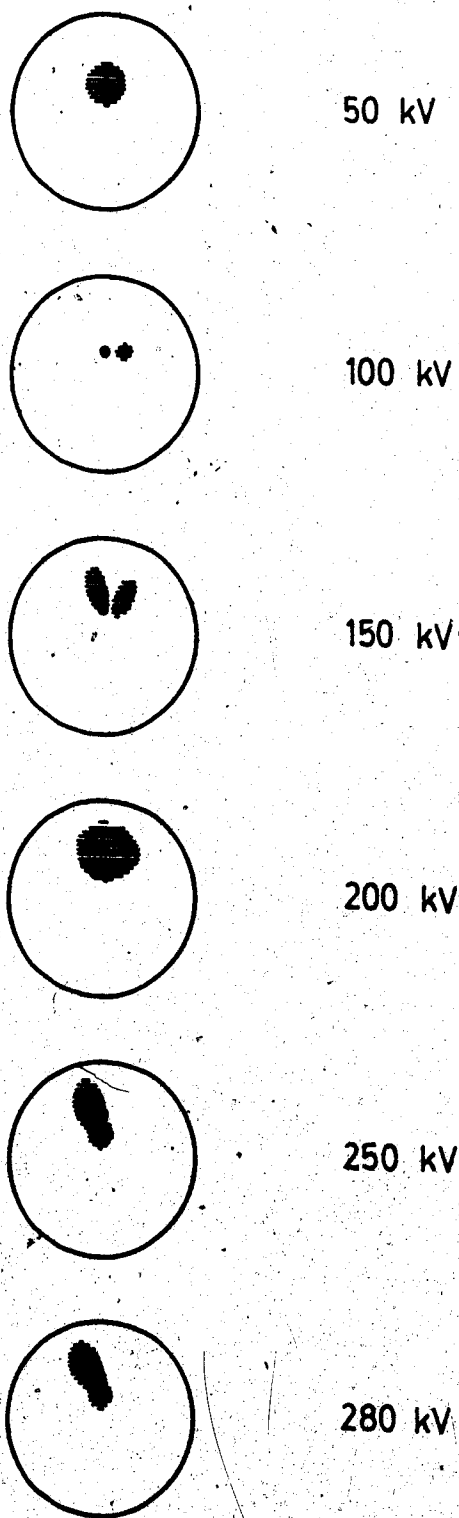


Figure 3.5 Accelerator Beam Current



ES

Figure 3.6 Beam Spots

of 1.7 mrad (0.10°) with the beam line axis—essentially, a parallel beam. An accounting of the space charge forces suggests that the waist is located close to the lens, and therefore, the beam, in fact, diverges through the mass filter and towards the mass selection aperture. In a similar fashion to the techniques of analysis used in Sec. 2.3.3.3, the waist is calculated to be 6.2 mm (0.25 in.) in diameter and located 78.4 mm (3.08 in.) from the lens center. At the mass selection aperture, the beam is predicted to be 6.8 mm (0.27 in.) in diameter. The aperture diameter is 4.76 mm (0.188 in.); hence, only about 49% of the ion current would be transmitted through the aperture, that is, 2.45  $\mu\text{A}$ , assuming a uniform current density. Of this, about 1  $\mu\text{A}$  is lost to the tube electrodes as evidenced by the increase in column current of 1  $\mu\text{A}$ , leaving a maximum of 1.45  $\mu\text{A}$  that can be collected at the target. Indeed, the largest observed current was 1.5  $\mu\text{A}$ . The divergence angle of the beam envelope is also limited by the aperture diameter. Assuming laminar space charge in the beam, the angle is 2.4 mrad (0.14°) at the aperture. The acceleration tube begins to influence ion beam trajectories at the fringe of its electric field pattern which is 70 mm (2.75 in.) beyond the aperture or 6 mm (3 in.) upstream of the first tube electrode (Galejs and Rose 1967, p. 305). At that point, the beam envelope is divergent with an angle of approximately 3.8 mrad (0.22°) to the beam line axis and is 5.4 mm (0.21 in.) in diameter. The virtual object location for the acceleration tube is then 784 mm upstream of the first tube electrode.

Continuing with point source Gaussian optics (Galejs and Rose 1967, pp. 312-313; El-Kareh and El-Kareh 1970, pp. 56-59) (see Fig. 2.5), the theoretical analysis shows that the acceleration tube produces a beam crossover upstream of the target and, hence, a divergent beam at the target location for all acceleration potentials except those below about 50 kV. Disregarding space charge expansion, the beam cross section, should be smaller as lower acceleration potentials are used. Wilson and Brewer (1973, p. 245), however, show that for a 5  $\mu\text{A}$   $\text{N}_2^+$  beam of 4.8 mm (0.19 in.) diameter, the effects of space charge cannot be ignored for acceleration potentials less than 100 kV in a 1000 mm (39.4 in.) tube. Therefore, as lower potentials are used, although the spot size should be smaller, the beam diameter expands due to



space charge forces. Figure 3.4 indicates that in going from 280 to 200 kV, during one particular run, the accelerator current fell by only 6.5%, but in going from 150 to 50 kV, during a different run, it fell 43%. The effects of space charge expansion of the beam at lower voltages along with optical aberrations and collisions between beam ions and residual gas atoms are likely so severe that a portion of the beam is lost to the acceleration tube electrodes. This accounts for the higher column currents that were observed.

Because of a misalignment of the acceleration tube during construction, the beam spot on the quartz window is off center. This misalignment is likely also the cause of the coma-like flare in the image shape, and as a consequence, correlation between Fig. 3.5 and Fig. 3.6 is difficult to verify. The expected trend in the experimental data is, nevertheless, apparent. At high acceleration potentials the beam diameter is large, while at low potentials the diameter is small although not as small as anticipated because of space charge expansion.

### 3.4 Radiation Pattern

In this device, radiation in the form of x rays is a by-product of the acceleration process. X rays are generated by the interaction of energetic secondary electrons with the surfaces of the acceleration tube and ion gun (Wilson and Brewer 1973, pp. 424-425). The pattern of x-ray intensity was recorded at various points in the laboratory area for a 280 kV 1.5  $\mu$ A N<sub>2</sub> beam. The data is given in Fig. 3.7 (see Fig. 2.30). No change in the pattern was apparent when secondary electron suppression at the beam in the target chamber was off, suggesting that the electrons originated within the acceleration tube—a result of collisions and charge exchange processes. The radiation survey meter was held at about the level of the beam line, and at each sampling point, it was oriented to read maximum intensity. As such, the source of greatest intensity seemed to be near the acceleration tube entrance, perhaps at the mass selection aperture. As set by the Atomic Energy Control Act, the maximum whole body exposure to radiation for nonatomic workers is 2.58  $\mu$ C/kg (10 mR) in a 40-hour week, or an average of 0.065 ( $\mu$ C/kg)/h (0.25 mR/h).

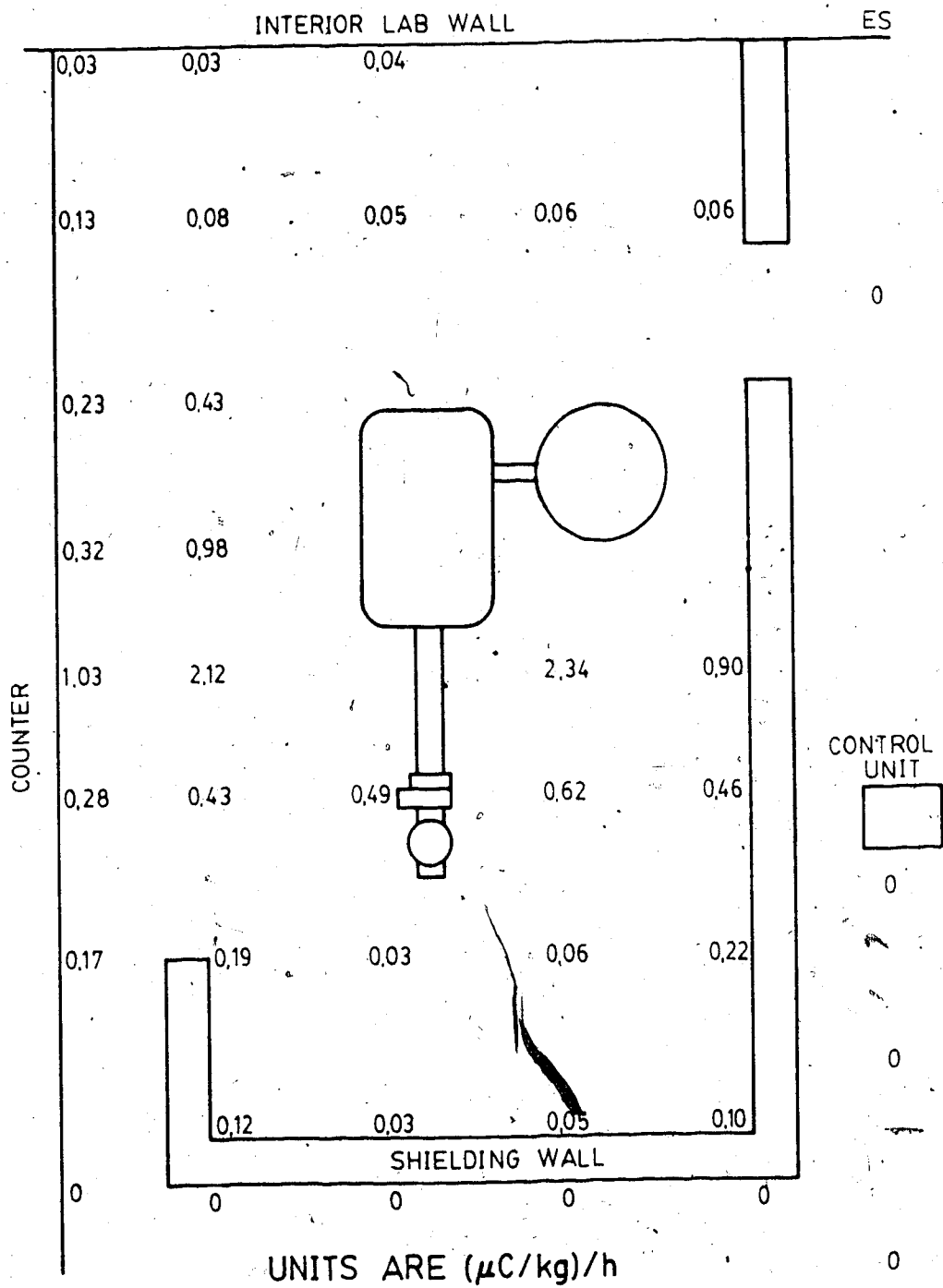


Figure 3.7 Radiation Intensity Pattern

### 3.5 Recommendations

Although the voltage holding capacity of the present acceleration tube is adequate, it was suggested in Sec. 2.3.2 that if higher acceleration potentials are to be used with the same acceleration tube that new spacer-resistors should be built. Apparently, contamination on the bore of the present spacer-resistors limits the voltage holding capacity of a single interelectrode section to 22 kV. Notwithstanding this performance, the total length of tube is not likely to be able to withstand 1 MV due to the long tube effect (Herb 1959, p. 87). Hence, if it were decided to use the acceleration tube at significantly higher voltages than the present 280 kV, it would be an advantage to build new spacer-resistors under cleaner conditions.

If lower gas pressure in the beam line is required, auxiliary apertures in the acceleration tube electrodes should be considered. Such apertures would increase the pumping conductance of the tube, but they would have to be oriented so that an extended acceleration path was not provided for a stray ion or electron flux.

To lower the intensity of background x-ray radiation, lead shielding could be placed around the beam line vacuum chamber near the junction between the acceleration tube and the ion gun.

In the course of running the accelerator system, several deficiencies in component performance have been noted. Among these is the electric power generation system inside the high voltage terminal. It has already been suggested in Sec. 2.3.4 that if more power was required the present electric generator should be replaced with an alternator and that the hydraulic motor should be serviced to repair possible damage.

Furthermore, the following modifications to the remote control apparatus should be considered. First, the ability to control vertical deflector voltage in the ion gun would be an asset. Second, the resolution of the controls should be improved, or at least, the control and monitor signals should be prevented from drifting. And third, it would be advantageous to have the monitored functions updated at a frequency higher than the present once per second.

A feature that could aid the setting of optimum filter voltages would be the addition of some form of beam previewer into the beam line of the ion gun. Such a device located near the acceleration tube entrance would allow the setting of filter voltages while monitoring the beam cross section. As it is now, settings that have been established in a test stand are used without alteration.

Of particular benefit would be a remote controlled needle valve for the ion source gas handling plant so that gas flow adjustments could be made under high voltage operation.

As a matter of convenience, part of the main high voltage terminal could be hinged to allow easier access to the ion gun controls. At present, it takes two people to set up the high voltage terminal.

To apply this accelerator to RBS and ion implantation, there would have to be additions to the target system. Besides ancillary control and diagnostic equipment, the following beam line components should be considered: variable slits, vertical and horizontal beam deflectors, an energy analyzer, a strong lens (that is, a quadrupole triplet), and a target manipulator (Wilson and Brewer 1973, pp. 467-473; Liebl 1977, pp. 277-281; Chu, Mayer, and Nicolet 1978, Chaps. 6 and 7; Bannenberg 1979; Jackson et al. 1979).

If beam currents greater than the present  $1.5 \mu\text{A}$  are required, there need to be changes to the existing beam line. Colutron Corporation suggests that to extract higher currents from the source a larger anode hole—up to 1.5 mm (0.06 in.) diameter from the present 0.5 mm (0.02 in.)—should be used. A more radical change would be to replace the present current regulated anode-to-cathode ion source power supply with a voltage regulated supply in order to be able to control ionization efficiency (Wilson and Brewer 1973, p. 14 and p. 86). Higher currents, though, means greater space charge expansion of the beam inside the ion gun. Higher beam voltages could reduce the problem, but the beam voltage cannot be raised above 5 kV, as specified by Colutron Corporation. This limitation can be circumvented by using a decelerating lens before and an accelerating lens after the filter (Hawkes 1972, pp. 194-196). Expansion of the beam may be overcome to some extent by installing a periodic focussing structure (Tien

1954) or another lens downstream of the filter, before the aperture. Higher beam currents can be delivered to the acceleration tube by increasing the diameter of the mass selection aperture—although at a cost of decreased mass resolution. A scheme to transmit more current through the tube might be to eliminate the focussing action at the acceleration tube entrance by installing a coarse wire mesh, thereby preventing a beam crossover within the tube and a possible loss of beam current. Increasing the aperture of the present tube, however, is not recommended on the basis of shielding requirements (see Sec. 2.2.1.2).

In summary, a possible beam line for generating and accelerating higher ion currents could have an ion source anode hole 1.5 mm (0.06 in.) in diameter, a periodic structure or lens following the filter, a larger mass selection aperture, and a wire screen at the acceleration tube entrance. If possible, these modifications should be installed one at a time to determine their effect on accelerator performance.

Further work on this project could include a thorough analysis of the operation of the mass filter looking at, for example, the correlation of electric and magnetic field patterns to the shape of the output beam cross section. Analysis of the effects of the fringe fields, and installation of magnetic shunt pieces can be attempted (Wählin 1964). Regarding the ion source, a detailed study of its operating characteristics would be valuable. To know its emittance characteristics (Wilson and Brewer 1973, pp. 185-189 and pp. 249-253) would be informative. An understanding of how the source behaves as a function of voltage, current, and gas pressure may suggest improvements that could be made, or at least, offer an avenue for explaining its present behaviour. A theoretical analysis of the plasma boundary (Harrison 1968; Kaufman 1977) may shed light on source behaviour as well.

#### 4. Conclusions

The objectives of this discourse were to introduce two accelerator design innovations and to show that a working accelerator facility which incorporates these innovations has been produced. The innovations are (1) an alternative acceleration tube construction and (2) a new system for the generation of electrical power inside a high voltage terminal.

The constant gradient acceleration tube design employs a string of internally-mounted voltage grading resistors. This innovation led to a simplification of tube construction and, consequently, a reduction in the cost of materials and component fabrication. The electrical and vacuum properties of the tube were satisfactory: the temperature of the vacuum mounted resistors remained low enough not to produce a significant outgassing load, and a nearly uniform interelectrode voltage was established. Moreover, the tube was successfully used to accelerate ions. Hence, following the plans presented here, an accelerator laboratory can build a constant gradient acceleration tube needing only modest financial resources and machine shop facilities.

The use of hydraulic equipment to transfer power to the high voltage terminal added flexibility to the design of the laboratory layout. In the present facility, many of the mechanical structures, such as terminal supports and radiation shielding, were carried over from a previous design. By using a fluid power scheme, the number of additions and changes to these structures that would be required to accommodate a power transfer apparatus were minimized, thereby saving time and money. That is, it was possible to locate equipment and route hydraulic lines so as to make optimum use of available laboratory space. In other words, a hydraulic apparatus such as the one described in this thesis, in which the motor unit can be located remotely from the accelerator room, could be used in other accelerator facilities where space is restricted.

The 280 kV ion accelerator that was built incorporates both of the aforementioned design innovations. In addition, it features a plasma-type positive-ion source, preacceleration mass filtering of the ion beam, an oil insulated Cockcroft-Walton high voltage generator, and a fiber optic channel to facilitate the control of terminal mounted equipment. All of the

accelerator components performed satisfactorily, both individually and collectively. The success of the project, however, was judged on the basis of the performance of the accelerator in a series of beam trials. In those trials, significant ion currents were accelerated, producing beam cross sections, at the target, that were well defined and stable. The results demonstrated that a viable accelerator system has been produced:

In summary, the two design innovations which are described in this dissertation contribute to low energy accelerator technology by increasing the equipment options available to the accelerator designer and by offering simple, low cost alternatives to existing practices. Moreover, while utilizing these innovations, a working accelerator system has indeed been produced.

## References Cited

- Ames, William F., *Numerical Methods for Partial Differential Equations*, 2nd ed. (Academic Press, New York, 1977).
- Arnold, W.R., *Rev Sci Instrum* 21, 796 (1950).
- Bannenberg, J.G., *Radiat Eff* 44, 3 (1979).
- Beuchner, W.W., R.J. Van de Graaff, A. Sperduto, L.R. McIntosh, and E.A. Burrill, *Rev Sci Instrum* 18, 754 (1947).
- Bromely, D. Allan, *Nucl Instrum Methods* 122, 1 (1974).
- Burcham, W.E., *Nature (London)* 160, 316 (1947).
- Carter, G. and W.A. Grant, *Ion Implantation of Semiconductors* (Edward Arnold, London, 1976).
- Chavet, I. and R. Bernas, *Nucl Instrum Methods* 47, 77 (1967).
- Chu, Wei-Kan, James W. Mayer, and Marc-A. Nicolet, *Backscattering Spectrometry* (Academic Press, New York, 1978).
- Cockcroft, J.D. and E.T.S. Walton, *Proc R Soc London, Ser A*: 129, 477 (1930).
- Cockcroft, J.D. and E.T.S. Walton, *Proc R Soc London, Ser A*: 136, 619 (1932a).
- Cockcroft, J.D. and E.T.S. Walton, *Proc R Soc London, Ser A*: 137, 229 (1932b).
- Coolidge, W.D., *J Franklin Inst* 202, 693 (1926).
- Dahl, Poul, *Introduction to Electron and Ion Optics* (Academic Press, New York, 1973).
- El-Kareh, A.B. and J.C.J. El-Kareh, *Electron Beams, Lenses, and Optics* (Academic Press, New York, 1970) Vol. 1.
- Galejs, A. and P.H. Rose, in *Focussing of Charged Particles*, edited by A. Septier (Academic Press, New York, 1967) Vol. 2, Chap. 5.1.
- Harrison, John L., *J Appl Phys* 39, 3827 (1968).
- Hawkes, P.W., *Electron Optics and Electron Microscopy* (Taylor and Francis, London, 1972).
- Hawley, R., in *High Voltage Technology*, edited by L.L. Alston (Oxford University Press, London, 1968), Chap. 4.
- Hedges, C.S., *Industrial Fluid Power*, 3 Vols. (Womack Machine Supply Co., 1969).
- Hepburn, Duncan, "Generation and Acceleration of Colloidal Beams", Ph.D. dissertation, University of Alberta, 1973.



- Hepburn, J.D., M.R. Shubaly, and J. Ungrin, in *Proceedings of the International Conference on Low Energy Ion Beams*, Institute of Physics Conference Series, Number 54, edited by I.H. Wilson and K.G. Stephens (Bristol and London, 1980), Chap. 5, pp. 158-162.
- Herb, R.G., in *Handbuch der Physik*, edited by S. Flügge and E. Creutz (Springer, Berlin, 1959), Vol. 44, pp. 64-104.
- Hollway, D.L., *Austral J Sci Res, A* 5, 430 (1952).
- Jackson, J.H., H.M. Bird, J.P. Flemming, G.J. Hofer, J.G. McCallum, P.J. Mostek, G.I. Robertson, A.F. Rodde, B. Weissman, and N. Williams, *Radiat Eff* 44, 59 (1979).
- Jiggins, A.H. and I.C. Demetsopoulos eds., *Proceedings of the Symposium on the Use of Low Energy Accelerators* (London, 1970) *Nucl Instrum Methods* 92, pp. 445-594 (1971).
- Kaufman, H.R., *AIAA J* 15, 1025 (1977).
- Klemperer, O. and M.E. Barnett, *Electron Optics*, 3rd ed. (Cambridge University Press, London, 1971).
- Kovarik, V.J., R.F. Lankshear, and Th. Sluyters, *IEEE Trans Nucl Sci* NS-18(3), 87 (1971).
- Laubert, R. and N. Wotherspoon, *IEEE Trans Nucl Sci* NS-12(3), 282 (1965).
- Lewin, Gerhard, *Fundamentals of Vacuum Science and Technology* (McGraw-Hill, New York, 1965).
- Liebl, H., in *Proceedings of the International Conference on Low Energy Ion Beams*, Institute of Physics Conference Series, Number 38, edited by K.G. Stephens, I.H. Wilson, and J.L. Moruzzi (Bristol and London, 1977).
- Liebmann, G., *Proc Phys Soc London, Sect B* 62, 219 (1949).
- Livingston M. Stanley and John P. Blewett, *Particle Accelerators* (McGraw-Hill, New York, 1962).
- Lorrain, Paul, René Béique, Paul Gilmore, Paul-Emile Girard, Alain Breton, and Pierre Piché, *Can J Phys* 35, 299 (1957).
- Menzinger, M. and L. Wählin, *Rev Sci Instrum* 40, 102 (1969).
- Michael, Irving, E.D. Berners, F.J. Eppling, D.J. Knecht, L.C. Northcliffe, and R.G. Herb, *Rev Sci Instrum* 30, 855 (1959).
- Miner, D.F. and J.B. Seastone, *Handbook of Engineering Materials* (Wiley, New York, 1955).
- Mott, R.L., *Applied Strength of Materials* (Prentice-Hall, Englewood Cliffs, 1978).
- Parks, H.G., in *Proceedings of the 11th Symposium on Electron, Ion, and Laser Beams*, edited by R.F.M. Thornley (Boulder, Colorado, 1979), pp. 229-238.
- Peck, R.A. and H.P. Eubank, *Rev Sci Instrum* 26, 444 (1955).

Reich, Herbert J., *Theory and Applications of Electron Tubes* (McGraw-Hill, New York, 1944).

Reinhold, G. and R. Minkner, *IEEE Trans Nucl Sci* NS-12(3), 820 (1965).

Reinhold, G., R. Minkner, and H. Adler, *IEEE Trans Nucl Sci* NS-12(3), 272 (1965).

Seliger, R.L., *J Appl Phys* 43, 2352 (1972).

Sidenius, G., in *Proceedings of the International Conference on Low Energy Ion Beams*, Institute of Physics Conference Series, Number 38, edited by K.G. Stephens, I.H. Wilson, and J.L. Moruzzi (Bristol and London, 1977), pp. 1-11.

Tien, Ping King, *J Appl Phys* 25, 1281 (1954).

Thompson, B.J. and L.B. Headrick, *Proc IRE* 28, 318 (1940).

Tuve, M.A., G. Breit, and L.R. Hafstad, *Phys Rev A* 35, 66 (1930).

Tuve, M.A., L.R. Hafstad, and O. Dahl, *Phys Rev A* 48, 315 (1935).

Van de Graaff, R.J., P.H. Rose, A.B. Wittkower, *Nature (London)* 195, 1292 (1962).

Van de Graaff, R.J., J.G. Trump, and W.W. Beuchner, *Rep Prog Phys* 11, 1 (1946).

von Engel, A., *Ionized Gases*, 2nd ed. (Oxford University Press, London, 1965).

Wählin, L., *Nucl Instrum Methods* 27, 55 (1964).

Wählin, L., *Nucl Instrum Methods* 38, 133 (1965).

Waidelich, D.L. and C.H. Gleason, *Proc IRE* 30, 535 (1942).

Weber, C., in *Focussing of Charged Particles*, edited by A. Septier (Academic Press, New York, 1967), Vol. 1, Chap. 1.2.

Wilson, Robert G. and George R. Brewer, *Ion Beams: With Applications to Ion Implantation* (Wiley, New York, 1973).

Wilson, R.G. and D.M. Jamba, *Nucl Instrum Methods* 91, 285 (1971).

Ziegler, James F., ed., *New Uses of Ion Accelerators* (Plenum, New York, 1975).

## Appendix: Operating Instructions

The arrangement of ion gun controls inside the high voltage terminal is given in Figs. 3.2 and 3.3. Figure 3.4 shows the remote control unit.

**Initial start-up.** The following procedures apply when the beam line upstream of the target chamber has been exposed to air for a long time, that is, more than one day. The ion source must undergo an outgassing regimen, as when ion source filaments are replaced.

1. Start the turbomolecular pump following the manufacturer's recommended procedure. Allow it to evacuate the entire beam line. Start the target chamber pressure gauge after about five minutes of pumping (follow the gauge manufacturer's instructions).
2. Pump the ion source through the source gas handling plant (GHP) by connecting the portable gas handling plant pump. Pumping should continue until the pressure at the target chamber is less than about 0.7 mPa ( $5 \cdot 10^{-6}$  Torr). This will take one or more days.
3. Go to the high voltage terminal and plug the power cord from the distribution panel into the extension outlet that supplies 117 V from the ac mains.
4. On the ion source control panel, make sure that the 4 kV switch is disabled, the filament selector and anode are off, and the source and furnace filament control switches are in LOC.
5. On the power distribution panel the MASTER switch should be set on. The ion source gauges will come on. (The meters may need to be tapped to unstick the indicator needle.) The FIL switch should then be set to ON.
6. Turn the filament selector switch to BOTH.
7. Record the target chamber pressure from the gauge control unit that is located on the remote control unit, and then raise both filament currents to 1 A. The target chamber pressure will rise to over 1.3 mPa ( $10^{-5}$  Torr), but after one day or more—depending on the length of time the beam line has been exposed to atmospheric air—it should return to below 0.7 mPa ( $5 \cdot 10^{-6}$  Torr).
8. When the target chamber has indeed dropped to less than 0.7 mPa increase the filament

- currents to 1.5 A. This time the target chamber pressure could rise to 10 mPa ( $10^{-4}$  Torr).
9. After about one day and if the pressure has recovered to less than 0.7 mPa, the filament currents can be raised to 2 A.
  10. Thereafter, continue to increment the currents by 1 A every day, or more frequently if target chamber pressure recovers. Beyond 5 A, the ion source cooling system should be run. To use the coolant system, open the faucet to start water flow to the heat exchanger, and turn on the circulation pump (yellow switch on the hydraulic system motor unit).
  11. At 15 A, if target chamber pressure is below 0.7 mPa, ion source outgassing is complete, and both filaments may be turned down, over a period of several hours, to zero.
  12. The ion source GHP should then be isolated by closing valve A (Fig. 3.2). The cooling system should be turned off, that is, stop the circulation pump and shut off the water flow.

A few days after the filaments are turned off, target chamber pressure should be less than 100  $\mu$ Pa ( $10^{-6}$  Torr). A thorough ion source outgassing can take more than two weeks. After this procedure has been followed once, however, it does not have to be repeated so long as the beam line is kept under vacuum. Therefore, avoid exposing the beam line to atmospheric air. If the target chamber must be accessed, the upstream portion of the beam line should be isolated under vacuum before venting the turbomolecular pump.

Running the accelerator with gas ions. This procedure applies if the beam line has already been outgassed and has since been kept under vacuum. Typically, target chamber pressure will be on the order of 40  $\mu$ Pa ( $3 \cdot 10^{-7}$  Torr) before a run. You will need the help of one assistant to perform step #18 of the start-up procedure and step #6 of the shut-down procedure.

1. Go to the remote control unit (RCU) and power on. Make sure that all ion gun controls are fully counter clockwise and all switches are in the off position.
2. Switch circuit breakers #16 (power hydraulic unit), #5 (acceleration voltage generator), and #25 (outside warning lights) to the on position.

3. Go to the high voltage terminal. Ion source gas flow metering valve, valve B in Fig. 3.2, should be closed, that is, turned fully clockwise (do not force it too tight), and valve A should be opened.
4. Gas from the portable gas handling plant can be admitted to the ion source gas reservoir through open valves C and D. Air, however, can be admitted directly.
5. Valve C is then closed and the portable gas handling plant is detached and placed behind the high voltage cable shield.
6. Plug the ion gun power cord into the generator outlet.
7. Go to the hydraulic system motor unit and turn the fan on to maximum. Have all laboratory personnel don ear protectors and switch both the coolant and hydraulic pumps on.
8. In the high voltage terminal, the 4 kV switch should be at DISABLE, filament selector should be off, filament controls should be on LOC and the controls turned fully counter clockwise, the anode should be off, and the lens should be off. The magnet switch should be on LOC and the controls turned fully counter clockwise. Ion gun power distribution switches should then be turned on in the following order: MASTER, VF/MAG/FO, FILS, ANODE. The ion source pressure meters may need a tap to unstick the needles.
9. Set the filament selector to FIL.
10. Set the source filament switch to REM.
11. Set the 4 kV control to ENABLE and the lens voltage switch to REM. With the switch in LOC, be careful not to touch the metal parts of the ion source GHP; the plastic knobs may, however, be handled.
12. Set the anode switch to REM, turn the anode to ON, and rotate the knob clockwise to the 6 o'clock position.
13. Set the filter magnet switch to REM.
14. Go to the RCU and advance the source filament current to a warm-up level—between 5 and 10 A, as indicated on the RCU monitor (see Fig. 3.4).

15. Return to the high voltage terminal and, using a DMM, set the filter voltages (see Sec. 2.3.3.3).
16. Gradually open the needle valve, that is, valve B, on the ion source gas handling plant, until discharge chamber pressure reads approximately 7 Pa (0.05 Torr). This will establish a target chamber pressure of about 1 mPa ( $10^{-5}$  Torr).
17. Open the faucet to start water flow to the cooling system.
18. Set the upper half of the main high voltage terminal in place (you will need help to do this). There is no need to move the secondary high voltage terminal about.
19. Go to the RCU and raise filament current to slightly over 15 A.
20. Switch the anode on to establish an electric discharge in the ion source. A discharge has been struck when an anode current of between 500 and 600 mA is indicated. The corresponding anode voltage will be between 10 and 30 V.
21. Record the discharge parameters. Representative values from a typical run were as follows: anode: 531 mA and 16 V; filament: 15.74 A and 14.31 V; discharge chamber pressure: 465 (arbitrary units); target chamber pressure: 1.3 mPa ( $9.7 \cdot 10^{-6}$  Torr).
22. Turn the outside warning lights on (the switch is on the south wall).
23. Turn the acceleration voltage on. Follow the directions given by the manufacturer when operating the high voltage power supply. Select any desired voltage up to 280 kV. No voltage conditioning is necessary. Record the acceleration tube column current and the power supply current.
24. Switch the ion gun extraction voltage (4 kV) on.
25. Set the magnet voltage for the corresponding ion species that is to be accelerated (see Sec. 2.3.3.3).
26. Raise the lens voltage to approximately 3200 V and monitor the beam current at the target.
27. Magnet and lens voltages will require adjustment to obtain maximum beam current.

During a run, it may be necessary to enter the accelerator area. If so, use a radiation survey meter to ensure the x-ray intensity is at a safe level (see Sec. 3.4). Enter the accelerator

area only to work near the target chamber and the immediate area. Avoid the high voltage terminals and acceleration tube. Shut down the accelerator if maintenance work is being performed.

To shut the accelerator down, carry out the following procedures.

1. Set RCU anode switch of the off position.
2. Turn filament current down to zero.
3. Turn magnet and lens voltages down to zero.
4. Turn extraction voltage off.
5. Turn the acceleration voltage off and extinguish the outside warning lights. Wait one minute or so until the voltage has fallen to zero before entering the accelerator area.
6. With the help of an assistant, uncover the main high voltage terminal.
7. Turn the needle valve off, but do not force it too tight.
8. Close ion source valve A and D.
9. Set the 4 kV switch to OFF and disable the extraction potential.
10. Set magnet switch to LOC control.
11. Turn the anode from the 6 o'clock position to OFF and switch the control to LOC.
12. Set the filament control switch to LOC.
13. Set the filament selector to OFF.
14. Power distribution switches should be shut off in the following order: ANODE, FILS, VF/MAG/FO; MASTER.
15. Both pumps on the hydraulic system motor unit should be turned off. Leave the fan on until laboratory equipment cools down. The portable GHP may be reconnected to the ion source if necessary.
16. Turn the water flow off.
17. Power the RCU off.
18. Place circuit breakers #25, #5, and #16 in the off position.

**Vacuum system operation.** The beam line should of course be kept under vacuum. At some point, however, it may be necessary to shut down the vacuum system. If so, the following procedures should be carried out.

1. Close valves A and C (Fig. 3.2) on the ion source GHP and disconnect the portable gas handling plant.
2. Turn the target chamber pressure gauge off.
3. The next step depends on the reason for the shut-down. If the entire beam line must be exposed to atmospheric air—for example, when the ion source filaments are replaced—simply follow the recommended shut-down procedure for the turbomolecular pump as given in the manufacturer's operating manual, venting the pump through the target chamber. On the other hand, when servicing of the target chamber is required or when the vacuum pumps need maintenance, the target chamber need only be exposed to air. In this case, close the gate valve that is located between the acceleration tube and target chamber before turning the turbomolecular pump off. This keeps the beam line above the target chamber under vacuum, thereby avoiding contamination of the beam line and permitting a faster pumpdown upon restarting the vacuum system.
4. Once the turbomolecular pump has coasted to a stop, close the gate above the pump and close the target chamber vent valve.
5. Circuit breaker #28 should then be placed in the off position.

To restart the vacuum system, procede as follows.

1. Place circuit breaker #28 in the on position.
2. Open the gate valve above the turbomolecular pump.
3. If the entire beam line was exposed to air, perform steps #1 and #2 of **Initial start-up**. The remainder of the initial start-up procedure may have to be followed if the beam line was exposed to air for more than one day.

Otherwise, with only the target chamber vented, start the turbomolecular pump. After the pump has run for about five minutes, restart the target chamber pressure gauge



according to the manufacturer's recommended procedure. When a pressure of about 7 mPa ( $5 \cdot 10^{-5}$  Torr) has been achieved in the target chamber (about 20 minutes after starting the pump), open the isolating gate valve upstream of the target chamber.

4. The accelerator may be run after target chamber pressure falls below 0.7 mPa ( $5 \cdot 10^{-6}$  Torr). This may take one or more days, depending on how long the vacuum system remained idle. Care must be exercised, however, to ensure that, upon raising ion source filament current to operating levels, the pressure in the target chamber does not rise too high, that is, above 1.3 mPa ( $10^{-5}$  Torr). If this happens, allow one or two additional days of pumping with the filament current at 10 A and the ac mains supplying electrical power. Then, try running the accelerator again.

If there is a power failure or power transient, the magnetic contactor switch will open, and this will cut power to all accelerator systems, including the vacuum equipment. The turbomolecular pump and the target chamber pressure gauge will go off. In addition, the gate valve above the turbomolecular pump will close. Before reconnecting the power, place the pump, gauge, and valve switches in the off position. Reconnect the power. Start the roughing pump on the turbomolecular pump unit. Then, after about one minute, start the turbomolecular pump itself. After the pump has run for about one or two minutes, open the gate valve and restart the pressure gauge. The gauge should not be kept on if the pressure reading is higher than 10 mPa ( $10^{-4}$  Torr). If this is the case, check that the target chamber vent valve is closed and continue pumping for a few more minutes. Try to restart the pressure gauge again.

## Vita

Name: Edmund Sumbar

Place of Birth: Calgary, Alberta

Year of Birth: 1954

### Academic History:

University of Alberta  
Edmonton, Alberta  
1972-76  
B.Sc. (Electrical Engineering), with distinction

University of Alberta  
Edmonton, Alberta  
1976-84  
Ph.D. candidate (Electrical Engineering)

### Honours and Awards:

J.M. Sharpe Memorial Prize 1975  
National Research Council of Canada Postgraduate Scholarship 1977-78  
National Research Council of Canada Postgraduate Scholarship 1978-79  
Natural Sciences and Engineering Research Council of Canada  
Postgraduate Scholarship 1979-80  
University of Alberta Dissertation Fellowship 1982-83

### Related Experience:

Teaching Assistant  
University of Alberta  
1976-84

### Publications:

- (1) "A novel ion acceleration tube design", submitted to *Review of Scientific Instruments*.
- (2) "Generating electrical power inside a high voltage accelerator terminal", in preparation.